

**ICE, CLOUD, and Land Elevation Satellite-2
(ICESat-2) Project**

**Algorithm Theoretical Basis Document (ATBD)
for
Land Ice Along-Track Height Product (ATL06)**

Prepared By: Denis Felikson, NASA Goddard Space Flight Center

With

**Benjamin Smith, David Hancock, Kaitlin Harbeck, LeeAnne Roberts,
Thomas Neumann, Kelly Brunt, Helen Fricker, Alex Gardner, Matthew
Siegfried, Susheel Adusumilli, Beata Csathó, Nicholas Holschuh, Johan
Nilsson, and Fernando Paolo.**



**Goddard Space Flight Center
Greenbelt, Maryland**

CHECK <https://ipdtdms.gsfc.nasa.gov>

Abstract

This document describes the theoretical basis of the land ice height processing algorithms and the products that are produced by the ICESat-2 mission. It includes descriptions of the parameters that are provided with each product as well as ancillary geophysical parameters used in the derivation of the products.

CM Foreword

This document is an Ice, Cloud, and Land Elevation Satellite-2 (ICESat-2) Project Science Office controlled document. Changes to this document require prior approval of the Science Development Team ATBD Lead or designee. Proposed changes shall be submitted in the ICESat-II Management Information System (MIS) via a Signature Controlled Request (SCoRe), along with supportive material justifying the proposed change.

In this document, a requirement is identified by “shall,” a good practice by “should,” permission by “may” or “can,” expectation by “will,” and descriptive material by “is.”

Questions or comments concerning this document should be addressed to:

ICESat-2 Project Science Office
Mail Stop 615
Goddard Space Flight Center
Greenbelt, Maryland 20771

Preface

This document is the Algorithm Theoretical Basis Document for the TBD processing to be implemented at the ICESat-2 Science Investigator-led Processing System (SIPS). The SIPS supports the ATLAS (Advance Topographic Laser Altimeter System) instrument on the ICESat-2 Spacecraft and encompasses the ATLAS Science Algorithm Software (ASAS) and the Scheduling and Data Management System (SDMS). The science algorithm software will produce Level 0 through Level 4 standard data products as well as the associated product quality assessments and metadata information.

The ICESat-2 Science Development Team, in support of the ICESat-2 Project Science Office (PSO), assumes responsibility for this document and updates it, as required, as algorithms are refined or to meet the needs of the ICESat-2 SIPS. Reviews of this document are performed when appropriate and as needed updates to this document are made. Changes to this document will be made by complete revision.

Changes to this document require prior approval of the Change Authority listed on the signature page. Proposed changes shall be submitted to the ICESat-2 PSO, along with supportive material justifying the proposed change.

Questions or comments concerning this document should be addressed to:

ICESat-2 Project Science Office
Mail Stop 615
Goddard Space Flight Center
Greenbelt, Maryland 20771

Review/Approval Page

Prepared by:

Denis Felikson
Research Scientist
NASA Goddard Space Flight Center
Cryospheric Sciences Laboratory
Code 615, Building 33, Room A209
8800 Greenbelt Rd.
Greenbelt, MD 20771

Reviewed by:

Alex Gardner
NASA Jet Propulsion Laboratory

***** Signatures are available on-line at: <https://ipdtdms.gsfc.nasa.gov> *****

Change History Log

Revision Level	Description of Change	Date Approved
1.0	Initial Release	
4.0	Minor changes made to document front matter; added brief abstract; clarified description of corrections applied to land-ice height variable (h_{li}).	

List of TBDs/TBRs

Item No.	Location	Summary	Ind./Org.	Due Date

Table of Contents

Abstract	ii
CM Foreword	iii
Preface	iv
Review/Approval Page	v
Change History Log	vi
List of TBDs/TBRs	vii
Table of Contents	viii
List of Figures	xi
List of Tables	xii
1 INTRODUCTION	1
2 BACKGROUND INFORMATION and OVERVIEW	2
2.1 Background	2
2.2 Physical Basis of Measurements	4
2.2.1 Height retrieval over approximately planar surfaces	4
2.3 Potential Errors	6
2.4 Land-ice Level-3 products: ATL06: Land-Ice Height	6
3 ALGORITHM THEORY: Derivation of ATL06 Land Ice Height Parameters	8
1.1 Representation of the surface	8
3.1.1 Land-ice height definition	10
3.2 Outline of processing	11
3.3 PE selection	11
3.3.1 Along-track segments	11
3.3.2 Local Coordinate Systems	14
3.3.3 Parameters describing selected PEs	15
3.3.4 Handling of invalid segments	19
3.3.5 Surface-window refinement and least-squares height estimate	20
3.4 First-Photon Bias	22
3.4.1 Mathematical Description for the First-Photon Bias	23
3.4.2 Correction Formulation for the First-Photon Bias	24
3.4.3 Statistics Derived from the First-Photon-Bias Correction	25

3.5	Transmit-pulse shape correction	30
3.6	Signal, Noise, and Error Estimates	32
3.6.1	Background PE rate	32
3.6.2	Signal PE count.....	33
3.6.3	Per-Photon Errors	33
3.6.4	Propagated Height Errors:	34
3.6.5	Uncorrected reflectance	34
3.7	Across-track slope calculation	35
3.8	Subsurface-Scattering Bias.....	35
3.9	Atmospheric-Scattering Bias	36
3.10	Segment geolocation	36
3.11	Noise-corrected robust estimators of spread	37
4	ATL06 Data product description	40
4.1	Data Granules	40
4.2	Segment_quality group.....	41
4.2.1	Signal_selection_status subgroup	42
4.3	<i>Land_ice_segments</i> group.....	42
4.3.1	geophysical subgroup	45
4.3.2	ground_track subgroup	48
4.3.3	bias_correction subgroup.....	50
4.3.4	fit_statistics subgroup.....	51
4.3.5	<i>DEM</i> subgroup.....	53
4.4	<i>residual_histogram</i> group.....	54
5	ALGORITHM IMPLEMENTATION: Land Ice Height (ATL 06/L3A)	56
5.1	Outline of Procedure	56
5.2	Input Parameters	56
5.3	Processing Procedure for Parameters.....	59
5.4	Top-Level Fitting Routine	60
5.5	Signal selection based on ATL03 flags	65
5.6	Backup PE-selection routine.....	66
5.7	Iterative Least-Squares Fitting Routine	68

5.8	Robust dispersion calculation from a collection of points, not including a background estimate.....	72
5.9	Robust dispersion calculation from a collection of points, including a background estimate.....	72
5.10	First- Photon Bias Correction.....	73
5.11	Gain-corrected median	74
5.12	Gain-corrected mean	76
5.13	Transmit-pulse-shape correction	77
5.14	Residual_histogram calculation.....	78
5.15	Transmit-echo-pulse initialization	80
6	TEST DATA AND SOFTWARE REQUIREMENTS	82
6.1	ATL06 Test Data Setup.....	82
7	Browse Products and Q/A statistics.....	83
7.1	Browse Products	83
7.2	Q/A Statistics	83
8	Appendix A: Glossary	84
	Glossary/Acronyms	90
	References	92

List of Figures

<u>Figure</u>	<u>Page</u>
Figure 2-1. ICESat-2 repeat-track schematic	3
Figure 2-2. Schematic of returns from different surface types	5
Figure 3-1. Surface return shape	8
Figure 3-2. Mean and median height biases	9
Figure 3-3. Reference point numbering schematic	11
Figure 3-4. Example PE selection.....	13
Figure 3-5. RGT coordinates	14
Figure 3-6 Segment fitting	15
Figure 3-7. First-photon bias correction	22
Figure 3-8. Accuracy of first-photon bias correction elevation recovery	27
Figure 3-9. Accuracy of first-photon-bias-correction signal strength recovery	28
Figure 3-10. Transmit-pulse-shape correction	30
Figure 5-1. Flow chart for top-level ATL06 processing.....	59
Figure 5-2. Flow chart for iterative ground fit.....	68
Figure 8-1. Spots and tracks, forward flight	87
Figure 8-2. Spots and tracks, forward flight	88

List of Tables

<u>Table</u>	<u>Page</u>
Table 3-1 <i>signal_selection_source</i> values	17
Table 3-2 Status parameters for signal-selection algorithms	18
Table 4-1 <i>Segment_quality</i> group	41
Table 4-2 <i>land_ice_segments</i> group	42
Table 4-3 Segment characteristics for <i>ATL06_quality_summary</i> to be zero	44
Table 4-4 <i>geophysical</i> subgroup	46
Table 4-5 <i>ground_track</i> subgroup	49
Table 4-6 <i>bias_correction</i> subgroup	50
Table 4-7 <i>fit_statistics</i> subgroup	51
Table 4-8 <i>DEM</i> subgroup	53
Table 4-9 Parameters in the <i>residual_histogram</i> group	54
Table 5-1. Inputs for ATL06	57

1 **1 INTRODUCTION**

2 This document describes the theoretical basis and implementation of the level-3 land-ice
3 processing algorithms. It currently includes ATL06, which provides geolocated land-ice surface
4 heights, and ATL11, which provides time series of surface heights. The higher-level products,
5 providing mapped height, and mapped height change will be described in supplements to this
6 document available 2021.

7 The ATL06 product provides the most basic derived values from the ATLAS instrument on
8 ICESat-2: the surface height at a given point on Earth’s surface at a given time relative to the
9 WGS-84 ellipsoid. ATL06 provides estimates of the ice-sheet surface height, and ancillary
10 parameters needed to interpret and assess the quality of these height estimates. ATL06 heights
11 represent the mean surface height averaged along 40-m segments of ground track, 20-m apart,
12 for each of ATLAS’s six beams. Segments within adjacent beams are aligned to facilitate
13 estimation of the across-track surface slope; they are also aligned from orbit to orbit so that
14 subsequent repeat tracks give height estimates for nearly the same location on the surface,
15 simplifying the estimation of height changes made through repeat-track analysis. Height
16 estimates from ATL06 can also be compared with other geodetic data and used as inputs to
17 higher-level ICESat-2 products, particularly ATL11, 14, and 15.

18 Higher-level products are based on the height estimates in ATL06. ATL11 provides heights
19 corrected for displacements between the reference tracks and the location of the ATLAS
20 measurements. ATL14 provides gridded height maps for selected epochs during the mission,
21 based on the corrected heights in ATL11. ATL15 provides height-change maps based on the
22 ATL14 height maps and height differences derived from ATL11.

23 In this document, Section 2 provides an overview of land-ice products and gives a brief summary
24 of the procedures used to derive products

25 Section 3 describes the algorithm used to generate the products.

26 Section 4 gives the processing steps and input data required to derive each parameter, and
27 describes the products in detail.

28 Section 5 gives a detailed procedure for deriving selected parameters

29 Section 6 describes test data and specific tests that NASA’s implementation of the algorithm
30 should pass.

31

32

33 **2 BACKGROUND INFORMATION AND OVERVIEW**

34 This section provides a conceptual description of ICESat-2’s ice-sheet height measurements and
 35 gives a brief description of the derived products.

36 **2.1 Background**

37 ATLAS on ICESat-2 determines the range between the satellite and the Earth’s surface by
 38 measuring the two-way time delay of short pulses of laser light that it transmits in six beams. It
 39 is different from previous operational ice-sheet altimeters in that uses a photon-counting
 40 detector. Previous altimeters (e.g. GLAS on ICESat-1, ATM, and LVIS) have used full-
 41 waveform digitizers that received millions or more photons for each transmitted pulse, allowing
 42 the receiver to generate a waveform, *i.e.* the return power as a function of time. ATLAS instead
 43 records a set of arrival times for individual photons, which are then analyzed to derive surface,
 44 vegetation, and cloud properties. Although ATLAS measures much weaker signals than full-
 45 waveform altimeters, it has three major design advantages over GLAS:

- 46 i) ATLAS has six beams arranged in three pairs (Figure 2-1), so that it samples each of
 47 three reference pair tracks with a pair of beams;
- 48 ii) ATLAS transmits pulses at 10 kHz, giving approximately one pulse every 0.7 m
 49 along track, more than two orders of magnitude finer than the 170-meter along-track
 50 of GLAS;
- 51 iii) ATLAS’s expected pointing control will be better than 90 m RMS, better than the
 52 100-200 m achieved by ICESat-1.

53 ATLAS’s six beams are spread over a small angle so that their projection onto the surface of the
 54 earth is a rectangular array with two rows and three columns, with about 3.3 km separation
 55 between each column and its neighbors, and 2.5 km between the rows. As ICESat-2 moves
 56 along its orbit, the ATLAS beams illuminate six tracks on the Earth’s surface; the array is rotated
 57 slightly with respect to the satellite’s flight direction so that tracks for the fore and aft beams in
 58 each column produce pairs of tracks, each pair separated by about 90 m (Figure 2-1). The
 59 separation between beams in each pair allows for measurement of the local surface slope in the
 60 across-track and along-track direction; this will allow ICESat-2 to make the most precise and
 61 detailed repeat estimates of ice-sheet height of any satellite to date.

62 ATLAS pulses are short, about 1.6 ns long (FWHM), and are transmitted every 0.1 ms (10 kHz);
 63 this fast repetition yields footprint centers separated by about 0.7 m in the along-track direction.
 64 Each pulse illuminates an approximately circular area on the ground ~17 m in diameter.
 65 ATLAS’s strong beams detect at most 12 reflected photons from each transmitted pulse. Great
 66 care is taken to detect only photons with the same wavelength as the transmitted laser pulse and
 67 to limit the field of view of the detectors to a region slightly larger than the illuminated
 68 “footprint” of each beam; therefore, ground-return photon events (PEs, meaning photons that are
 69 detected) may readily be distinguished from solar background PEs because they are clustered in
 70 time, while background PEs are distributed evenly in time and arrive much less frequently.

71 The high (~45-meter RMS) accuracy of ICESat-2’s pointing control means that pairs for
 72 consecutive repeats of each RPT (Reference Pair Track) are likely to overlap. The fine along-

73 track sampling and the multi-beam capability allow height products to be defined for segments
 74 that are consistent in along-track position for repeated measurements along the same RPT.
 75

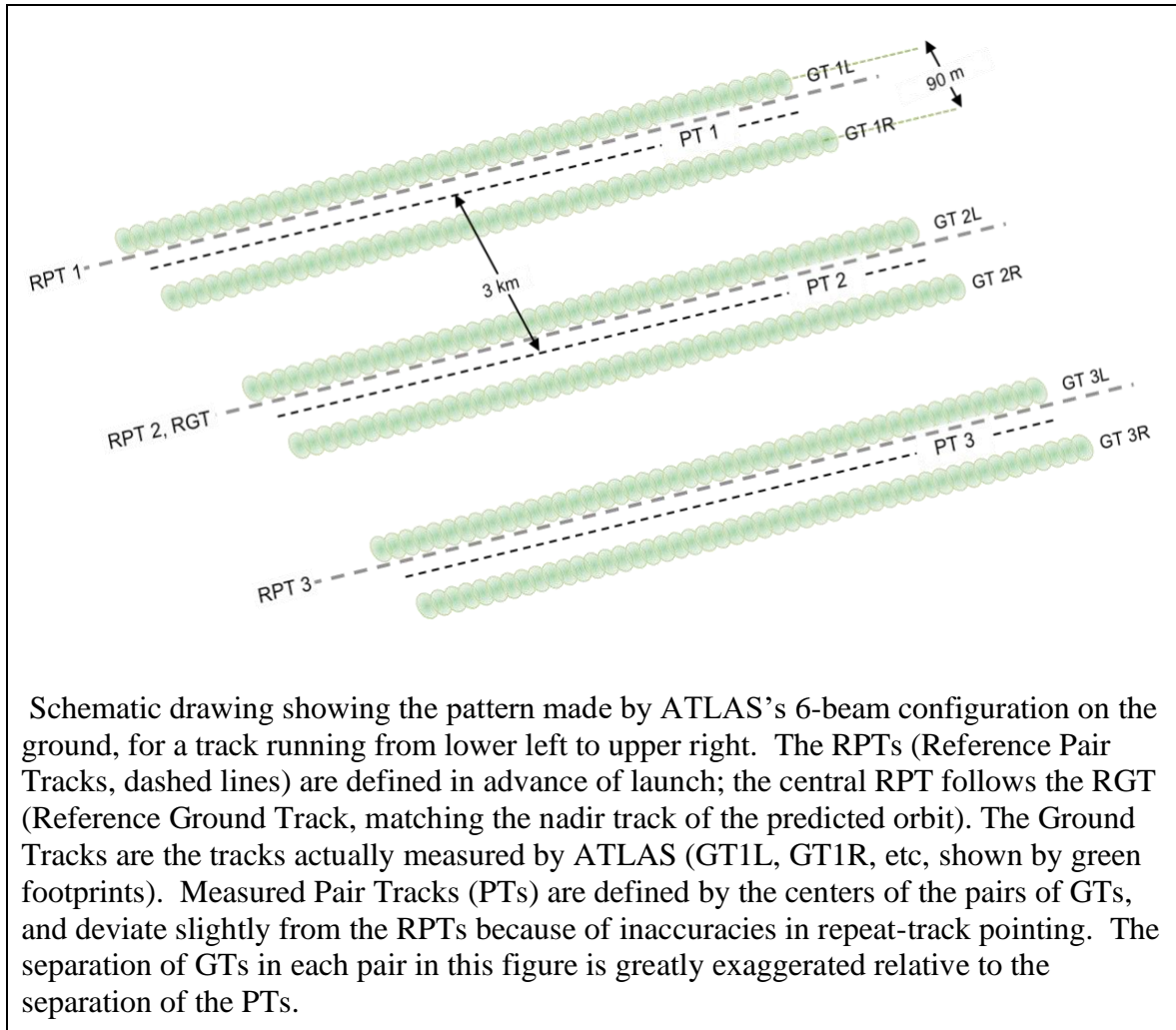


Figure 2-1. ICESat-2 repeat-track schematic

76
 77 Further processing of ATL06 heights will produce heights corrected for surface slope and
 78 curvature that give the estimated time-varying height for selected points on the RPTs and at
 79 track-to-track crossover points (ATL11). These shape-corrected heights will be processed further
 80 to give i) height maps for selected time intervals (semi-annual or annual, ATL14) and ii) annual
 81 height-change maps for the Antarctic and Greenland ice sheets (ATL15)
 82

83 **2.2 Physical Basis of Measurements**

84 **2.2.1 Height retrieval over approximately planar surfaces**

85 Light from the ATLAS lasers reaches the earth’s surface as flat disks of down-traveling photons,
 86 approximately 50 cm in vertical extent, and spread over about 17 m horizontally. On land ice,
 87 photons are scattered once, or many times, by snow and ice grains, into every direction,
 88 including towards the satellite; a tiny fraction return to the ATLAS telescope’s focal plane, and a
 89 few of these are counted by the detector electronics and recorded as Photon Events (PEs). Over
 90 the vast majority of the earth’s land ice, the surface is smooth, with small (single-degree)
 91 variations in surface slopes at scales less than a few hundred meters. This allows us to
 92 approximate the surface profiles measured by ATLAS with short linear segments. We aggregate
 93 PEs received by ATLAS into 50% overlapping along-track segments of a fixed length (40 m),
 94 whose centers are 20 m apart. We then fit these PEs with sloping line segments; for each
 95 segment, we estimate both the along-track slope and the height at the center of the segment.
 96 When both beams in a pair provide height measurements, we also calculate the across-track
 97 slope for the pair. Any height variation not captured by this fitting process will be treated as
 98 surface roughness.

99 The time variation in surface height is determined by fitting a simple spatial function to the
 100 heights from multiple repeat measurements, and using this function to correct the measurements
 101 for the height variations caused by spatial sampling of sloped and curving surfaces. This
 102 function is fit to the subset of the repeat measurements that we assess to be of the highest quality,
 103 but corrected height estimates are provided for all available repeats, and data-quality metrics are
 104 provided to allow users to decide which heights to use.

105 **2.2.2 Effects of surface slope and roughness**

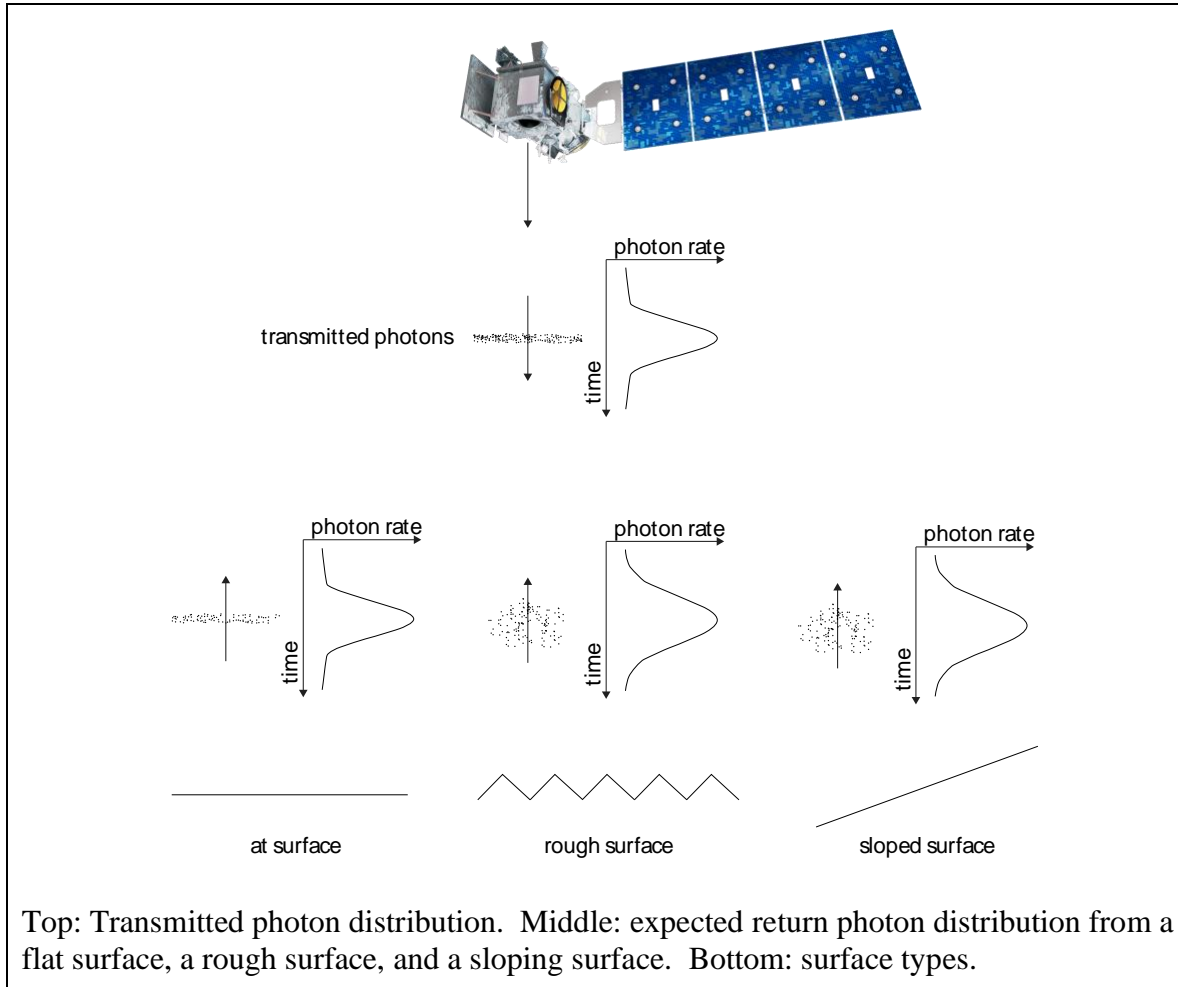
106 Figure 2-2 shows how slope and roughness contribute to the shape of the return pulse. For many
 107 areas of glaciers, the ground may be treated as a rough planar surface, and the laser pulse as
 108 having a Gaussian distribution in space, with intensity falling to $1/e^2$ of its peak value over a
 109 distance $W/2$. The laser pulses also have an approximate Gaussian distribution in time, with
 110 standard deviation σ_{tx} . If the incident beam is not parallel to the surface normal, photons from the
 111 edge of the footprint farthest from the satellite will be delayed relative to photons from the edge
 112 nearest the satellite. At the same time, a rough surface will yield early photons and late photons,
 113 further spreading the returned photons. If the angle between the beam and the surface normal is
 114 φ , and the surface height within the footprint has a Gaussian distribution with RMS deviation R
 115 relative to the plane of the surface, then the measured temporal distribution of the returned
 116 photons will be Gaussian as well (Yi & Bentley, 1999), with a temporal standard deviation equal
 117 to the quadratic sum of the spreads due to the transmitted pulse, the surface slope, and the
 118 roughness:

$$\sigma_R = \left[\sigma_{tx}^2 + \left(\frac{2\sigma_{beam}}{c} \tan\varphi \right)^2 + \left(\frac{2R}{c} \right)^2 \right]^{1/2} \quad 1$$

119 For ATLAS, σ_{beam} is expected to be around 4.25 m (one quarter of W), and σ_{tx} around 0.68 ns,
 120 corresponding to a FWHM (Full Width at Half Maximum) of 1.6 ns, so spreading due to sloping

121 surfaces will be smaller than the transmit-pulse duration for slopes up to approximately 1.3
 122 degrees.

Figure 2-2. Schematic of returns from different surface types



123 Surface roughness on a 17-m scale is likely to be small except in heavily crevassed glacier
 124 margins and in heavily channeled ablation zones. Although analysis of the return pulse shape
 125 does not allow us to distinguish the effects of roughness from those of slope, the geometry of
 126 ATLAS’s tracks, with pairs of beams separated by 90 m, allows estimates of the across-track
 127 slope at scales modestly larger than a single footprint, while the along-track component of the
 128 slope can be estimated from the along-track sequence of heights.

129 **2.2.3 Distinguishing return PEs and background PEs**

130 At the same time as signal photons are received by the ATLAS detector, background photons
 131 from sunlight are continually entering the telescope. Most of these are eliminated by filters that
 132 allow only photons with wavelengths close to the laser wavelengths through, but some pass these
 133 filters, and their timing is also recorded. The time distribution of the returned signal photons
 134 depends on the geometry and reflectance of the ice surface, and on scattering and attenuation in
 135 the atmosphere. We distinguish signal PEs from background PEs by their clustering in time.

136 Sunlight scattered from bright (*i.e.* snow-covered) surfaces will produce detected PEs at rates up
137 to around 12 MHz. For comparison, a return with as few as three PEs distributed over one half
138 meter of range produces a brief return rate of 900 MHz. Signal returns are also distinct from the
139 background because they are spatially contiguous, so that PEs will be clustered in time in a
140 consistent way from one shot to the next.

141 **2.3 Potential Errors**

142 Errors in ATLAS land-ice products can come from a variety of sources:

- 143 1) Sampling error: ATLAS height estimates are based on a random sampling of the surface
144 height distribution;
- 145 2) Background noise: Random-noise PEs are mixed with the signal PEs, so sampled PEs
146 will include random outliers;
- 147 3) Complex topography: The along-track linear fit and across-track polynomial fit do not
148 always resolve complex surface topography.
- 149 4) Misidentified PEs: The ATL03 product will not always identify the correct PEs as signal
150 PEs;
- 151 5) First-photon bias: This is an error inherent to photon-counting detectors that results in a
152 high bias in the mean detected PE height that depends on signal strength;
- 153 6) Atmospheric forward scattering: Photons traveling downward through a cloudy
154 atmosphere may be scattered through small angles but still be reflected by the surface
155 within the ATLAS field of view; these will be delayed, producing an apparently lower
156 surface;
- 157 7) Subsurface scattering: Photons may be scattered many times within ice or snow before
158 returning to the detector; these will be delayed, producing a surface estimate with a low
159 bias.

160 These errors are each treated in a different way during the ATL06 processing:

161 1) and 2) are treated as random errors, and their effects are quantified in the error estimates
162 associated with the products.

163 3) and 4) will produce relatively large errors, and will need to be addressed with consistency
164 checks on the data during the generation of higher-level products.

165 5) will be corrected routinely during ATL06 processing (see Section 3.0).

166 6) and 7) require information about cloud structure and ice-surface conditions that will not be
167 available at the time of processing of ATL06. Correcting for these errors remains an active
168 avenue for research.

169 **2.4 Land-ice Level-3 products: ATL06: Land-Ice Height**

170 The ATL06 product provides surface height estimates organized by reference -pair track (RPT),
171 in a format designed to facilitate comparison between different repeat measurements on the same
172 RPT. It also combines information from the two beams in each PT to give across-track slope
173 estimates. A variety of parameters are provided that indicate the quality of the surface-height
174 estimates and the signal and noise levels associated with the measurement. Note that in cycles 1

175 and 2 of the mission, ICESat-2 did not point at the RPTS, and ICESat2's pairs are offset by up to
176 2 km from the RPT locations. The first cycle that was collected over the RPTS was the third.

177 We define ATL06 heights based on fits of a linear model to ATL03 height data from short
178 (40 m) segments of the ground track, centered on reference points spaced at 20-m intervals
179 along-track. We refer to height estimates for these short segments as "segment heights", and
180 segment's horizontal location is that of the reference point, displaced in a direction perpendicular
181 to the RGT to match the GT offset. The choice of 40 m for the segment length provides data
182 from slightly more than two independent (non-overlapping) ATL03 heights (based on 17-m
183 footprints) for the along-track slope estimate, so that this component of the slope can be
184 eliminated as a cause of vertical scatter in the PE height distribution. The spacing between
185 reference points is 20 m, so that each segment overlaps its neighbors by 50%. Defining
186 overlapping segments in this way increases the chances that a segment will overlap a locally
187 smooth area within a crevasse field, potentially improving elevation-rate recovery in these areas.

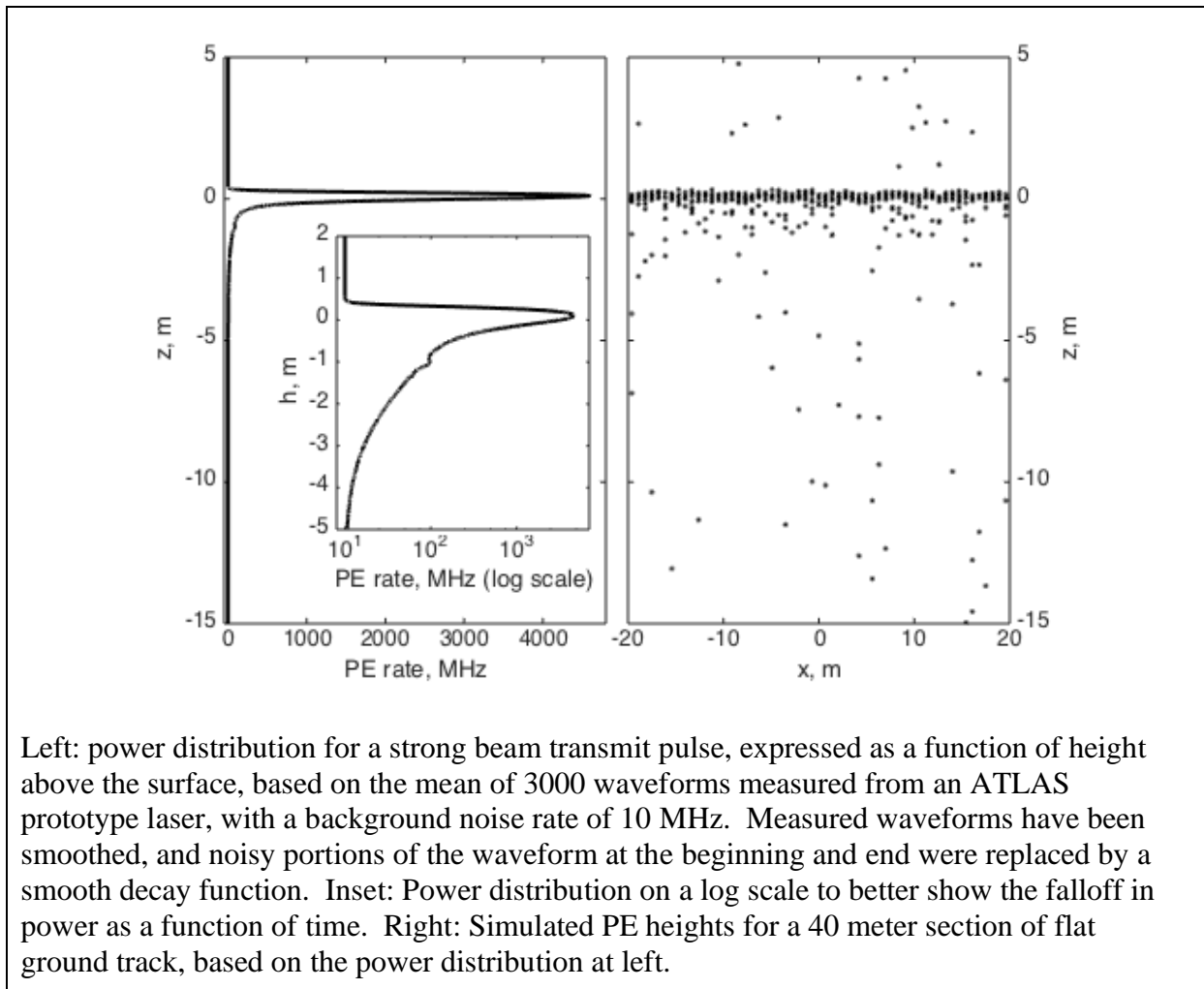
188 We use the same along-track sampling for both beams in each beam pair, and, for each cycle, use
189 the same reference point each time we calculate a segment height. This allows for direct
190 comparison between segment heights from the same RPT, without the need to interpolate in the
191 along-track direction. The ATL03 PE used for each segment can be determined by associating
192 the */gtxx/land_ice_segments/segment_id* parameter in ATL06 with the
193 */gtxx/geolocation/segment_id* parameter in ATL03: segment *m* in ATL06 includes PEs from
194 ATL03 segments *m-1* and *m* (here *xx* represents the ATLAS beam, with *gt1l* and *gt1r* providing
195 the left and right beams for pair 1).

196 A minimal representation of the data is given in datasets in the ATL06 product in the
197 */gtxx/land_ice_segments* groups. In these groups, we give the latitude, longitude, height, slope,
198 vertical error estimate, and a quality flag for each segment. This represents the minimum set of
199 parameters needed by most users; a wide variety of parameters describing the segment fit, the
200 input data, and the environmental conditions for the data are available in the subgroups within
201 the *gtxx* groups.

202 **3 ALGORITHM THEORY: DERIVATION OF ATL06 LAND ICE HEIGHT**
 203 **PARAMETERS**

204 In this section, we describe the ATL06 height derivation from lower-level ATLAS data
 205 (primarily the PE heights, locations, and times provided by ATL03). This process provides
 206 height estimates and segment geolocations for a set of points (called reference points) spaced
 207 every 20 m along each of ATLAS's pair tracks. One height is calculated for each beam in each
 208 pair, for each reference point, for each cycle of ICESat-2's orbit.

Figure 3-1. Surface return shape



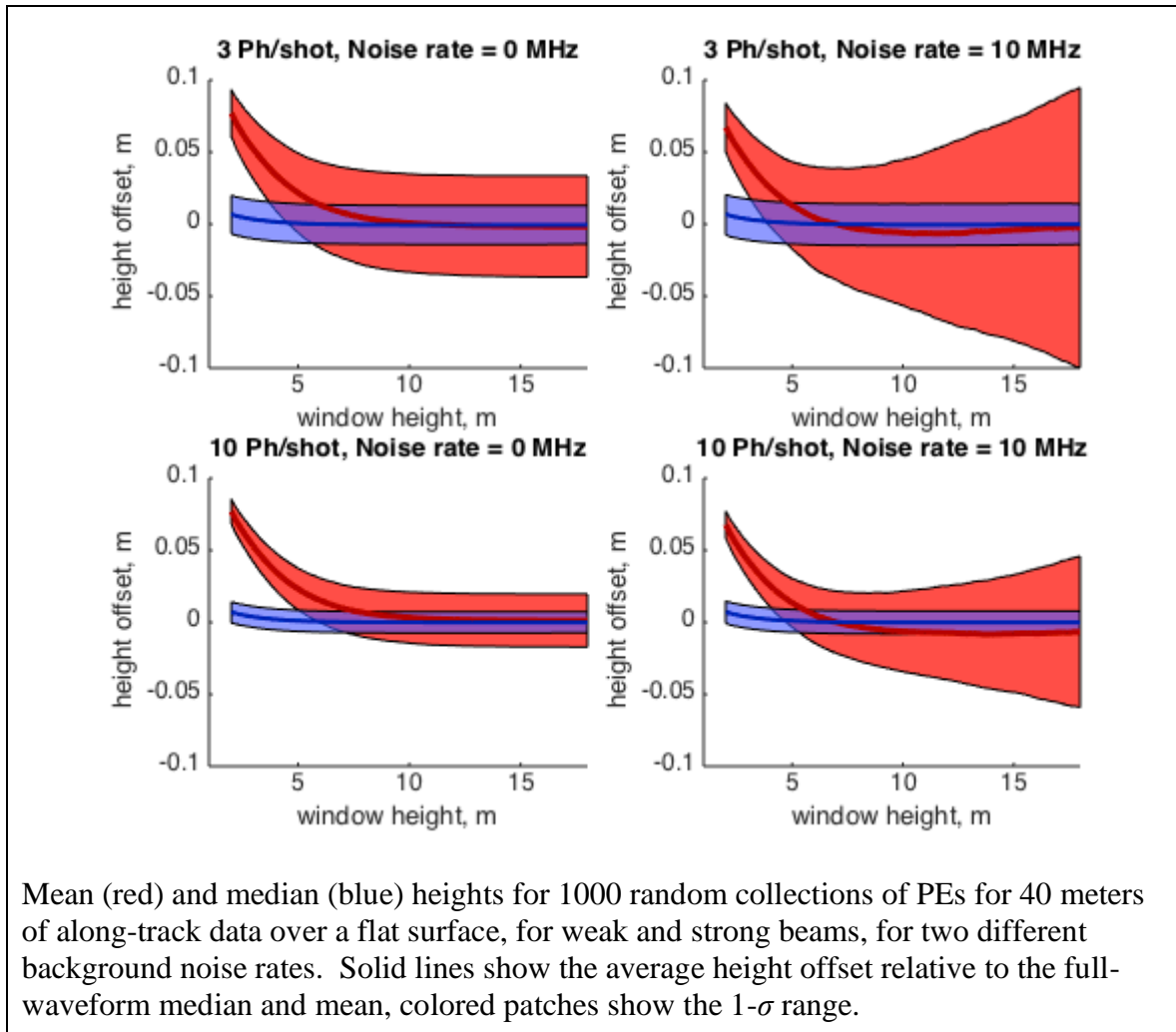
209 **1.1 Representation of the surface**

210

211 Figure 3-1 shows the expected surface-return power as a function of height above the surface,
 212 based on waveforms measured from a prototype ATLAS laser, for sunlit ice-sheet conditions
 213 with a background PE rate of 10 MHz, and a random set of photon heights generated based on

214 this waveform for a 40-meter along-track segment. The return has a sharp peak in power at the
 215 ground, but it is asymmetric, with a leading edge (on the +z side) that is sharper than the trailing
 216 edge (on the -z side), and with a long ‘tail’ of energy on the -z side caused by a slow decay in
 217 laser power at the end of the pulse. This produces a dense collection of PEs at the surface height,
 218 with scattered PEs above and below, some of which come from the sun and some of which come
 219 from the tail of the waveform.

Figure 3-2. Mean and median height biases



220

221 One way to characterize the surface height for this segment would be to calculate the mean of all
 222 PE heights within a pre-determined height range (the ‘surface window’). For simplicity, one
 223 might choose a large surface window of 10-20 m to ensure the capture of all return PEs.
 224 However, this choice would lead to significant noise and potential bias in the estimated surface
 225 heights. The noise would come about because the mean of a distribution of heights is sensitive to
 226 the extreme values of the distribution, so the photons at the edge of the distribution would
 227 produce sampling errors in the recovered heights. The bias could come about if the shape of the

228 transmit pulse were to change over time, because of temperature changes or because of aging of
229 the lasers. If this were to happen, the mean recovered surface height could change even if the
230 true surface height did not, again because the mean is sensitive to outlying data. Figure 3-2
231 shows the expected bias and scatter magnitudes as a function of the width of the surface window
232 for the means of 1000 random collections of PEs based on the waveform in Figure 3-1.
233 Selecting a small surface window results in a narrow (2 cm or less) scatter of values around the
234 mean, because the range of PE heights in the window is small. However, this leads to a 7-8 cm
235 bias in the surface height, because the tail of the distribution is cut off. Selecting a large surface
236 window leads to a small bias, but, particularly when background noise is large, it leads to scatter
237 in the surface heights, potentially as large as ± 10 cm.

238 We ameliorate this problem in two ways: First, we use an iterative process to select a small
239 surface window that includes the majority of the signal PEs but few background PEs. Second,
240 we express the surface height as the median of the PE heights within the surface window. We
241 select the median instead of the mean because it is less sensitive to sampling error for
242 distributions containing a uniform, ‘background’ component. Median height offsets shown in
243 Figure 3-1 have a spread of less than 2 cm, have maximum biases less than 7 mm, and are nearly
244 independent of the surface-window height. This represents a large improvement in accuracy and
245 precision over the mean, and further processing (discussed in 3.5) can correct for the remaining
246 bias in the median heights.

247 In the course of processing photon-counting data, we frequently need to estimate the spread of a
248 distribution of PE heights. For other types of data, we might choose to make this estimate based
249 on the standard deviation of the sample of heights, but because our measurements contain a
250 mixture of signal and noise PEs, the standard deviation often overestimates the spread of the
251 data. Instead, we generally use the RDE (Robust Dispersion Estimator), which is equal to half
252 the difference between the 16th and the 84th percentiles of a distribution. For Gaussian-
253 distributed data, this statistic is approximately equal to the standard deviation, and for data
254 containing a mixture of a large fraction of signal and a small fraction of noise, it can give an
255 estimate of the spread of the signal that is relatively insensitive to the noise. In some cases, we
256 use a version of this statistic that estimates the spread of the signal component of a distribution
257 that contains a mixture signal (Gaussian- or near-Gaussian-distributed) PEs and background
258 (uniformly distributed) PEs. In these cases, we estimate the 50th and 75th percentiles of the signal
259 component and scale the difference between these percentiles based on the expected width of
260 these percentiles for a Gaussian distribution. We refer to this measure as “robust spread
261 including background” and describe its implementation in section 5.

262 **3.1.1 Land-ice height definition**

263 The land-ice height is defined as estimated surface height of the segment center for each
264 reference point, using median-based statistics. We calculate this the sum of the least-squares
265 height fit, the first-photon-bias median correction, and the pulse-truncation median correction.
266 Height increment values on the product allow removal of the corrections and calculation of the
267 segment mean height, and first-photon-bias and pulse-truncation corrections appropriate to the
268 segment mean.

269

270 **3.2 Outline of processing**

271 The outline of the process is as follows for each cycle for each along-track point. First, heights
 272 and along-track slopes are calculated for each beam in each pair:

- 273 1. PEs from the current cycle falling into the along-track bin for the along-track point are
 274 collected (3.3)
- 275 2. The heights and surface windows are iteratively refined (3.3.5.2)
- 276 3. Corrections and error estimates are calculated based on the edited PEs. (3.4, 3.5, 3.6)

277 Once these steps are complete, based on the height values for the two beams,

- 278 4. The across-track slope is calculated (3.7)

279 Each of these steps is described in turn below.

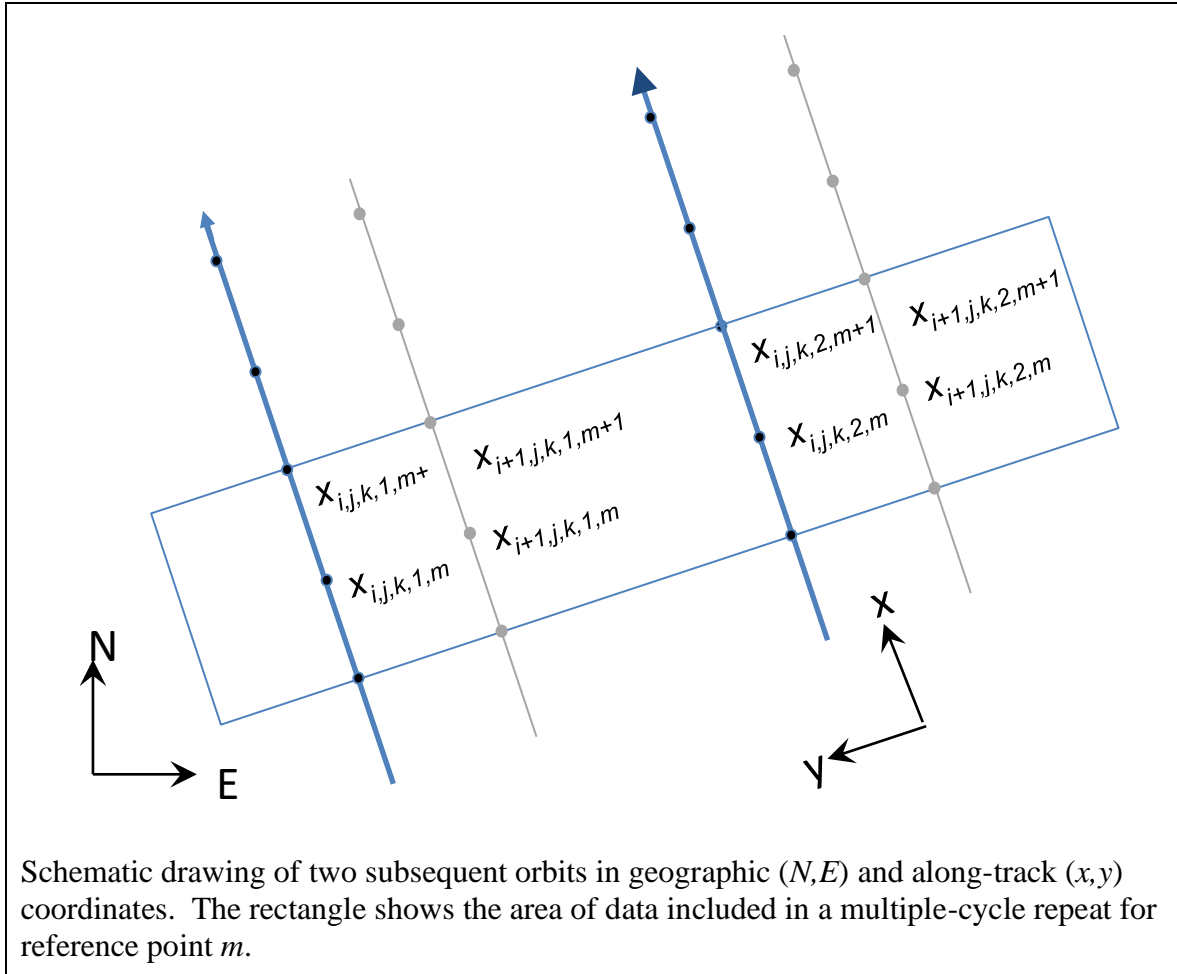
280 **3.3 PE selection**

281 ATL03 provides PE locations and timings for each beam. The first step in ATL06 processing is
 282 to select groups of PEs that determine the segment height at each along-track point. Processing
 283 is only carried out if the ATL03 *podppd_flag* indicates that the PE geolocation was of high
 284 quality for all pulses in the segment, otherwise the segment is skipped.

285 **3.3.1 Along-track segments**

286 Our height- and height-change schemes rely on dividing the data into repeatable along-track
 287 segments. We define these segments relative to the pre-defined RGT (see ATL06 Appendix A
 288 for definitions related to the ICESat-2 ground and reference tracks) and use them to select groups
 289 of PEs for each beam and each pass, and to define local coordinates relative to the RGT. We
 290 define a set of reference points, spaced every 20 m in the along-track coordinate x along the
 291 RGT, which specify the locations of the height estimates reported in ATL06. One set of
 292 reference points is defined for each RPT (Reference Pair Track). An ATL06 segment of data
 293 includes all PEs whose x coordinates are within approximately 20 m of that of a given reference
 294 point, for a total length of 40 m, so that each segment overlaps its neighbors by 50%. Each
 295 individual segment is fit with a least-squares model that gives the slope and height of the
 296 segment (Figure 3-3 and Section 3.1.2.4), and height corrections are derived based on the
 297 residuals to this model.

Figure 3-3. Reference point numbering schematic



298

299 Along-track segments are designated by five subscripts (Figure 3-3):

300 -i, the cycle number, numbered from the start of the mission;

301 -j, the track number, numbered consecutively within the cycle;

302 -k, the pair number, numbered from left to right across the satellite swath;

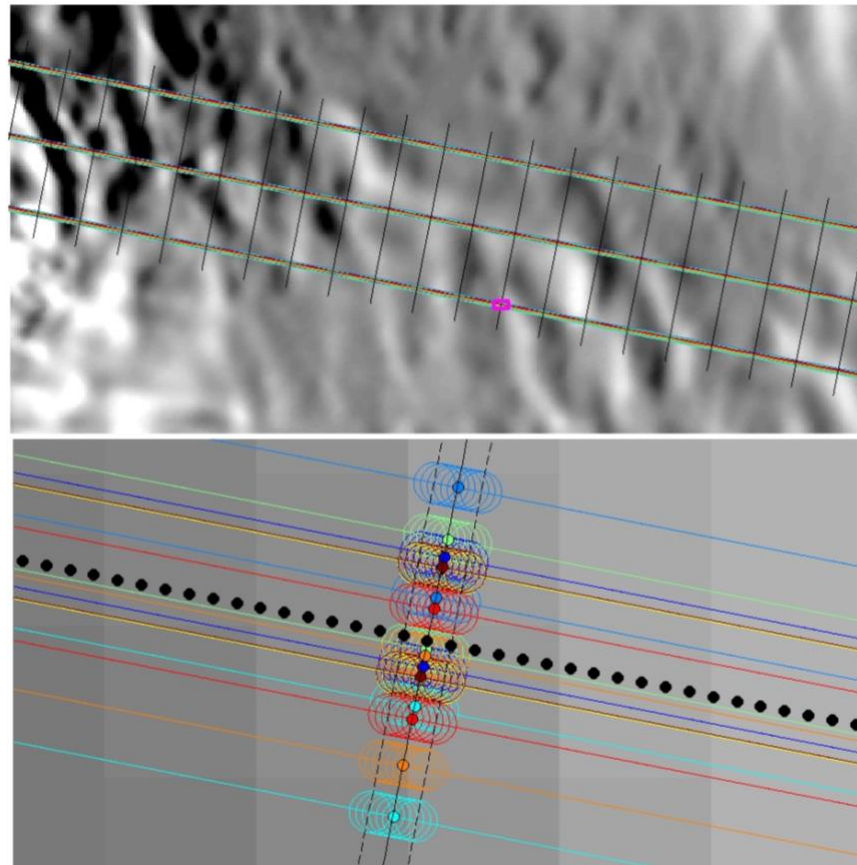
303 -l, the beam number within the pair, numbered from left to right;

304 -m, the reference point number, counted from the equator crossing of the RGT.

305 An along-track repeat measurement for a segment is made up of segments with the same j , k , and
 306 m , meaning that the track, the pair, and the along-track coordinates of the measurements are the

307 same. Each cycle, i , contributes measurements from two beams, with different l values, to the
 308 repeat; these different measurements allow the across-track slope to be constrained
 309 independently from the height change, and the along-track segment fitting procedure allows us to
 310 correct for the along-track slope. Both ATL03 and ATL06 use this segment numbering scheme;
 311 however, ATL06 segments are 40 m long and overlap their neighbors by 50%, while ATL03
 312 segments are 20 m long and are disjoint. ATL06 segments are defined as including PE from pairs
 313 of adjacent ATL03 segments, and are numbered to match the second of the two, so that ATL06

Figure 3-4. Example PE selection



Selecting PEs for a reference point. Top: GT locations for eight simulated repeat measurement of track 188 (colored lines). Black lines are plotted every 2 km in the along-track coordinate x . Bottom: selected footprint locations for a reference point on PT 3 (circles, every 10th shown). Lines and circles are color coded by repeat. Solid points show reference-point locations, dashed lines show the 40-m along-track extent of the segments, filled circles show segment centers. Background image from (Scambos and others, 2007)

314 segment m includes ATL03 segments m and $m-1$.

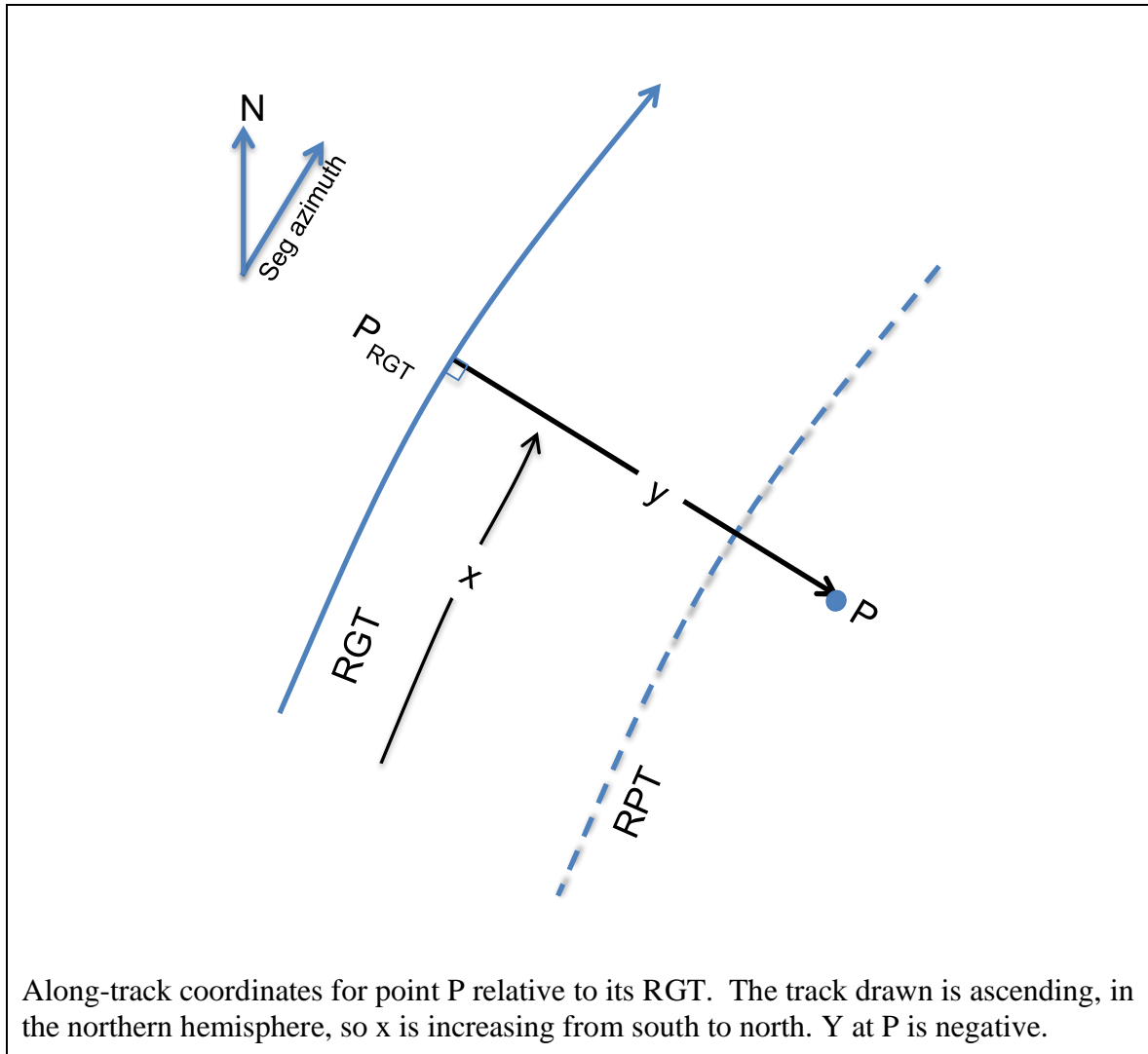
315 **3.3.2 Local Coordinate Systems**

316 To select the PEs associated with each reference point, the height data are grouped in local
 317 coordinates. The local coordinate system is defined in the ATL03G ATBD. Briefly, the
 318 coordinate system is defined separately for each RGT with an x coordinate that follows the RGT,
 319 starting at its equator crossing going north. The y coordinate is measured perpendicular to the x
 320 coordinate and is positive to the left. Thus, the x coordinate runs from zero to around forty
 321 thousand km for each track, the y coordinate runs from approximately -3.3 km for the right beam
 322 pair to approximately 3.3 km for the left beam pair, although its values may be larger if ATLAS
 323 is pointed off nadir.

324 To calculate along-track coordinates for any point P adjacent to an RGT, we define the x
 325 coordinate to be equal to the x coordinate of the nearest point on the RGT, P_{RGT} . The y
 326 coordinate is equal the distance between P and P_{RGT} , measured to the left of the along-track
 327 direction (Figure 3-5). This calculation is carried out for each PE in ATL03: The x coordinate
 328 for each PE is equal to the sum of the ATL03 parameters */geolocation/segment_dist_x* and
 329 */heights/dist_ph_along*. The y coordinate is equal to the ATL03 *dist_ph_across* parameter. Our
 330 reference points are defined to be equal to the start of the first ATL03 segment, so that ATL06
 331 segment m encompasses all PE from ATL03 segments $m-1$ and m .

332

Figure 3-5. RGT coordinates



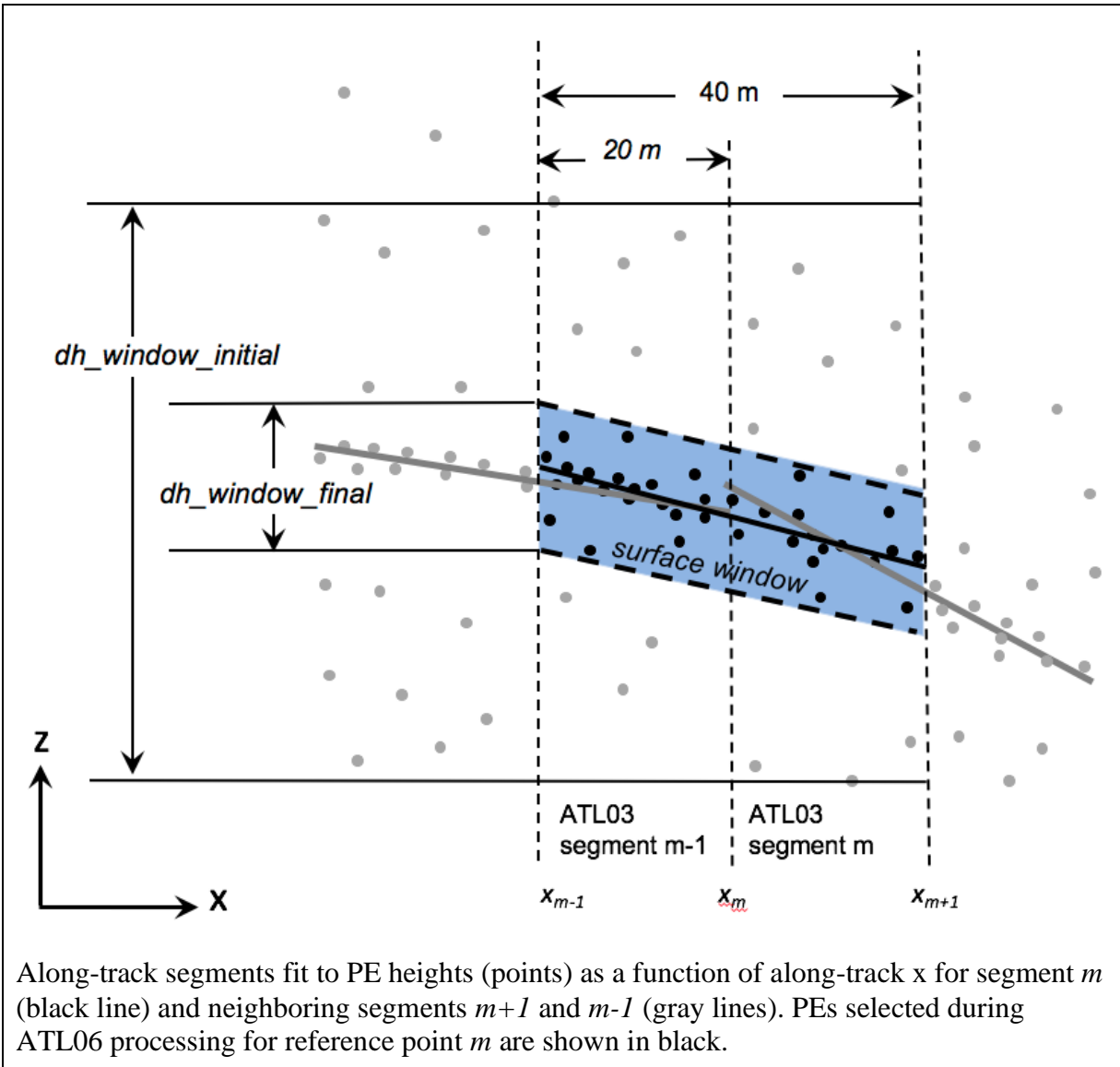
333

334 The AL06 along-track coordinate for each segment is given by the parameter x_{atc} . The across-
 335 track coordinate is given by y_{atc} , and the angle between the along-track vector and local north
 336 is given in the parameter $seg_azimuth$. To allow easy referencing between ATL06 and ATL03,
 337 we provide the number for the second ATL03 segment in each ATL06 segment in the variable
 338 $segment_id$.

339 3.3.3 Parameters describing selected PEs

340 ATL06 heights and slopes are estimated by piecewise-linear fits to PEs within each overlapping
 341 40-m segment. Since ATL06 segments are 40-meters long and overlap by 50%, we can collect
 342 the photons for each segment, m , by selecting all ATL03 PE that have $segment_id$ equal to $m-1$
 343 or m .

Figure 3-6 Segment fitting



344

345 The initial PE selection is shown in Figure 3-6. ATL03 data give a ground-finding confidence
 346 flag that indicates whether each PE was detected high confidence (SNR > 100, flag value of 4),
 347 medium (100 < SNR < 40, flag value of 3) low confidence (SNR < 40, yet still passes threshold
 348 test, flag value of 2), or is included because it falls within 10m of the detected surface (flag value
 349 of 1).

350 An initial surface window is valid if it contains at least 10 PE, and if the along-track distance
 351 between the first and last PE is greater than 20 m. This ensures that there are enough PE to
 352 determine both the height and slope of the segment. We define three possible sources for signal-
 353 selection data:

- 354 1. ATL03 confident PE ($signal_selection_source=0$): PE with $confidence_flag$ values > 1
 355 (low or better confidence)

- 356 2. All ATL03 detected PE (*signal_selection_source=1*): PE with *confidence_flag* flag
 357 values ≥ 1 (including low or better, and pad PE).
 358 3. A backup signal-finding algorithm (*signal_selection_source=2*)

359 3.3.3.1 Setting the surface window based on ATL03 flagged PE.

360 If sources 1 or 2 define a valid surface window, we calculate the slope of that window using an
 361 initial least-squares fit to h as a function of x for the flagged PE. Based on the slope of this
 362 window, we calculate *sigma_expected* using equation 1, and calculate the robust spread of the
 363 residuals for the flagged PE (correcting for the background PE rate), *r_flagged*. If ATL03
 364 confident PE define a window (case 1), the minimum surface window size, w_{min} , is set to 3 m,
 365 and if ATL03 confident PE do not define a window but the combination of ATL03 detected and
 366 pad PE do (case 2), w_{min} is set to 10 m. The initial surface window, *w_surface_window_initial*
 367 is then set to $\max(w_{min}, 6 \sigma_{expected}, 6 r_{flagged})$. The residuals for all of the segment PE
 368 are then calculated, and PE with residuals within $\pm w_{surface_window_initial}/2$ are selected and
 369 passed on to the iterative along-track fitting.

370 3.3.3.2 Setting the surface window using the backup signal-finding algorithm

371 If any ATL03 PE are detected but they do not define a window or if no ATL03 PE are present, a
 372 backup algorithm is used. First, if any ATL03-flagged PE are present, the along-track slope of
 373 the initial window is set to zero, its width is set to 10 m, and it is centered vertically on the mean
 374 height of the flagged PE. If the PE within this window fail the along-track-spread test or the ten-
 375 PE test, then PE within 40 m along track of the reference point are examined to find the 10-
 376 meter-high by 80-meter-long window, centered on the reference point, containing the largest
 377 number of PE. Typically, there will be a range of center heights whose PE counts are not
 378 significantly different from the maximum; if the maximum count is C_{max} , then any window with
 379 a count greater than $C_{max} - C_{max}^{1/2}$ will be included. The initial window will extend from 5 m
 380 below the minimum of these centers to 5 m above the top of these centers, and its length is set to
 381 40 m. If this best window does not contain a good distribution of PE (i.e. more than 10 PE, with
 382 a horizontal spread greater than 20 m), the segment is considered invalid. If C_{max} is less than 16
 383 (the number of PE that would be detected in an 80-meter long window with a signal strength of
 384 10 PE/40 m, minus one standard deviation), no PE are selected, and the signal selection is
 385 marked as invalid.

Table 3-1 *signal_selection_source* values

Value	Meaning
0	Signal selection succeeded using ATL03 confident-or-better flagged PE
1	Signal selection failed using ATL03 confident-or-better flagged PE but succeeded using all flagged ATL03 PE

2	Signal selection failed using all flagged ATL03 PE, but succeeded using the backup algorithm
3	All signal-finding strategies failed.

386
 387 The *signal_selection_source* parameter describes the success or failure of each step in this
 388 process, and Table 3-1 describes the meaning of each value. For each signal-selection algorithm
 389 that was attempted, the *signal_selection_status_confident*, *signal_selection_status_all*, and
 390 *signal_selection_status_backup* parameters in the *segment_quality* group give details of the
 391 success or failure of each part of the algorithm. The *signal_selection_source* parameter is
 392 provided for all segments (successful or not) in the *segment_quality* group, and is provided for
 393 segments for which at least one pair has an elevation in the *fit_statistics* subgroup.

Table 3-2 Status parameters for signal-selection algorithms

<i>Signal_selection_status_confident</i>	
0	Signal selection succeeded using ATL03 low-or-better confidence PEs
1	Signal selection using ATL03 low-or-better confidence PEs failed the 20-meter-spread test
2	Signal selection using ATL03 low-or-better confidence PEs failed the 10-photon-count test
3	Signal selection using ATL03 low-or-better confidence PEs failed both tests
<i>Signal_selection_status_all</i>	
0	Signal selection succeeded using all ATL03 flagged PEs (or algorithm not attempted)
1	Signal selection using all ATL03 flagged PEs failed the 20-meter-spread test
2	Signal selection using all ATL03 flagged PEs failed the 10-photon-count test
3	Signal selection using all ATL03 flagged PEs failed both tests

<i>Signal_selection_status_backup</i>	
0	Signal selection succeeded using the backup signal finder after centering the window on flagged PE (or backup signal finder not attempted)
1	Signal selection succeeded using the backup signal finder after searching for the strongest-signal window using four adjacent ATL03 segments
2	Signal selection using the backup signal finder failed the 20-meter-spread test
3	Signal selection using the backup signal finder failed the 10-photon-count test
4	Signal selection using the backup signal finder failed both tests

394

395 The final, refined window is described in the *fit_statistics* subgroups. The height of the window
 396 is given as *dh_window_final*, and the number of pulses that might contribute PE to the ATL06
 397 segment is given in the *n_seg_pulses* parameter. Note that not all of the pulses in the segment
 398 necessarily contribute to the received PEs if the signal strength is low. We calculate
 399 *n_seg_pulses* based on the speed of the nadir point, v_{nadir} , of the spacecraft along the ground
 400 track, the pulse repetition frequency, and the nominal 40-m length of the ATL06 segment:
 401 $N_{seg_pulses} = PRF \times 40 \text{ m} / v_{nadir}$. This parameter has non-integer values, because it is intended
 402 to represent the expected number of pulses in each segment. There is no straightforward way to
 403 determine exactly which pulses might have targeted a particular ground segment.

404 **3.3.4 Handling of invalid segments**

405 Segments must pass a series of tests before their elevations are reported in the ATL06
 406 *gtxx/land_ice_segments* groups. The signal selection routines must return at least 10 PE, spread
 407 over at least 20 m. Fitting does not proceed if these criteria are not met. For segments that
 408 continue to the surface window refinement routine, after the surface window refinement is
 409 complete, the final PE count and surface-window height are checked against the *snr_significance*
 410 parameter, to ensure that the probability of the measured signal-to-noise ration resulting from a
 411 random signal selection is small. Only segments with *snr_significance* < 0.05 (indicating that,
 412 given a random-noise input, the algorithm would converge to the calculated SNR less than 5% of
 413 the time) proceed to the next stage.

414 These criteria allow a significant number of low-quality segment heights to be reported in
 415 ATL06. This intended for the benefit of users who need to measure surface heights under
 416 marginal conditions. To help other users remove these segments, the

417 *land_ice_segments/ATL06_quality_summary* parameter gives a synopsis of the parameters
 418 relevant to segment quality (Table 4-3), any one of which could indicate unusable data. The
 419 subset of segments with *ATL06_quality_summary* = 0 are unlikely to contain blunders due to
 420 signal-finding errors. This choice of parameters may reject useful elevations collected over
 421 rough, strongly sloping, or low-reflectivity surfaces and under clouds so obtain more height
 422 estimates, users may need to examine additional parameters in ATL06, or regenerate a similar
 423 flag for themselves based on a less-stringent set of parameters.

424 A variety of data flags are available to indicate why a particular segment does not have a
 425 reported height parameter. In many cases, the strong-beam segment in a pair will have a
 426 reported height, and the weak beam will not; in these cases, a full record is available for the
 427 weak-beam segment, providing all parameters up to the step where the fitting process failed. In
 428 cases where neither the strong nor the weak beam returned a surface height, the *segment_quality*
 429 group provides the *signal_selection_source* parameter, which will show a value of 3 if all signal-
 430 selection strategies failed. Only in cases where both segments passed the signal-selection tests
 431 but did not pass the *snr_significance* < 0.05 test will there be an entry in *segment_quality* and no
 432 entry in the remainder of the ATL06 records.

433

434 Users wishing to apply more- or less-stringent criteria to the data than those described above can
 435 examine the refined surface window width *fit_statistics/w_surface_window_final*, the signal-to-
 436 noise ratio, *fit_statistics/snr*, the range-based-error parameter, *land_ice_segments/h_li_sigma* and
 437 the uncorrected reflectance, *r_eff*, to ensure that they are within expected ranges.

438 3.3.5 Surface-window refinement and least-squares height estimate

439 The ATL06 ground-finding algorithm refines the ATL03 surface detection estimate by iterative
 440 fitting of the initially-selected ATL03 PEs with the along-track segment model, rejecting PEs
 441 with large residuals to the model at each step (3.3.5.2). After the iterations are terminated, the
 442 final model height, based on this fit, *h_mean*, is used as an input to the next stage of the
 443 algorithm, in which the model residuals are used to derive corrections to the model height.

444 3.3.5.1 Least-squares fitting

445 For each segment, we first calculate a least-squares best-fitting segment to the initially selected
 446 ATL03 PEs, then use an iterative procedure based on the least-squares fit to refine this window.
 447 Each time we perform the least-squares fit, we construct a design matrix, \mathbf{G}_0 , from the vector \mathbf{x} ,
 448 of along-track coordinates for the selected PEs:

$$\mathbf{G}_0 = [1 \ \mathbf{x}] \quad 2$$

449 The segment height and along-track slope are calculated based on \mathbf{G}_0 and the vector of ATL03
 450 heights, \mathbf{h} , as:

$$[h_{fit}, \frac{dh}{dx}] = (\mathbf{G}_0^T \mathbf{G}_0)^{-1} \mathbf{G}_0^T \mathbf{h} \quad 3$$

451 The residuals to this model are then calculated:

$$r_o = h - \mathbf{G}_0 [h_{fit}, \frac{dh}{dx}] \quad 4$$

452

453 3.3.5.2 Iterative ground-window refinement

454 The initial surface window height may be as large as 20 meters from top to bottom, larger in
 455 rough terrain or when the signal-to-noise ratio is small. This means that it may include many
 456 noise PEs mixed with the signal PEs. If included in the calculation, these will lead to large
 457 random errors in the surface slope and height. We can increase the proportion of signal PEs by
 458 shrinking the surface window, but need to avoid shrinking it so much that we lose signal PEs.
 459 To do this, we seek to find a window centered on the median height of the surface-return PEs,
 460 whose height is three times the spread of the surface PE height residuals. Because the spread and
 461 the median of the surface PEs are not initially known, we use an iterative procedure to shrink the
 462 size of the surface window, estimating the median and spread at each step.

463 We have two ways of calculating a value for the spread of the surface return, which we combine
 464 as part of our calculation of the width of the surface window. The first is to predict the RMS
 465 spread of the surface return using an initial estimate of the surface-slope vector and Equation 1 to
 466 give *h_expected_RMS*, assuming zero roughness. The second is to calculate it based on the
 467 spread of the residuals to the current model, σ_o . In low-signal-to-noise conditions, we include a
 468 correction for the background signal level in this calculation (described in 3.11). Since either of
 469 these might provide a good estimate of the spread of the surface PEs we take the maximum of
 470 these two values as our spread estimate. To avoid excessive trimming, we eliminate PEs only if
 471 their residual magnitude is greater than the maximum of 1.5 m and three times our spread
 472 estimate.

473 We initialize the iterative procedure with the PE selection described in the previous two sections.
 474 In cases where the signal selection was initialized with flagged PE (*signal_selection_source=0*
 475 *or 1*), the iterative ground-window refinement is forced to use only PE included in the initial
 476 selection. In all other cases, iterations after the first may include PE that were not included in the
 477 initial selection, so the window may expand or migrate as iterations progress. In either case the
 478 PE that might be selected are the *selectable* PE.

479 At each step, we

- 480 a) Perform a least-squares fit to the currently selected PEs using equation 3, giving a current
 481 model estimate, $[h_{mean}, dh/dx]$ and residuals to the model, r .
- 482 b) Calculate the median and background-corrected RDE (see 3.11) of the distribution of the
 483 residuals for the selected PEs, r_{med} and σ_o , and update *h_expected_RMS* based on the
 484 current dh/dx estimate. The residual spread (σ_o) is limited to a maximum value of 5 m.
- 485 c) Calculate the residuals of all of the *selectable* PEs to the current model estimate, r .

486 d) Select PEs from among the *selectable* PEs for which $|r-r_{med}| < H_window/2$, where
 487 $H_window = \max(6 \sigma_o, 6 h_expected_RMS, 0.75 H_window_last, 3 \text{ m})$.

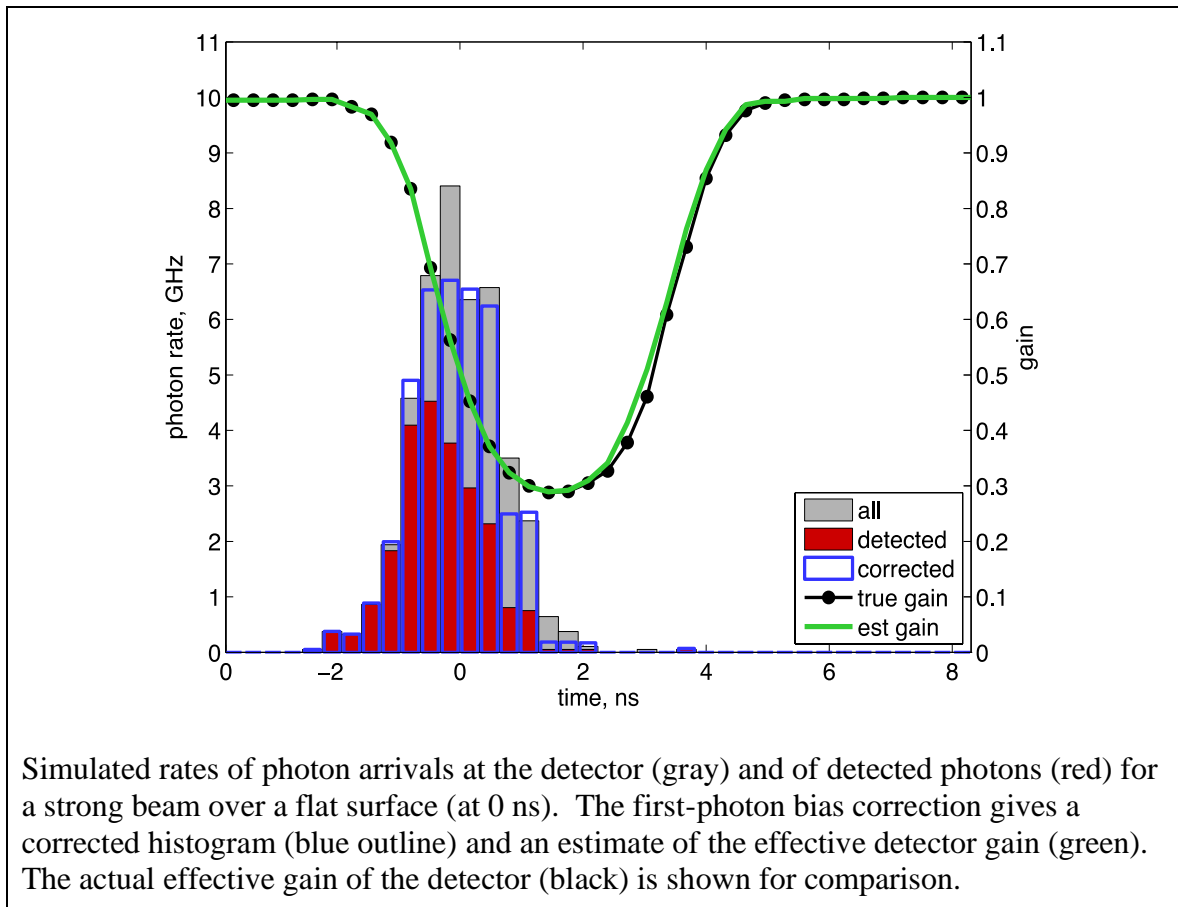
488 The iterations are terminated if no further PEs are eliminated in a given step. If a given iteration
 489 eliminates PE such that the selected PE no longer define a window, then that step is reversed,
 490 and the iterations are terminated. The inclusion of $0.75 H_window_last$ as the minimum size of
 491 the window in each step of the calculation attempts to ensure that the calculation does not
 492 converge too fast to a spurious value of h_mean .

493

494 The window width after the final step is reported as $w_surface_window_final$, and the number of
 495 PEs in the window is reported as $n_fit_photons$. The final slope of the along-track segment is
 496 reported as dh_fit_dx . The median residual to the along-track fit is given in the parameter
 497 med_r_fit , and is used to convert between a mean-based height estimate for each segment and a
 498 median-based estimate.

499 **3.4 First-Photon Bias**

Figure 3-7. First-photon bias correction



500

501 The first-photon bias (FPB) results from an inherent problem with the photon-counting detectors
 502 selected for ATLAS. For a short time, t_{dead} , after an individual pixel of each detector detects a
 503 photon, it cannot detect another. This means that photons early in a ground return are more
 504 likely to be detected than those later on, and, for a symmetric return-photon distribution, the
 505 mean surface height estimate is biased upwards, an effect that is largest for more intense pulses
 506 and for pulses from flat surfaces where the return energy is concentrated in a short period of
 507 time. Note that for ATLAS's asymmetric transmit pulse, the first-photon bias may result in either
 508 positive or negative height errors, because for small roughness values, the FPB suppresses
 509 detection the early, intense part of the waveform, while the tail of the waveform is unaffected,
 510 resulting in a negative height bias. For larger roughness values, FPB affects the tail and the peak
 511 more equally, and the bias becomes positive. For clarity, we will describe modeling results using
 512 a simulated symmetric Gaussian transmit pulse, but the corrections provided on the ATL06
 513 products may have either positive or negative signs.

514 For ATLAS, t_{dead} is quite short, at approximately 3.2 ns, and there are multiple pixels in each
 515 detector (16 for the strong beams, 4 for the weak), to which photons are assigned at random as
 516 they reach the detector, resulting in fewer photons reaching each pixel while it is inactive.
 517 Despite this, up to several cm of bias may be observed for flat bright surfaces. Figure 3-7 shows
 518 simulated instantaneous photon rates for photons incident on the detector, and of detected
 519 photons for returns from a flat, smooth surface for a strong spot, under moderately saturated
 520 conditions (1.2 photons per pixel per pulse), aggregated over 40 m. Background PE are not
 521 included in the simulation, but their effect is likely to be minor, because their contribution to the
 522 total PE count is, in strong-signal conditions, a small fraction of the total, and the correction is
 523 negligible if the signal is not strong.

524 We have found that we can generate a correction for the first-photon bias based on a model of
 525 the detector for PEs aggregated over a 40-m ground-track segment. In this algorithm, we
 526 generate a histogram representing the distribution of heights around the ground return for the
 527 segment, as represented by the histogram of PE residuals to the best-fitting sloping segment
 528 model. We then estimate the effective gain of the detector, a function that represents the
 529 probability that a photon would have been detected if it reached the detector. We use this
 530 function to correct the received histogram to an estimate of the histogram of all the photons,
 531 detected and undetected. Statistics of this histogram are used to improve estimates of the
 532 surface height.

533 Using the residuals to the best-fitting segment in this calculation assumes that each pulse
 534 experiences the same distribution of photon-arrival times, shifted in time by the along-track
 535 surface slope, so that a typical distribution can be found by correcting for the along-track slope.
 536 If the surface slope or the reflectance has strong variations within a segment this assumption will
 537 fail, but for segments where the correction is large (i.e., in the interior of the ice sheets), it should
 538 not introduce large errors because ice-sheet surfaces are typically very homogeneous.

539 3.4.1 Mathematical Description for the First-Photon Bias

540 The photon distribution incident on the detectors is written as a function of $t_i - t_g$, where t_i is the
 541 PE time and t_{gi} is the time of the ground return. In practice, this is calculated as $t_i - t_{gi} = -r c/2$,

542 where r is the height residual to the best-fitting segment. We can express the histogram over N
 543 PE times as:

$$N(t; t_i - t_{gi}) = \sum_{i=1:N} \sum_{t_i - t_{gi} \in (t, t + \Delta t]} 1 \quad 5$$

544 Only some of these photons are detected: After a photon hits a detector, that detector cannot
 545 detect another photon until it becomes active, after receiving no photons for a time t_{dead} . This can
 546 be expressed by a function giving the status of each pixel for each pulse at time t :

$$A(t, p, pixel) = \begin{cases} 1 & \text{if pixel is active at time } t \text{ for pulse } p \\ 0 & \text{if pixel is inactive at time } t \text{ for pulse } p \end{cases} \quad 6$$

547 The detected photon distribution is then:

$$N_d(t; t - t_g) = \sum_{i=1:N} \sum_{t_i - t_{gi} \in (t, t + \Delta t]} A(t_i - t_{gi}, pixel_i, P_i) \quad 7$$

548 If the photon distribution in $t - t_g$ is constant over the pulses and over all pixels, then we can write:

$$N_d(t - t_g; \Delta t) = G(t - t_g) N(t - t_g; \Delta t) \quad 8$$

549 Where:

$$G(t - t_g) = \frac{1}{N_{pulses} N_{pixels}} \sum_{pulses, pixels} A(t - t_g) \quad 9$$

550 This function is effectively a gain for this collection of pulses. It ranges between zero, when all
 551 pixels are inactive, and one, when all pixels are active. The detector gain is shown by the black
 552 line in Figure 3-7. It falls rapidly from unity to about 0.3 during the early part of the surface
 553 return, then recovers gradually over a period slightly longer than t_{dead} , about 3.2 ns.

554 3.4.2 Correction Formulation for the First-Photon Bias

555 We implement the gain correction based on channel dead-time estimates from ATL03 and a
 556 histogram of residual times relative to the best-fitting segment model from 3.3.5.2, truncated by
 557 $\pm h_window_final/2$. We represent the deadtime for the detector with the mean deadtime for all
 558 channels in the detector, and assume that all pixels (and channels) have identical sensitivity.
 559 Although the algorithm's function does not depend strongly on the spacing of the histogram bins,
 560 our test software has used a bin spacing of 0.05 ns. We express the timing for the correction as a
 561 function of time relative to the ground-return time, under the assumption that for an entire
 562 segment, the return shape will be consistent relative to the ground-return time:

$$\tau = t - t_g \quad 10$$

563 Our strategy in this calculation is to correct an initial histogram of PE arrivals for the effects of
 564 detector dead time ($G < 1$) by dividing $N_d(\tau)$ by $G(\tau)$:

$$N_{est}(\tau; \Delta t) = \frac{1}{G(\tau)} N_d(\tau, \Delta t) \quad 11$$

565 To correct waveforms for the effects of dead time, we can use an *a posteriori* estimate of $G(\tau)$
 566 calculated with a simple model of the detector. In this model, we calculate a detected
 567 distribution, N_d , as the histogram of PE arrivals relative to the ground bin for a single-segment
 568 (40 m) section of track. For each bin in the histogram, we then determine the average number of
 569 pixels in the detector that were inactive. This is calculated:

$$P_{dead}(\tau) = \frac{\text{number of photons in } [\tau - t_{dead}, \tau)}{N_{pix} N_{pulses}} \quad 12$$

570

571 The estimated gain is then $1 - P_{dead}$. This calculation can be carried out efficiently by convolving
 572 the histogram of residuals with a rectangular window of height $1/N_{pix}N_{pulses}$, and shifting the
 573 result by the width of the window.

574 For our simulated example (in Figure 3-7) the recovered gain (green) is approximately equal to
 575 the true detector gain; this example is fairly typical of other simulations of this process, where
 576 the estimated gain is usually within a few percent of the true gain. There are visible differences
 577 between the corrected photon-timing histogram (blue) and the incident photon histogram, but the
 578 effects of these variations on the recovered heights are relatively small and have approximately
 579 zero bias.

580 3.4.3 Statistics Derived from the First-Photon-Bias Correction

581 The output of the gain estimation is a corrected histogram of height differences relative to a
 582 reference surface. Statistics of this histogram (e.g. its vertical centroid, its median) can be
 583 calculated as they would for the uncorrected PE heights. Since these statistics are calculated on
 584 the histogram of uncorrected photon residuals, their values give the correction relative to the
 585 mean of the PE heights. Thus, to calculate the corrected mean or median surface height, we add
 586 the gain-corrected mean or median of the residuals, respectively, to the uncorrected mean height.
 587 Because we expect the transmitted pulse to be skewed, we expect the median height correction to
 588 be much larger than the mean height correction.

589

590 3.4.3.1 Mean Height Correction

591 The mean height correction based on the corrected histogram is:

$$fpb_mean_corr = \sum \frac{N_{corr,i}}{N_{tot}} dz_i \quad 13$$

592 Here dz_i are the bin centers of the histogram of the PE residuals (i.e. the difference between the
 593 PE heights and the linear segment fit. The error in the mean correction is found using the error
 594 propagation formula for a centroid, assuming that the measured PE counts are Poisson
 595 distributed and ignoring the error in the gain estimate. For each bin in the corrected histogram,
 596 the corrected count at that bin has an error:

$$\sigma_{N,corr,i} = \frac{N_{0,i}^{1/2}}{G_i} \quad 14$$

597 The error in the mean height based on the corrected counts is then:

$$\sigma_{f_{pb-corr}} = \left[\sum \left(\sigma_{N,corr,i} \frac{dz_i - f_{pb-corr}}{N_{corr,tot}} \right)^2 \right]^{1/2} \quad 15$$

598 3.4.3.2 Median Height Correction

599 The median correction and its error are calculated from the CDF (Cumulative Distribution
 600 Function) of the corrected histogram as a function of dz :

$$CDF(dz_0) = \sum_{dz_i < dz_0} \frac{N_{corr,i}}{N_{corr,tot}} \quad 16$$

601 The median of the corrected histogram is found by interpolating into dz as a function of $CDF(dz)$
 602 at an abscissa value of 0.5:

$$median\ f_{pb} = CDF^{-1}(0.5) \quad 17$$

603 Because CDF is a function of the residuals to the linear segment-fit model, the median calculated
 604 in this way gives an offset relative to h_mean .

605 The uncertainty of the median interpolated from the CDF is the slope of the inverse function of
 606 $CDF(dz)$ with respect to CDF times the statistical uncertainty in the CDF at the median point:

$$\sigma_{med} = \left. \frac{dz}{dCDF} \right|_{CDF=0.5} \sigma_{CDF}(h_{med}) \quad 18$$

607 The statistical uncertainty in the CDF achieves half its total variance at the median, so we can
 608 calculate its uncertainty at the median as:

$$\sigma_{cdf}(dz_{med}) = \left[\frac{1}{2} \sum \frac{\sigma_{N,corr,i}^2}{N_{tot,corr}^2} \right]^{1/2} \quad 19$$

609 We estimate the slope of the CDF based on the 60th and 40th percentiles of dz, calculated from
 610 the CDF of dz, and noting that 20% of the residuals should fall within this range. The error in
 611 the median correction is then:

$$fpb_md_corr_sigma = \frac{dz_{60} - dz_{40}}{0.2} \sigma_{cdf}(dz_{med}) \quad 20$$

612 For both the mean and the median corrections, the error calculated in this way gives the total
 613 error in the surface height due to the Poisson sampling in the data. It does not take into account
 614 the effects of the along-track distribution of the photons, as the propagated least-squares error
 615 (equation 19) does, so the error in the final, corrected height measurement (*h_li_sigma*) is the
 616 maximum of *sigma_h_mean* and *fpb_med_corr_sigma*. Note that neither the combined error nor
 617 the median error calculated above are rigorous estimates of the error guaranteed to work under
 618 all circumstances. However, numerical experiments have shown that these error estimates match
 619 the RMS spread of recovered values to within ~10% for numbers of PEs greater than ~20. For
 620 smaller numbers of PE, the error estimates may be up to 20% too small.

621 3.4.3.3 Corrected Return Count

622 The corrected number of returned photons is calculated:

$$fpb_{N_photons} = \sum N_{corr} \quad 21$$

623 This sum is carried out over the ground window calculated during ground-bin refinement
 624 (3.3.5.2). This is similar to the dead-time correction on ATL03.

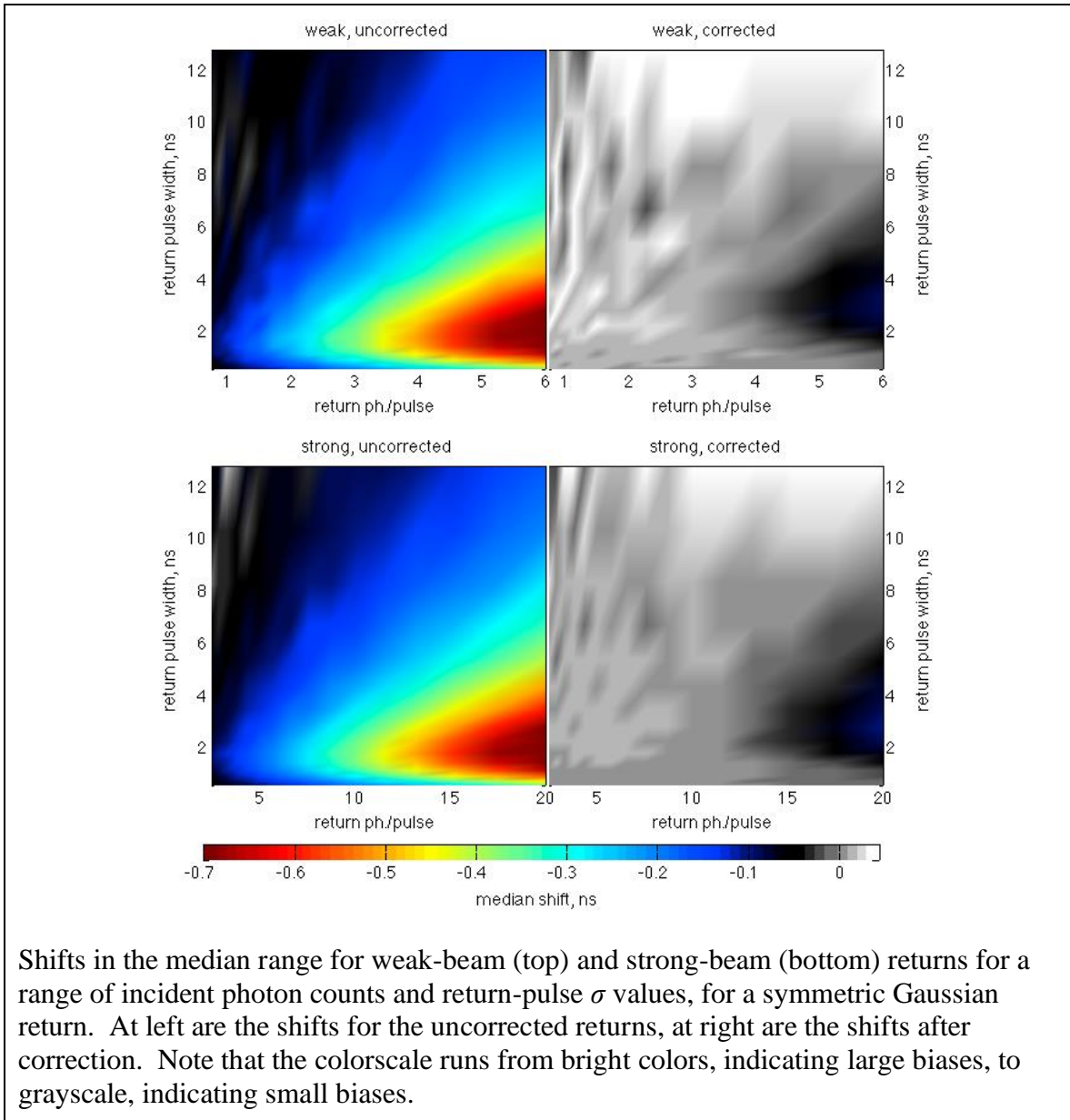
625 3.4.3.4 Correction Validity

626 The correction should provide accurate height and signal-strength corrections as long as there are
 627 at least a few active detector pixels during each time increment. If the estimated detector gain for
 628 a segment falls below $2/(N_seg_pulses \times n_pixels)$, the correction values are set to their invalid
 629 value (*NaN*), so that any value that uses these corrections (e.g. *h_li*, *fpb_n_corr*) will also be
 630 marked invalid.

631

632 3.4.3.5 Accuracy of the first-photon bias correction

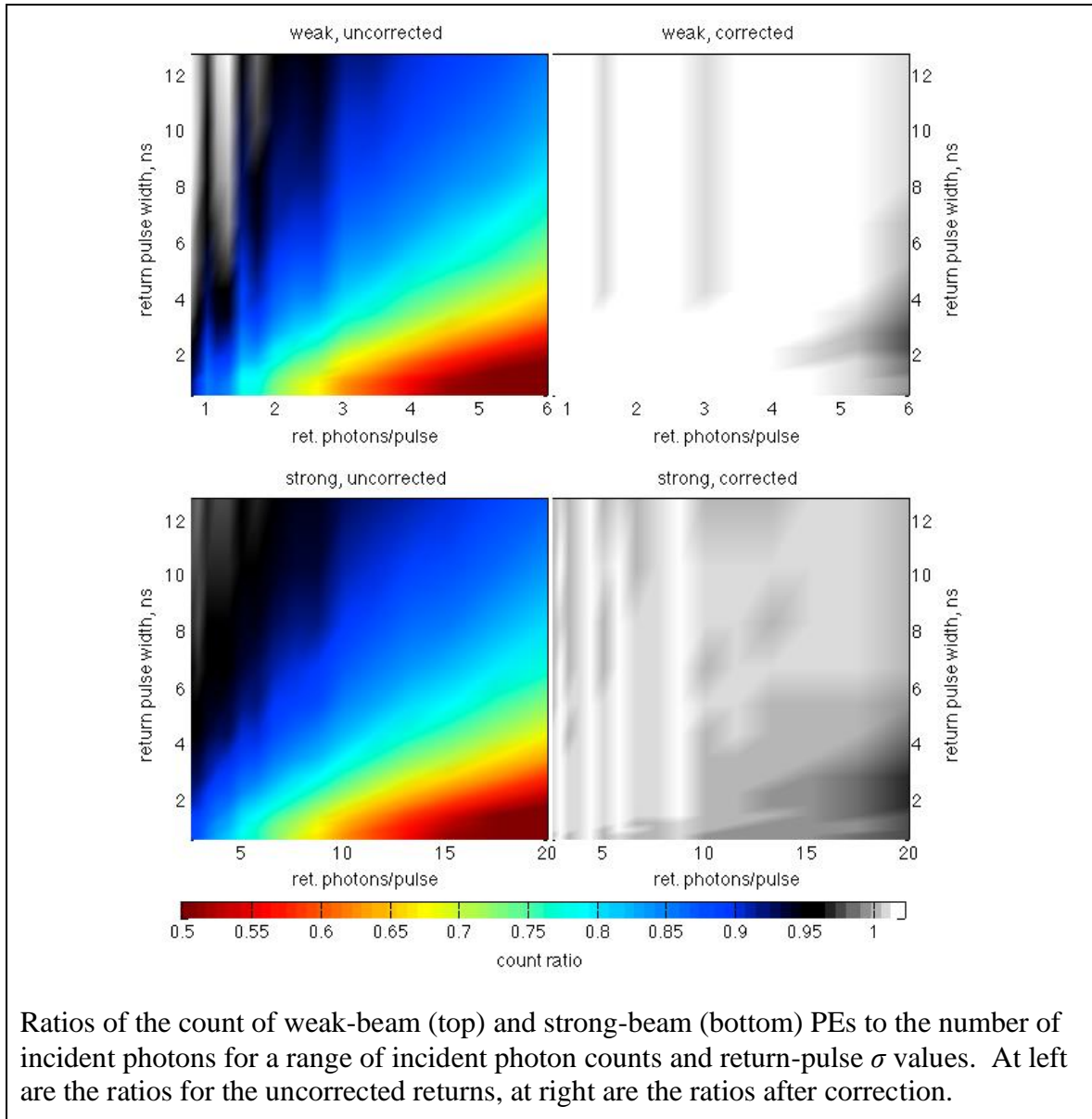
Figure 3-8. Accuracy of first-photon bias correction elevation recovery



Shifts in the median range for weak-beam (top) and strong-beam (bottom) returns for a range of incident photon counts and return-pulse σ values, for a symmetric Gaussian return. At left are the shifts for the uncorrected returns, at right are the shifts after correction. Note that the colorscale runs from bright colors, indicating large biases, to grayscale, indicating small biases.

633 We assess the potential accuracy of this calculation with a simple simulation of elevation
 634 recovery for a strong and a weak ATLAS beam. For each realization of this simulation, we
 635 generate random arrival times for a collection of N_{inc} incident return-pulse photons, with
 636 standard deviation σ_{inc} . These photons are assigned at random to detector pixels (4 pixels for a
 637 weak beam, 16 for a strong beam) and are labeled as detected or undetected based on the detector
 638 model described in 3.4 with a dead time of 3.2 ns. Based on these PE times, we then calculate a
 639 corrected arrival-time histogram as described in 3.4.2 and calculate statistics for this distribution
 640 as described in 3.4.3.

Figure 3-9. Accuracy of first-photon-bias-correction signal strength recovery



641

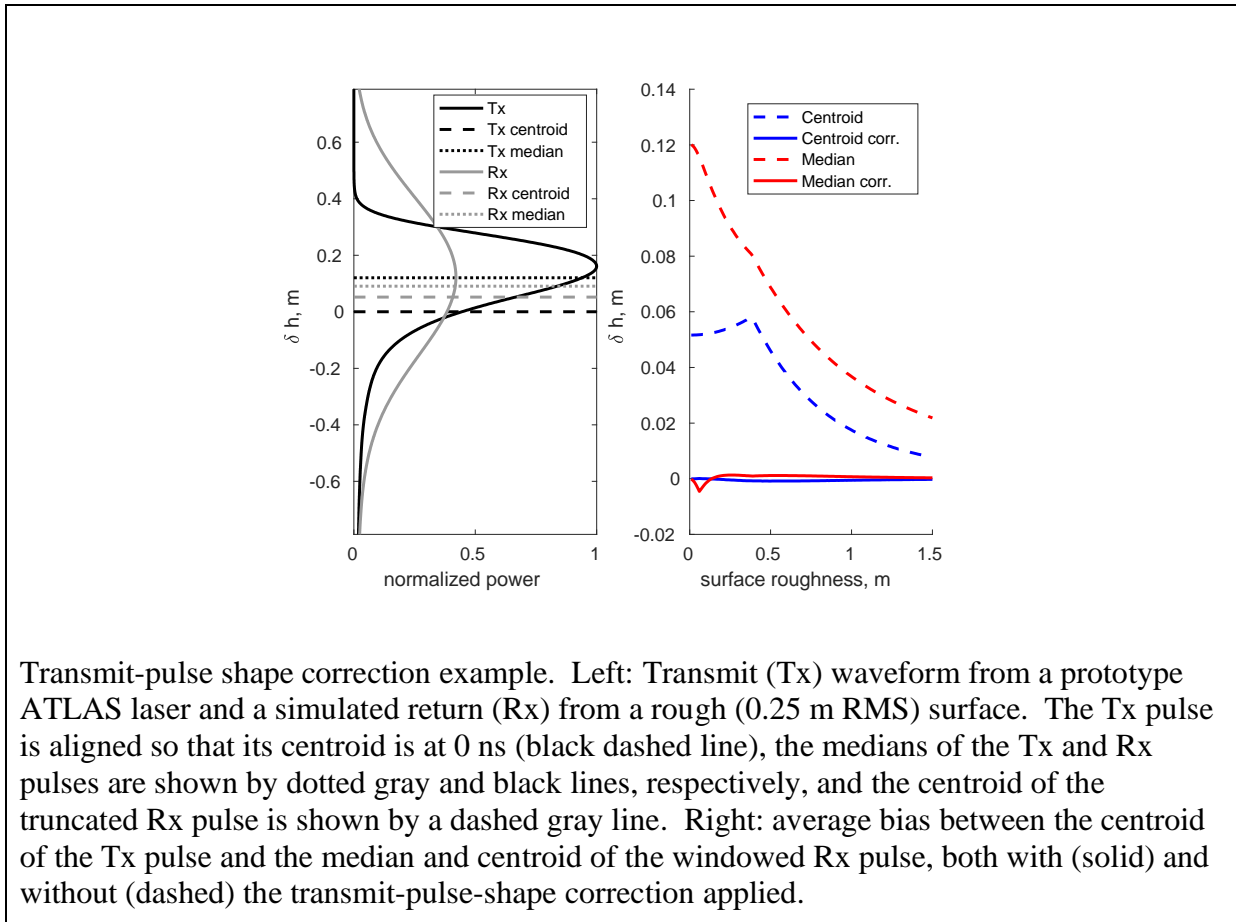
642 Results of this simulation are shown in Figure 3-8 and Figure 3-9. For the strongest simulated
 643 returns, with around two photons per pulse per detector pixel, uncorrected time biases are as
 644 large as -0.7 ns, corresponding to positive elevation biases of about 0.1 m. For these returns,
 645 only about 60% incident photons are detected. For expected return strengths, of 0.8 photons per
 646 pulse per pixel, elevation biases are smaller, around -0.2 ns, and about 85% of incident photons
 647 are detected. The largest elevation errors come for return-pulse widths of around 2 ns, and the
 648 largest loss of signal photons happens for the smallest pulse widths and the strongest returns.

649 Applying the correction removes the majority of the bias, both for return times and for signal
 650 strengths. Corrected returns have much smaller time biases, accurate to 0.1 ns (1.5 cm) for the

651 strongest (2 photons/pixel/pulse) returns, and 0.02 ns (0.03 cm) for expected (0.8 ph/pixel/pulse)
 652 return strengths. Corrected PE counts are within 2% of the incident counts.

653 **3.5 Transmit-pulse shape correction**

Figure 3-10. Transmit-pulse-shape correction



654

655 The ATL06 surface-fitting routine and the ATL06 first-photon bias correction both give
 656 estimates of the median height of the surface for each segment, relative to the centroid of the
 657 transmit pulse, for a ‘windowed’ collection of photons of limited vertical extent (typically ± 1.5
 658 m around the median height). However, the ATL03 PE heights are calculated relative to an
 659 estimate of the centroid of the entire transmit pulse. Because the transmitted pulse is not
 660 symmetric in time around its centroid, its median is different from its mean, and the centroid of
 661 any truncated subset of the photons from this pulse will have a nonzero bias relative to those
 662 from the full waveform. This introduces a potential bias in ATL06 height estimates.

663 The magnitude of the bias depends on three factors: the shape of the ‘tail’ of the transmitted
 664 waveform, the width of the surface window, and the effective surface roughness (i.e. the total
 665 broadening introduced by surface slope and roughness). The effects of the tail shape and the

666 surface-window height were described previously (1.1). The effect of increasing effective
 667 surface roughness is to increase the scatter in the PEs, producing returns that are closer to
 668 symmetrical, as shown for 0.25 m noise in Figure 3-10 (left panel). This larger scatter results in
 669 return-waveform medians that have smaller biases than those from a smooth surface, and in
 670 smaller biases in the truncated-waveform centroids. Figure 3-10 (right panel) shows the
 671 magnitude of biases in return centroids and medians for prototype-laser waveforms, broadened to
 672 simulate the effects surface roughness values between 0 and 1.5 meters. For each waveform, we
 673 calculated the centroid and median surface height relative to the centroid and median of the
 674 transmitted pulse, using a surface window height of a maximum of 3 m and three times the RDE
 675 of the returned PEs. The worst of the biases, for the zero-roughness median, is around 15 cm,
 676 and biases decrease with increasing roughness. The bias in the centroid is smaller than that of the
 677 median, but both are large relative to other expected instrumental biases.

678 We have found that we can correct for this effect by modeling expected return-pulse shapes and
 679 calculating the biases for these shapes, then subtracting the bias from the measured height
 680 estimates. The model is based on transmitted-waveform shapes measured periodically during the
 681 ICESat-2 orbit using the transmitter-echo-pulse (TEP). Using this TEP waveform and the width
 682 of the return, we estimate the extent to which reflection from the sloped, rough surface has
 683 broadened the return, and smooth the TEP waveform to broaden it to the same width. We then
 684 truncate the broadened synthetic waveform around its mean using the surface window
 685 determined in 3.3, then calculate the median and centroid of the broadened, truncated waveform.
 686 This gives corrections to the median and mean surface heights.

687 Note that at the time of writing of this document the relationship between the absolute values of
 688 the photon times measured in the TEP and the transmit times of the lasers has not been
 689 established. On-orbit calibration exercises and further analysis of pre-launch calibration data
 690 should be helpful in this regard, but for now, we take the TEP as a measurement of the shape of
 691 the waveform, not the timing of the transmission. Accordingly, we shift the time values on the
 692 TEP measurements obtained from ATL03 so that the centroid of the signal photons arrival times
 693 is equal to zero, and assume that this shifted TEP represents the transmit pulse.

694 To estimate the broadened transmit-pulse shape, we begin with an estimate of the transmitted
 695 pulse shape derived from ATL03, $P_{tx}(t)$, and $RDE(t_i)$, our estimate of the degree to which the
 696 distribution of surface returns, t_i , has been spread by its reflection from a rough or sloping
 697 surface:

$$\sigma_s^2 = \max \left((0.01 \text{ ns})^2, RDE(t_i)^2 - RDE(P_{tx}(t))^2 \right) \quad 22$$

698 The $\max((0.01 \text{ ns})^2, \dots)$ function here is included to ensure that the broadening estimate is
 699 positive. From this we generate an estimate of the surface broadening function $S(t)$:

$$S(t) = \exp \left(-\frac{t^2}{2\sigma_s^2} \right) \quad 23$$

700 The estimated broadened pulse shape, $P_B(t)$ is the temporal convolution of $P_{tx}(t)$ and $S(t)$:

$$P_B(t) = P_{tx}(t) * S(t) \quad 24$$

701 We apply a windowing function, $W_s(t)$, to account for the truncation of the surface return during
 702 the ground-bin-selection process:

$$W_s(t) = \begin{cases} 0 & |t - \text{mean}(P_B(t))| > h_window_final/2 \\ 1 & |t - \text{mean}(P_B(t))| \leq h_window_final/2 \end{cases} \quad 25$$

703

704 The height correction for the median based on this waveform estimate is then:

$$dh_{tx} = \frac{c}{2} \text{median}_t(P_B(t)W_s(t)) \quad 26$$

705 Here $\text{median}_t()$ represents the temporal median of a function:

$$\text{median}_t(f(t)) \equiv t \text{ such that } \int_{-\infty}^t f(t')dt' = \frac{1}{2} \int_{-\infty}^{\infty} f(t')dt' \quad 27$$

706 The correction for the mean is identical, but uses the mean instead of the median in equation 26.
 707 Figure 3-10 shows that after applying this correction, the remaining bias in the median and mean
 708 heights is less than 3 mm. The value calculated in equation 26 is included in the standard
 709 surface-height estimate, h_{li} , and is provided in the tx_median_corr and tx_mean_corr fields in
 710 the $bias_correction$ parameter subgroup.

711

712 3.6 Signal, Noise, and Error Estimates

713 Before we can calculate the error in the retrieved surface height, we must form estimates of
 714 relative contributions of signal and noise PEs to the observed PE count. Under ideal conditions,
 715 when the signal level is high and the background count rate is low, few noise PEs will be present
 716 among those selected by editing process described above. However, under cloudy conditions
 717 when the sun is above the horizon this will often not be true, and it is important that the error
 718 estimates reflect the potential presence of background PEs.

719 3.6.1 Background PE rate

720 The background PE rate ($bckgrd$ in the *geophysical* subgroup) is derived from the ATL03
 721 parameter $/bckgrd_atlas/bckgrd_rate$, and is derived from a 50-shot, 200Hz count of PE within
 722 the ATLAS signal-finding window, corrected for the number of PE detected by the ATL03
 723 ground-finding algorithm. In general, we expect this parameter to be sufficiently accurate to
 724 allow us to predict the number of PE within 10 m of the ground to a precision of better than 10
 725 PE/segment.

726 The expected background rate, E_{bckgrd} , is also predicted based the solar elevation, assuming a
 727 flat, Lambertian surface at the ground. The calculation of this parameter is described in the
 728 ATL07 ATBD, section 4.2.3.1. This parameter, when compared against the measured $bckgrd$, is
 729 a potential indicator of the surface reflectance and cloud properties.

730 3.6.2 Signal PE count

731 The total number of PEs selected in the window, as a function of the number of signal PEs, the
 732 background rate, the number of pulses in the window, and the background window height is:

$$N_{tot} = N_{sig} + N_{BG} \quad 28$$

733 The number of background PEs in the window has a mean value:

$$N_{BG} = 2 N_{pulses} h_{window} BGR/c \quad 29$$

734 Subtracting the two gives an estimate of the number of signal PE, N_{signal} . Because the number of
 735 background PE is a Poisson random variable, the calculated N_{signal} may be less than zero in
 736 weak-signal conditions. The ratio between the number of signal and noise photons is reported as
 737 $fit_statistics/snr$.

738 To help distinguish high-quality surface returns from returns that are likely a result of
 739 signal-finding blunders, we provide the $fit_statistics/snr_significance$, which gives the
 740 probability that in the absence of any real ground signal, a segment with at least the observed
 741 SNR would be found by the ATL06 signal-selection routine, for the initial range of heights,
 742 $h_range_initial$ and background rate $bckgrd$. If ATL03 detected photons were used in the signal
 743 selection ($signal_selection_source$ of 0 or 1, or $signal_selection_status_backup$ of 0),
 744 h_range_input is equal to the range of photon heights. Otherwise it is set to the full range of PE
 745 heights provided from ATL03 for the segment. The values of $snr_significance$ are calculated
 746 from a look-up table based on 1,000,000 realizations of random noise for background-noise
 747 values, $bckgrd_table$, between 1 and 10 MHz, and for initial window sizes, w_table , between 3
 748 and 80 meters. For each set of random-noise PE, the backup signal-selection algorithm is run to
 749 select the input PE for the iterative ground-window refinement routine (3.3.5.2), which is then
 750 run to convergence, and the final SNR is recorded. Then, for each value of $bckgrd_table$ and
 751 w_table , the probability of reporting a segment with an SNR value greater than a set of values
 752 between -10 and 10, in steps of 0.1, is calculated, and the value is stored in F_table . To find
 753 $snr_significance$ for each segment, we interpolate into F_table as a three-dimensional linear
 754 function of h_range_input , $bckgrd$, and snr for that segment.

755 3.6.3 Per-Photon Errors

756 Noise PEs are vertically distributed throughout the window with a standard deviation of
 757 approximately

$$\sigma_{BG} = 0.287 h_{window} \quad 30$$

758 where the factor 0.287 equals the standard deviation of a uniform random variable on a unit
759 interval.

760 The signal PEs have an approximate skewed Gaussian distribution, whose width depends on the
761 transmit-pulse duration, the surface roughness, the surface slope, and the footprint width, as
762 described in equation 1, with additional broadening possible due to atmospheric or subsurface
763 scattering. For ice-sheet surfaces and near-vertical beams we assume that the angle between the
764 beam and the surface slope is equal to the magnitude of the surface slope. The total standard
765 deviation of the surface return heights, $\sigma_{\text{photon,est}}$ is then:

$$\sigma_{\text{photon,est}} = \left(\frac{N_{BG}\sigma_{BG}^2 + N_{\text{signal}}\sigma_{\text{signal}}^2}{N_{BG} + N_{\text{signal}}} \right)^{1/2} \quad 31$$

766 With the exception of the surface roughness, all of the quantities needed for this equation are
767 estimated from the data: the slope spreading is estimated from the along-track component of the
768 surface slope and the transmitted pulse width using equation 1, and the background and signal
769 PE counts are estimated from the total number of PEs and the background rate. If we assume the
770 roughness to be zero, and neglect atmospheric and subsurface scattering errors, equation 31 gives
771 a minimum error estimate. An alternate estimate of the per-PE error is the vertical spread of PEs
772 relative to the along-track fit, $h_{\text{rms_misfit}}$. We combine these two estimates by setting our error
773 estimate, σ_{photon} , to the maximum of $h_{\text{rms_misfit}}$ and $\sigma_{\text{photon,est}}$.

774 3.6.4 Propagated Height Errors:

775 Given the established per-PE error, σ_{photon} , the error propagation for the linear fitting equation
776 gives an estimate of the covariance matrix for the fit (Menke, 1989):

$$\mathbf{C}_{\text{fit}} = ((\mathbf{G}^T\mathbf{G})^{-1} \mathbf{G}^T)((\mathbf{G}^T\mathbf{G})^{-1} \mathbf{G}^T)^T \sigma_{\text{photon}}^2 \quad 32$$

777 The height error estimate, σ_{h_mean} is the square root of the upper-left element of \mathbf{C}_{fit} .
778 This error is combined with the sampling error estimated during the first-photon-bias calculation
779 to give the total surface ranging error, $h_{\text{li_sigma}}$. The error in the along-track slope
780 $\sigma_{dh_fit_dx}$, is equal to the square root of the lower-right element of \mathbf{C}_{fit} .

781 3.6.5 Uncorrected reflectance

782 The uncorrected reflectance gives the ratio of the measured return energy to the energy expected
783 from a white surface, through a nominal clear atmosphere (Yang and others, 2013). Following
784 the strategy outlined in the ATL09 ATBD, we calculate:

$$r_{\text{eff}} = \frac{\pi E_{RX} r^2 F}{N_{\text{seg_pulses}} E_{TX} A T_{\text{opt}}} \quad 33$$

785 Here E_{RX} is the received energy, r is the range to the surface, A is the telescope area, and T_{opt} is a
786 factor that combines the optical efficiency of the instrument optics and the detector sensitivity. F
787 is a calibration factor that will be determined and maintained as part of the atmospheric science

788 operations. E_{TX} is the transmitted energy per pulse from the ATL03 parameter tx_pulse_e . We
 789 calculate E_{RX} based on the number of returned PE as:

$$E_{RX} = (f_{pbN} - N_{BG}) \frac{hc}{\lambda} \quad 34$$

790 Here f_{pbN} is the dead-time-corrected segment signal photon count, N_{BG} is the background-photon
 791 count (from equation 29), and hc/λ is the energy received per photon. Note that this is the same
 792 calculation as equation 4.7 in the ATL09 ATBD, except that we use the ATL06 first-photon-
 793 bias-corrected photon count, instead of the correction factor used in ATL09. For an atmospheric
 794 transmittance 0.95, we expect to see r_{eff} of about 0.88 over unit-reflectance surfaces.

795 3.7 Across-track slope calculation

796 After the iterative editing process is complete, the across-track slope is computed for the pair
 797 based on the first-photon-bias-corrected median heights for the two segments:

$$\frac{dh}{dy} = \frac{h_{LI,R} - h_{LI,L}}{y_{ATC,R} - y_{ATC,L}} \quad 35$$

798 If only one beam has returned a height, then *across_track_slope* is set to *invalid* for both beams.

799 3.8 Subsurface-Scattering Bias

800 The subsurface-scattering, or volume-scattering, bias comes from photons that experience
 801 multiple scattering within the snow or ice before returning to the satellite. Ice absorbs green
 802 light only weakly, with attenuation lengths of tens of meters or more, but ice grains in firn and
 803 air bubbles in ice both scatter green light strongly (Warren and others, 2006). While most
 804 photons from an ATLAS pulse are expected to exit the surface of a firn pack within a fraction of
 805 a nanosecond, others will likely be delayed significantly, producing a long tail on the histogram
 806 of return times. Averaging return times of PEs from this tail with PEs from the surface return
 807 leads to a delay in the mean PE return time, and a downward bias in the apparent surface height.
 808 The median surface height is modestly less sensitive than the mean, because it less sensitive to
 809 outlying data values far from the central peak of the return distribution. This error and its
 810 temporal variability is expected to be small for fine-grained snow surfaces such as those found
 811 on the Antarctic Plateau and in central Greenland, but it may be more significant in coastal areas
 812 where seasonal snow melt leads to large temporal variations in the surface grain size.

813 The magnitude of the subsurface-scattering bias delay depends in part on the scattering density
 814 of the snow and its bulk absorbance, both of which are determined by the density and grain or
 815 bubble size close to the surface, and on the impurity content of the snow or ice. Since none of
 816 these properties may be known at the time of ATLAS processing, each must be determined
 817 independently using external information about the snow, such as meteorological model output
 818 or infrared reflectance data.

819 We do not expect to be able to offer an accurate correction for this effect with our current
 820 understanding of the process. This remains an area of active research.

821 3.9 Atmospheric-Scattering Bias

822 A second important source of bias in ATLAS height measurements may come from atmospheric
823 scattering of the down-going laser pulse. Scattering by ice particles in the atmosphere redirects
824 much of the light through small angles, often less than about one degree. These photons may fall
825 outside the field of view of the ATLAS detectors, in which case they will be lost and will have
826 no impact on altimetry beyond attenuation of the received pulse, or they may reflect from the
827 surface within the field of view, in which case they may then be detected by ATLAS. However,
828 because their down-going path was longer than the assumed straight down-and-back path
829 assumed in the PRD model, they will give erroneously long ranges, and therefore low surface
830 heights. This effect is increasingly severe for thicker clouds, which scatter more photons, and for
831 clouds closer to the surface, where photons scattered through large angles may still remain in the
832 field of view.

833 Under cloudy conditions, the received pulse contains a mixture of scattered and unscattered
834 photons, yielding a tail of delayed photons on the downward side of the return pulse; mean and
835 median delays for a segment's aggregate PEs will depend on the relative fraction of the two
836 groups of photons, and the mean path delay per photon. This process has been modeled and
837 found to produce 1-cm level biases on ATLAS height retrievals under most circumstances (Yang
838 and others, 2011) but since the bias may be correlated over large spatial scales it may have a
839 non-negligible impact on continental-scale surface-change retrievals.

840 As is the case with the subsurface-scattering bias, parameters relating to a possible correction
841 must be determined from datasets external to ATLAS, likely from atmospheric models that give
842 an estimate of the cloud optical depth and the particle size. Potential corrections and data editing
843 strategies for this effect remain an active topic of research.

844

845 3.10 Segment geolocation

846 After ground-window refinement we calculate the final location of the segment. The segment
847 location is defined as the reference-point location plus the across-track unit vector times the
848 mean across-track coordinate of the selected PEs.

849 To calculate the latitude and longitude of each segment, including the offset between the
850 segment and the reference point, we use the latitude, longitude, and along-track distance
851 provided by ATL03 for the selected PE. We assume that latitude and longitude for the selected
852 PE in the segment are linear functions of along-track distance, and fit a linear function, f_{lat} , to the
853 PE latitudes, and a second linear function, f_{lon} , to the PE longitudes, each as a function of $x-x_0$.
854 The intercepts of these functions give the segment latitude and longitude.

855 Geolocation errors in the along- and across-track direction are calculated based on the ATL03
856 parameters σ_{geo_AT} , and σ_{geo_XT} and the radial orbit error, σ_{geo_r} .

857 With the surface-slope vector and the geolocation estimate we can calculate the geolocation
858 contribution to the uncertainty in the surface height:

$$\sigma_{geo,h} = \left(\sigma_{geo,r}^2 + \left(\sigma_{geo,AT} \frac{dh}{dx} \right)^2 + \left(\sigma_{geo,XT} \frac{dh}{dy} \right)^2 \right)^{1/2} \quad 36$$

859 This value is reported in the *land_ice_segments* group as *sigma_geo_h*, and the contributing
860 *sigma_geo_r*, *sigma_geo_xt*, and *sigma_geo_at* are reported in the *ground_track* group.

861 3.11 Noise-corrected robust estimators of spread

862 Many of the parameters in this document are based on ordinal statistics. These statistics use the
863 percentiles of a distribution, which are defined based on the cumulative distribution function
864 (CDF) of the distribution. We define the CDF of a discrete sample of values S as:

$$C(x; S) = \frac{\text{the number of values in } S \text{ that are less than } x}{\text{the number of values in } S} \quad 37$$

865 For a binned distribution (e.g. a histogram or a probability distribution function), $C(x; D(x_0))$, we
866 define the CDF as

$$C(x; D(x_0)) = \frac{\int_{x_1}^x D(x') dx'}{\int_{x_1}^{x_2} D(x') dx'} \quad 38$$

867 Here x_1 and x_2 are the bounds over which the distribution is defined. The percentiles of a
868 distribution are found by calculating the inverse function of the CDF of the distribution:

$$p(r; D) = C^{-1}\left(\frac{r}{100}; D\right) \quad 39$$

869 Thus the median of a distribution D is:

$$\text{Median}(D) = x \text{ such that } C(x; D) = 0.5 \quad 40$$

870 We also define the robust dispersion estimate (RDE) of a distribution as

$$RDE(D) = \frac{p(0.84; D) - p(0.16; D)}{2} \quad 41$$

871 This is analogous to the standard deviation of a normal distribution, which is equal to half the
872 difference between its 84th and 16th percentiles, but is less influenced by outlying background
873 values.

874

875 In most cases, distributions of ATLAS PEs include a mix of signal and noise PEs. In these
876 cases, the noise PEs and the signal PEs both contribute to the distribution D. We expect the
877 noise PEs are generally uniformly distributed, so we can assume that

$$C(x; D) = \frac{BGR(x - x_1) + \int_{x_1}^x D_{signal}(x')dx'}{\int_{x_1}^{x_2} D(x')dx'} \quad 42$$

878 Here D_{signal} is the distribution of the signal PEs, and $bckgrd$ is the background PE rate, in units of
879 x^{-1} . We can solve this for C_{signal} :

$$C(x; D_{signal}, BGR) = \frac{\int_{x_1}^x D_{signal}(x')dx'}{N_{signal}} = \frac{\int_{x_1}^x D(x')dx' - \frac{BGR(x - x_1)}{N_{total}}}{N_{signal}} \quad 43$$

880 Here $N_{total} = \int_{x_1}^{x_2} D(x')dx'$ and $N_{signal} = N_{total} - (x_2 - x_1)BGR$.

881 Estimating the percentiles of D_{signal} is complicated because $C(x; D_{signal}, bckgrd)$ generally does
882 not have an inverse function in x . However, if we evaluate $C(x; D_{signal}, bckgrd)$ for a set of
883 values, x_i , we can find x_{LT} , the largest value of x_i for which $C(x; D_{signal}, bckgrd) < r/100$ and x_{GT} ,
884 the first value of x_i for which $C(x; D_{signal}, bckgrd) > r/100$, and interpolate linearly into $[x_{LT}, x_{GT}]$
885 as a function of $[C(x_{LT}; D_{signal}, bckgrd), C(x_{GT}; D_{signal}, bckgrd)]$ at the point $r/100$.

886 The above procedure defines the background-corrected percentiles of a distribution. Based on
887 this we define the noise-corrected median of a distribution, which we designate: $median(D;$
888 $bckgrd)$. We define the noise-corrected RDE of a distribution somewhat differently from its
889 uncorrected counterpart. For low-noise distributions, the standard deviation of the population
890 can accurately be estimated as half the difference between its 16th and 84th percentiles. In the
891 presence of significant noise, the standard deviation can be estimated more accurately based on
892 the difference between the 25th and 50th percentiles of the distribution, divided by a correction
893 factor of 1.349, equal to the width of the central 50% of a normalized Gaussian distribution.

894

895 The surface-window-refinement procedure in section 3.3.5 uses least-squares fitting and the
896 RDE to progressively narrow the surface window. This procedure will not converge under all
897 circumstances. Consider an initial surface window spanning from $-H/2$ to $H/2$, with noise rate
898 R (in PE/m), containing s signal PEs at the center of the window. The normal (non-background-
899 corrected) RDE will find a spread of:

$$\hat{\sigma} = 0.34 H - \frac{s}{R} \quad 44$$

900 If s is small, $\hat{\sigma} \approx 0.34 H$ so the three-sigma interval will have a width of $2.04 H$, and the
901 refinement will not converge. Convergence requires $6\hat{\sigma} < H$, or:

$$s > 1.73HR \quad 45$$

902 For a background rate of 10MHz (0.067 PE/m) and a weak beam (three surface PE per pulse),
903 the procedure will converge if $H < 26$ m. For a strong beam (10 PE per pulse), it will converge if
904 $H < 86$ m. The convergence intervals become smaller in proportion to the signal PE count as the
905 surface return is weakened by cloud attenuation or by reduced surface reflectance.

906 The noise-corrected RDE and median improve on the performance of their uncorrected
907 counterparts, but their performance is limited by the accuracy of the signal-level estimate. The
908 estimate of N_{signal} has an approximate error of $(N_{\text{pulses}}(HR+s))^{1/2}$ due to the Poisson statistics of
909 the PE. In contrast to the non-robust RDE and median, the process works increasingly well as
910 more shots are aggregated, because N_{signal} increases in proportion to N_{pulses} , while its error
911 increases in proportion to $N_{\text{pulses}}^{1/2}$. If we require that $N_{\text{pulses}} s > a\sigma_n$, we find convergence
912 intervals:

$$H < \frac{N_{\text{pulses}}s^2 - a^2s}{a^2R} \quad 46$$

913 For 10 MHz noise, 3 PE/pulse, and for 57 pulses, this gives $s > 3\sigma_n$ for $H < 806$ m, implying
914 that the accuracy of the signal-level estimate will not be the limiting factor for any reasonable
915 initial window size.

916

917

918 **4 ATL06 DATA PRODUCT DESCRIPTION**

919 Here we describe how the parameters appear in the ATL06 product. The ATL06 parameters are
 920 arranged by beam, and within each beam in a number of groups and subgroups. Where
 921 parameter descriptions in the ATL06 data dictionary are considered adequate, they are not
 922 repeated in this document.

923 **4.1 Data Granules**

924 ATL06 data are provided as HDF5 files. The HDF format allows several datasets of different
 925 spatial and temporal resolutions to be included in a file. ATL06 files contain data primarily at the
 926 single-segment resolution, divided into different groups to improve the conceptual organization
 927 of the files. Each file contains data from a single cycle and a single RGT.

928 Within each file there are six top-level groups, each corresponding to data from GT: *gt1l*, *gt1r*,
 929 *gt2l*, etc. The subgroups within these *gtxx* groups are *segment_quality*, *land_ice_segments*, and
 930 *residual_histogram*.

931 In the *segment_quality* group, the data are nearly dense, providing signal-selection and location
 932 information for every segment attempted (i.e. those that contain at least one ATL03 PE) in the
 933 granule, at the 20-meter along-track segment spacing. Datasets in this group can be used to check
 934 the geographic distribution of data gaps in the ATL06 record.

935 In the *land_ice_segments* group, data are sparse, meaning that values are reported only for those
 936 pairs for which adequate signal levels (i.e. more than 10 PE, *snr_significance* > 0.05) were found
 937 for at least one segment: This means that within each pair, every dataset has the same number of
 938 values, and that datasets are pre-aligned between pairs, with invalid values (NaNs) posted where
 939 the algorithm provided a value for only one beam in a pair. Conversely, if neither beam in a pair
 940 successfully obtained a value for *h_li*, that segment is skipped for both beams in the pair. The
 941 *segment_id*, timing, and geolocation fields for the valid segments should allow the along-track
 942 structure of the data to be reconstructed within these sparse groups. For segments without valid
 943 heights that still appear on the product (because the other beam in the pair did contain a valid
 944 height) the latitude and longitude are reported for the mean location of all PE for the segment (if
 945 any PE are present) or as the location for the valid segment in the pair, displaced by the 90-meter
 946 within-pair separation (if no PE are present).

947 The *residual_histogram* group is at lower resolution than the other groups, giving the distribution
 948 of PE relative to the segment heights at a horizontal resolution of 200 m, or around 280 pulses.
 949 The *segment_id_list*, *x_atc_mean*, *lat_mean*, and *lon_mean* fields in this group all can be used to
 950 connect the *residual_histogram* group to the per-segment groups.

951 In the native format archived at the National Snow and Ice Data Center (NSIDC), each granule
 952 (file) of data contains segments from a single pass over a one-degree increment of latitude for a
 953 particular RGT, with corresponding data from all six beams. Over most of the globe, ICESat-2
 954 travels in a roughly north-south direction, so each granule will contain approximately 111 km of
 955 data for each beam, or approximately 5660 segments. The granules containing the southernmost
 956 extent of Antarctica, south of 87S, will contain a considerably longer stretch of data, but because
 957 this area will likely be of most interest to researchers investigating continental-scale Antarctic
 958 mass balance, the additional coverage will likely be desirable. We expect that because most

959 users will obtain their data through subsetting services provided by the NSIDC, the native
 960 granule structure will be of minor importance.

961 **4.2 Segment_quality group**

962 The segment_quality group contains a nearly dense record of the success or failure of the
 963 surface-finding strategies, and gives the locations of the reference points on the RPTs. It
 964 contains a record of the success or failure of the surface-finding strategies, and gives the
 965 locations of the reference points on the RPTs.

966 Locations provided within this group are for the reference points on the pair tracks, not for the
 967 segments themselves. This means that both beams in a pair will have the same location (because
 968 they are not displaced relative to the reference point), and that the actual segment locations will
 969 usually be displaced from the values in *reference_pt_lat* and *reference_pt_lon* in this group by
 970 more than 45 m in the across-track direction. The laser beam and spot numbers corresponding to
 971 the ground tracks are available in the attributes of the *ground_track* group.

972

Table 4-1 Segment_quality group

Parameter	Units	Description
<i>delta_time</i>	seconds	Elapsed GPS seconds since the reference epoch. Use the metadata attribute <i>granule_start_seconds</i> to compute the full GPS time.
<i>segment_id</i>	unitless	segment number corresponding to the second of two ATL03 segments in the ATL06 segment, counted from the RGT equator crossing
<i>reference_pt_lat</i>	degrees	Latitude of the reference segment location on the RPT
<i>reference_pt_lon</i>	degrees	Longitude of the reference segment location on the RPT
<i>record_number</i>	unitless	For those segments that have adequate signal strength, this parameter gives the record for the pair within the other groups in the granule.
<i>signal_selection_source</i>	unitless	Indicates the last algorithm attempted to select the signal for ATL06 fitting, see table Table 3-1.

		A value of 3 indicates that all algorithms failed.
--	--	--

973

974 **4.2.1 Signal_selection_status subgroup**

975 This subgroup includes the *Signal_selection_status_confident*, *Signal_selection_status_all*, and
 976 *Signal_selection_status_backup* parameters. Their values are described in Table 3-2. Its density
 977 structure matches that of the *segment_quality* group.

978

979 **4.3 Land_ice_segments group**

980 The primary set of derived ATL06 parameters are given in the *land_ice_segments* group (Table
 981 4-2). This group contains geolocation, height, and standard error and quality measures for each
 982 segment. This group is sparse, meaning that parameters are provided only for pairs of segments
 983 for which at least one beam has a valid surface-height measurement. This group contains the
 984 *bias_correction*, *fit_statistics*, *ground_track*, and *geophysical* subgroups, which all have the same
 985 sparsity structure as the *land_ice_segments* group.

986

987

Table 4-2 land_ice_segments group

Parameter	Units	Description	Defined
<i>ATL06_quality_summary</i>	Unitless	Flag indicating: 0: No likely problems identified for the segment 1: One or more likely problems identified for the segment	4.3
<i>delta_time</i>	Seconds	Elapsed GPS seconds since the reference epoch. Use the metadata attribute <i>granule_start_seconds</i> to compute the full gpstime.	Interpolated to the segment center from ATL03
<i>h_li</i>	Meters	Standard land-ice segment height determined by land ice algorithm, corrected for first-photon bias, representing the median-based height of the selected PEs	Equation 47

<i>h_li_sigma</i>	Meters	Propagated error due to sampling error and FPB correction from the land ice algorithm	Equation 48
<i>sigma_geo_h</i>	meters	Total vertical geolocation error due to PPD and POD, including the effects of horizontal geolocation error on the segment vertical error	3.10
<i>latitude</i>	degrees north	Latitude of segment center, WGS84, North=+	3.10
<i>longitude</i>	degrees east	Longitude of segment center, WGS84, East=+	3.10
<i>segment_id</i>	counts	Segment number, counting from the equator. Equal to the <i>segment_id</i> for the second of the two 20-m ATL03 segments included in the 40-m ATL06 segment	ATL03

988

989 The standard surface height will be given on the ATL06 product as *h_li*. This height is the
 990 segment-center height obtained from the along-track slope fit, with the mean-median correction
 991 applied so that it represents the median surface height for the segment. By default, *h_li* will be
 992 corrected for all height increments in the *geophysical* parameter group except for the ocean tide,
 993 the equilibrium tide, and the dynamic atmosphere correction (*dac*); this includes earth, load, and
 994 pole tides, and troposphere corrections. Since these parameters are included in the standard
 995 ATL03 PE height, no correction is applied at the ATL06 stage. Using the names for product
 996 variables:

$$h_{li} = h_{mean} + fpb_{med_corr} + tx_{med_corr} \quad 47$$

997 Tide and troposphere corrections may be removed from *h* by adding the values provided in the
 998 ATL06 *geophysical* group. The correction values for the waveform-based corrections are
 999 provided in the *bias_correction* group, so that users may convert, for example, from a median-
 1000 based height estimate to a mean-based estimate.

1001 The errors in the standard land-ice height product are calculated as the maximum of the median
 1002 error (calculated during the first-photon-bias correction) and the linear-fit error (calculated in
 1003 3.6), ignoring errors in the tidal and atmospheric corrections.

$$h_{li_sigma} = \max(\sigma_{h_fit}, fpb_{med_corr_sigma}) \quad 48$$

1004 This value does not include the effects of geolocation errors on the height estimate, because
 1005 while the components of h_li_sigma should be uncorrelated at the segment-to-segment scale, the
 1006 geolocation errors are likely to be correlated on much longer scales. The vertical component of
 1007 the geolocation error, as calculated from the surface-slope vector and the mean horizontal
 1008 geolocation accuracies of the selected PEs are given in parameter $sigma_geo_h$ (see 3.10). The
 1009 error on a single segment height measurement taken independently of all adjacent measurements
 1010 should be $(h_li_sigma^2 + sigma_geo_h^2)^{1/2}$. Averaged over several tens of segments with a
 1011 consistent surface slope, the error should approach $sigma_geo_h$, but the relative scatter between
 1012 individual adjacent segments should be h_li_sigma .

1013 The geolocation of the segment is given in geographic coordinates by parameters *latitude* and
 1014 *longitude*. These each represent the horizontal centers of the segments. The corresponding
 1015 along-track coordinates are given in the *ground_track* group as *x_atc* and *y_atc*.

1016 The *land_ice_segments* group includes the *ATL06_quality_summary* parameter, which indicates
 1017 the best-quality subset of all ATL06 data. A zero in this parameter implies that no data-quality
 1018 tests have found a problem with the segment, a one implies that some potential problem has been
 1019 found. Users who select only segments with zero values for this flag can be relatively certain of
 1020 obtaining high-quality data, but will likely miss a significant fraction of usable data, particularly
 1021 in cloudy, rough, or low-surface-reflectance conditions. Table 4-3 gives the parameter values
 1022 needed for *ATL06_quality_summary* to be reported as zero. The last of these characteristics, the
 1023 vertical density of photons, helps remove the effects of a common problem where the ATL03
 1024 photon selection identifies a cloud top as a likely surface return. In these cases, ATL06 can
 1025 converge to a large (10+ m) vertical window containing tens of signal photons. Requiring a
 1026 minimum ratio between the number of photons and the height of the window eliminates most
 1027 clouds, and eliminates only a few returns from rough or steep surfaces.

Table 4-3 Segment characteristics for *ATL06_quality_summary* to be zero

Characteristic	Threshold	Description
h_robust_spread	< 1 m	Robust spread of photons less than one meter suggests moderate spreading due to slope or roughness
h_li_sigma	< 1 m	Errors in surface height are moderate or better
snr_significance	< 0.02	Surface detection blunders are unlikely
Signal_selection_source	<=1	Signal selection must be based on ATL03 photons
N_fit_photons/ W_surface_window_final	>1 PE /m for weak beams, > 4 PE/m for strong beams	The vertical density of photons in the final surface window.

1028
1029
1030

1031 **4.3.1 geophysical subgroup**

1032 The *geophysical* group (Table 4-4) contains tidal and atmospheric corrections that may be added
1033 to or removed from *h_li*, and inferred atmospheric properties that may be used to determine
1034 whether the elevation of a given segment might be affected by atmospheric forward scattering.
1035 Note that the *neutat_delay* parameter and all *tide_* parameters in this group are applied by default
1036 except for *tide_ocean* and *dac* (dynamic atmosphere correction).. The sign of the parameters is
1037 such that adding the parameter value to *h_IS* removes the correction (for applied corrections) and
1038 subtracting the parameter includes the correction (for *tide_ocean*). These parameters are
1039 interpolated from the corresponding ATL03 parameters for the ‘nominal photons’, interpolated
1040 as a piecewise linear function of along-track distance to the segment centers. This group is
1041 sparse, meaning that parameters are provided only for pairs of segments for which at least one
1042 beam has a valid surface-height measurement.

1043 The ocean-tide value (*tide_ocean*) and dynamic atmosphere correction(*dac*) are provided to
1044 allow interested users to correct for tides and the inverse-barometer effect over ice shelves.
1045 These parameter are not applied because the locations of ice-sheet grounding lines (defining the
1046 inland extent of floating ice shelves) are not always precisely known, and may change over time.
1047 Different users will want to apply the ocean-tide model to different areas within the grounding
1048 zone.

1049 This group also include parameters related to solar background and parameters indicative of the
1050 presence or absence of clouds. Some of these parameters are derived from the ATLAS
1051 atmospheric channel, and should help identify segments strongly affected by clouds or blowing
1052 snow: parameters *cloud_flg_asr* and *cloud_flg_atm* give estimates of the probability of clouds
1053 between ATLAS and the ground, based on the apparent surface reflectance and on atmospheric
1054 backscatter, respectively. Their values are described in the ATL09 ATBD, and should be
1055 evaluated against the standard that cloud optical thickness greater than 0.5 in the lower 3 km of
1056 the atmosphere is required to produce a substantial altimetry error. (Yang and others, 2011) .
1057 Note that over surfaces other than bright snow (e.g. over blue ice or dirty snow) the
1058 *cloud_flg_asr* may indicate clouds when none are present.

1059 Blowing snow has a larger potential to produce altimetry errors, and has been assigned its own
1060 flag; the estimated height of a detected blowing-snow layer is given in *bsnow_h*, which is set to
1061 zero if no such layer can be detected; the confidence with which a blowing-snow layer can be
1062 detected or ruled out is given in *bsnow_conf*. For both flags, cautious users may require a value
1063 of 0 or 1 (clear with high/medium confidence) but under sunlit conditions, neither flag may
1064 clearly indicate cloud-free conditions. The estimated optical thickness of blowing snow layers,
1065 if found, is given in *bsnow_od*.

1066

1067

Table 4-4 geophysical subgroup

Parameter	Units	Description	Defined
<i>bckgrd</i>	Hz	Background count rate, derived from the ATL03 50-shot average, interpolated to the segment center.	Interpolated from ATL03
<i>bsnow_conf</i>	unitless	Blowing snow confidence. -3=surface not detected; -2=no surface wind; -1=no scattering layer found; 0=no top layer found; 1=none-little; 2=weak; 3=moderate; 4=moderate-high; 5=high; 6=very high	ATL09
<i>bsnow_od</i>	unitless	Blowing snow layer optical depth	ATL09
<i>bsnow_h</i>	meters	Blowing snow layer top height	ATL09
<i>cloud_flg_asr</i>	counts	Cloud flag (probability) from apparent surface reflectance. 0=clear with high confidence; 1=clear with medium confidence; 2=clear with low confidence; 3=cloudy with low confidence; 4=cloudy with medium confidence; 5=cloudy with high confidence	ATL09
<i>cloud_flg_atm</i>	counts	Number of layers found from the backscatter profile using the DDA layer finder.	ATL09
<i>layer_flag</i>	counts	This flag is a combination of multiple flags (<i>cloud_flag_atm</i> , <i>cloud_flag_asr</i> , and <i>bsnow_con</i>) and takes daytime/nighttime into consideration. A value of 1 means clouds or blowing snow are likely present. A value of 0 indicates the likely absence of clouds or blowing snow.	ATL09

<i>e_bckgrd</i>	Hz	Expected background count rate based on sun angle, surface slope, for unit surface reflectance	Calculated following ATL07
<i>msw_flag</i>	unitless	Multiple Scattering warning flag. The multiple scattering warning flag (ATL09 parameter <i>msw_flag</i>) has values from -1 to 5 where zero means no multiple scattering and 5 the greatest. If no layers were detected, then <i>msw_flag</i> = 0. If blowing snow is detected and its estimated optical depth is greater than or equal to 0.5, then <i>msw_flag</i> = 5. If the blowing snow optical depth is less than 0.5, then <i>msw_flag</i> = 4. If no blowing snow is detected but there are cloud or aerosol layers detected, the <i>msw_flag</i> assumes values of 1 to 3 based on the height of the bottom of the lowest layer: < 1 km, <i>msw_flag</i> = 3; 1-3 km, <i>msw_flag</i> = 2; > 3km, <i>msw_flag</i> = 1. A value of -1 indicates that the signal to noise of the data was too low to reliably ascertain the presence of cloud or blowing snow. We expect values of -1 to occur only during daylight.	ALT09
<i>r_eff</i>	unitless	Effective reflectance, uncorrected for atmospheric effects.	Equation 33
<i>solar_azimuth</i>	degrees_east	The direction, eastwards from north, of the sun vector as seen by an observer at the laser ground spot.	ATL03 <i>solar_azimuth</i> parameter, interpolated to the segment center from the reference photons
<i>solar_elevation</i>	degrees	Solar Angle above or below the plane tangent to the ellipsoid surface at the laser spot. Positive values mean the sun is above the horizon, while negative values mean it is below the horizon. The effect of atmospheric refraction is not included. This is a low-precision value,	ATL03 <i>solar_elevation</i> parameter, interpolated to the segment center from the reference photon

		with approximately TBD degree accuracy.	
<i>tide_earth</i>	meters	Earth tide	Inherited from ATL03
<i>dac</i>	meters	dynamic atmosphere correction	Inherited from ATL03
<i>tide_load</i>	meters	Load Tide	Inherited from ATL03
<i>tide_ocean</i>	meters	Ocean Tide	Inherited from ATL03
<i>tide_pole</i>	meters	Pole Tide	Inherited from ATL03
<i>tide_equilibrium</i>	meters	Equilibrium tide	Inherited from ATL03
<i>neutat_delay_total</i>	meters	Total neutral atmospheric delay correction (wet+dry)	Inherited from ATL03

1068

1069 In some circumstances, the estimated background rate may also give an indication of cloud
 1070 conditions. The estimated background rate is provided in parameter *bckgrd*, which may be
 1071 compared with the background rate expected for a unit-reflectance Lambertian surface, with a
 1072 slope equal to the measured surface slope, *E_bckgrd*. In sunlit conditions, these parameters
 1073 together allow an estimate of the total sub-satellite reflectance. The effective, uncorrected surface
 1074 reflectance, *r_eff*, based on first-photon-bias-corrected PE count and the range to the ground,
 1075 may be compared to these numbers; if *bckgrd* is approximately equal to *e_bckgrd*, the
 1076 atmosphere and the surface must together have a reflectance close to unity; if *r_eff* is
 1077 approximately equal to unity, this indicates that the surface below the satellite is likely snow, and
 1078 likely cloud free; if *bckgrd* is approximately equal to *e_bckgrd* and *r_eff* is small, clouds must be
 1079 present, and if *bckgrd* is less than *e_bckgrd*, the surface must be dark, and, most likely not snow
 1080 covered.

1081 Also included in this group are the solar azimuth (*solar_azimuth*) and elevation
 1082 (*solar_elevation*), used in estimating the expected background rates.

1083 4.3.2 ground_track subgroup

1084 The *ground_track* subgroup (Table 4-5) contains parameters describing the GT and RGT for
 1085 each segment, as well as angular information about the beams. All the components needed to
 1086 identify a given segment's orbit number, reference track, pair track, and beam number are given,
 1087 along with the azimuth and elevation of the beam relative to the ellipsoid surface normal. The
 1088 orientation of the RPT with respect to local north is given in *seg_azimuth*.

1089 Note that in land-ice products, the ground tracks and pair tracks are numbered separately from
 1090 the laser beams: the ground tracks are numbered from left to right relative to RGT, and the
 1091 ground track number is associated with group names within the product: From left to right, they
 1092 are *gt1l*, *gt1r*, *gt2l*, *gt2r*, *gt3l*, and *gt3r*. The laser beams are numbered from left to right relative
 1093 to the spacecraft flight direction. When the spacecraft is flying with its x axis pointing forwards,
 1094 the beam numbers are in the same order (beam numbers 1...6 correspond to tracks *gt1l*...*gt3r*),
 1095 but when it is in the opposite orientation, the laser-beam numbers are reversed relative to the
 1096 ground-track numbers (beam numbers 1...6 correspond to tracks *gt3r*...*gt1l*).

1097 This group is sparse, meaning that parameters are provided only for pairs of segments for which
 1098 at least one beam has a valid surface-height measurement. Data-set attributes give:

1099 -the reference ground track number

1100 -the correspondence between laser beam numbers and ground tracks

1101 -the cycle number

1102 The RMS accuracy of the horizontal geolocation for the segment is described by the geolocation
 1103 error ellipse, which is calculated based on the PE-medians of the ATL03 parameters
 1104 *sigma_geo_xt*, *sigma_geo_at* and *sigma_geo_r*. The along-track and across-track coordinates of
 1105 the segments are provided by parameters *x_atc* and *y_atc*.

Table 4-5 ground_track subgroup

Parameter	Units	Description	Derived
<i>ref_azimuth</i>	degrees	The direction, eastwards from north, of the laser beam vector as seen by an observer at the laser ground spot viewing toward the spacecraft (i.e., the vector from the ground to the spacecraft).	ATL03
<i>ref_coelv</i>	degrees	Coelevation (CE) is direction from vertical of the laser beam as seen by an observer located at the laser ground spot.	ATL03
<i>seg_azimuth</i>	degrees	The azimuth of the pair track, east of local north	3.1.2.2
<i>sigma_geo_at</i>	meters	Geolocation error in the along-track direction	3.10
<i>sigma_geo_xt</i>	meters	Geolocation error in the across-track direction	3.10
<i>sigma_geo_r</i>	Meters	Radial orbit error	3.10

<i>x_atc</i>	meters	The along-track x-coordinate of the segment, measured parallel to the RGT, measured from the ascending node of the equatorial crossing of a given RGT	3.1.2.2
<i>y_atc</i>	meters	Along-track y coordinate of the segment, relative to the RGT, measured along the perpendicular to the RGT, positive to the right of the RGT.	3.1.2.2

1106

1107 **4.3.3 bias_correction subgroup**

1108 The *bias_correction* subgroup (Table 4-6) contains information about the estimated first-photon
 1109 bias, and the transmit-pulse-shape bias. The standard correction applied in *h_li* is
 1110 *fpb_med_corr+tx_med_corr*, and its error is *fpb_med_corr_sigma*. The alternate, mean-based
 1111 correction, is *fpb_mean_corr*, with error *fpb_mean_corr_sigma*. The median-based elevation,
 1112 without the first-photon-bias correction, may be recovered by subtracting *fpb_med_corr* and
 1113 adding *med_r_fit*. For example, users who prefer to use the mean statistics instead of the median
 1114 statistics would use *h_li - fpb_med_corr - tx_med_corr + fpb_mean_corr + tx_mean_corr* as their
 1115 height estimate.

1116 The corrected photon count is given as *fpb_n_corr*; this gives an estimate of the number of
 1117 photons in the surface window as estimated during the FPB correction. The transmit-pulse-shape
 1118 corrections (*tx_med_corr* and *tx_mean_corr*) are also given.

1119

Table 4-6 bias_correction subgroup

Parameter	Units	Description	Derived
<i>fpb_mean_corr</i>	meters	First-photon bias correction to the mean segment height	3.4.3.1
<i>fpb_mean_corr_sigma</i>	meters	Estimated error in <i>fpb_mean_corr</i>	3.4.3.1
<i>fpb_med_corr</i>	meters	First-photon-bias correction giving the difference between the mean segment height and the corrected median height	3.4.3.2
<i>fpb_med_corr_sigma</i>	meters	Estimated error in <i>fpb_med_corr</i>	3.4.3.2
<i>fpb_n_corr</i>	counts	Estimated window photon count after first-photon-bias correction	3.4.3.3

<i>med_r_fit</i>	meters	Difference between uncorrected mean and median of linear-fit residuals	3.3.5.2
<i>tx_med_corr</i>	meters	Estimate of the difference between the full-waveform transmit-pulse mean and the median of a broadened, truncated waveform consistent with the received pulse	3.5
<i>tx_mean_corr</i>	meters	Estimate of the difference between the full-waveform transmit-pulse mean and the mean of a broadened, truncated waveform consistent with the received pulse	3.5

1120

1121 **4.3.4 fit_statistics subgroup**

1122 The *fit_statistics* subgroup gives a variety of parameters describing the segment fit and its
 1123 residuals. These parameters may be used to determine whether a particular segment is
 1124 potentially usable if it is not identified as problem-free in the
 1125 *land_ice_segments/ATL06_quality_summary* flag.

Table 4-7 fit_statistics subgroup

Parameter	units	Description
<i>dh_fit_dx</i>	unitless	Along-track slope from along-track segment fit
<i>dh_fit_dx_sigma</i>	Unitless	Propagated error in the along-track segment slope
<i>dh_fit_dy</i>	Unitless	Across-track slope from segment fits to weak and strong beams; the same slope is reported for both laser beams in each pair
<i>signal_selection_source</i>	Unitless	Flag describing the source of the information used to select the signal PE. See Table 3-1

<i>signal_selection_source_status</i>	Unitless	Indicates the status of the last signal selection algorithm attempted (see <i>signal_selection_source</i>). Values for this flag are given in the sections of Table 3-2.
<i>h_mean</i>	meters	Mean surface height, not corrected for first-photon bias or pulse truncation.
<i>sigma_h_mean</i>	meters	Propagated height error due to PE-height sampling error for height from the along-track fit, not including geolocation-induced error
<i>h_expected_rms</i>	meters	Expected RMS misfit between PE heights and along-track segment fit
<i>h_rms_misfit</i>	meters	RMS misfit between PE heights and along-track segment fit
<i>h_robust_sprd</i>	meters	RDE of misfit between PE heights and the along-track segment fit.
<i>n_seg_pulses</i>	counts (pulse ID)	The number of pulses potentially included in the segment (floating-point number)
<i>n_fit_photons</i>	counts	Number of PEs used in determining <i>h_li</i> after editing
<i>w_surface_window_final</i>	meters	Width of the surface window, top to bottom
<i>snr</i>	unitless	Signal-to-noise ratio in the final refined window

<i>snr_significance</i>	unitless	Probability that signal-finding routine would converge to at least the observed SNR for a random-noise input. Small values indicate a small likelihood of a surface-detection blunder.
-------------------------	----------	--

1126

1127 **4.3.5 DEM subgroup**

1128 This subgroup (Table 4-8) contains DEM elevations interpolated at the segment centers. It
 1129 contains only three parameters: the DEM elevation (*dem_h*), the geoid height (*geoid_h*), and the
 1130 DEM source (*dem_flag*). The best DEMs available in time for the ICESat-2 launch may be
 1131 significantly better than those available at present (February 2015), but the best current choices
 1132 are:

- 1133 • For Antarctica, the REMA DEM : <https://www.pgc.umn.edu/data/rema/>, filtered to 40-m
 1134 resolution before interpolation to the ICESat-2 segment centers, with gaps filled with
 1135 ATL06 data from cycles 1 and 2.
- 1136 • For the Arctic, the Arctic DEM, based on stereophotogrammetry
 1137 <https://www.pgc.umn.edu/data/arcticdem>. The DEM should be filtered to 40-m
 1138 resolution before interpolation to the ICESat-2 reference points.
- 1139 • For areas outside the poles, a multi-sensor global DEM, posted at 7.5 arcsec
 1140 (http://topotools.cr.usgs.gov/gmted_viewer).

1141 This group is sparse, meaning that parameters are provided only for pairs of segments for which
 1142 at least one beam has a valid surface-height measurement.

Table 4-8 DEM subgroup

Parameter	Description
<i>dem_h</i>	Height of the DEM, interpolated by cubic-spline interpolation in the DEM coordinate system to the PE location
<i>dem_flag</i>	source for the DEM. 1=Antarctic DEM, 2=Arctic DEM, 3=global DEM.
<i>geoid_h</i>	Geoid height, meters

1143

1144 **4.4 residual_histogram group**

1145 This group contains histograms of the residuals between PE heights and the least-squares fit
 1146 segment heights, at 200-meter along-track resolution. It is intended to allow visualization of the
 1147 surface-return shapes, and investigation of changes in the return pulse shape or of near-surface
 1148 scattering, such as that due to dense blowing snow. Each column of the histogram gives the
 1149 number of PE in a set of bins distributed between -50 and +50 m around the surface. The
 1150 distribution of these bins is as follows:

- 1151 From 50 to 20 m below the surface, bins are spaced at 1 m
- 1152 From 20 m to 10 m below the surface, bins are spaced at 0.5 m
- 1153 From 10 m to 4 m below the surface, bins are spaced at 0.25 m
- 1154 From 4 m to 2 m below the surface, bins are spaced at 2 cm
- 1155 From 2 m below the surface to 2 m above the surface, bins are spaced at 1 cm
- 1156 From 2 m to 4 m above the surface, bins are spaced at 2 cm
- 1157 From 4 to 10 m above the surface, bins are spaced at 0.25 m
- 1158 From 10 to 20 m above the surface, bins are spaced at 0.5 m
- 1159 From 20 m above the surface to 50 m above the surface, bins are spaced at 1 m.

1160 This distribution of bin edges gives 749 (N_{bins}) vertical bins, with 750 edges. The heights of
 1161 the bin tops are given in the *bin_top_h* parameter, listed in order from bottom to top. For any bin
 1162 in the histogram, the bottom elevation is equal to the top of the previous bin, and the elevation of
 1163 the bottom of the bottom bin is 1 m below its top. The residuals from collections of 10 along-
 1164 track ATL06 segments are combined into each histogram; because adjacent ATL06 segments
 1165 overlap by 50%, only those PE within 10 m of each segment center in the along-track direction
 1166 are included in the histograms. Only those segments with high-quality signals
 1167 (*ATL06_quality_summary* =0) are included in the histogram, and a list of the *segment_id* values
 1168 of included segments is provided in the group (recall that the *segment_id* for a segment
 1169 corresponds to the second of the two ATL03 segments included in each ATL06 segment). To
 1170 allow reconstruction of the per-pulse signal levels, the sum of the number of pulses in the valid
 1171 segments is given for each histogram, and the *background_per_m* parameter is given to indicate
 1172 the number of background photons expected in each vertical meter of each histogram. The
 1173 expected number of photons in each histogram bin can be found by multiplying the height
 1174 difference between the edges of the bin by *background_per_m*. The counts for any histogram
 1175 bins that are not entirely encompassed by at least one of the two possible telemetry band window
 1176 ranges are marked as invalid.

1177

Table 4-9 Parameters in the residual_histogram group

Parameter	Dimensions	Description
-----------	------------	-------------

<i>count</i>	N_bins x N_hist	Residual count in 1-cm bins, for PE within 10 (horizontal) m of segment centers for each histogram. Bin-top heights may be found in <i>residual_histogram/bin_top_h</i> .
<i>delta_time</i>	1xN_hist	Elapsed GPS seconds since the reference epoch. Use the metadata attribute <i>granule_start_seconds</i> to compute the full gpstime. Calculated from the mean of the <i>delta_time</i> for the segments in each histogram bin.
<i>bin_top_h</i>	N_bins	Height of the top of each histogram bin, listed in increasing order. The bottom of each bin is equal to the top of the next-lowest bin, and the bottom of the lowest bin is 1 m below its top
<i>bckgrd_per_m</i>	1xN_hist	Number of background PE expected for each vertical meter of the histogram based on the observed background rate (<i>bckgrd</i>)
<i>segment_id_list</i>	10xN_hist	Segments ids included in each column of the histogram
<i>lat_mean</i>	1x N_hist	Mean latitude of the segments included in the histogram
<i>lon_mean</i>	1x N_hist	Mean longitude of the segments included in the histogram
<i>pulse_count</i>	1xN_hist	Number of pulses potentially included in the histogram (pulses are counted if they are in the central 20 m of each segment, even if no PE from the pulse are selected)
<i>x_atc_mean</i>	1x N_hist	Mean along-track coordinate of the segments included in the histogram.

1178

1179

1180 **5 ALGORITHM IMPLEMENTATION: LAND ICE HEIGHT (ATL 06/L3A)**

1181 This section gives detailed procedures for estimating heights from ATL03 PEs. The procedures
1182 are presented as an outline of the steps that need to be programmed to calculate the main
1183 parameters from each group; we assume that after interaction with the programming team these
1184 outlines will be updated to ensure their accuracy and consistency with the rest of this document.

1185 **5.1 Outline of Procedure**

1186 The following steps are performed for each along-track reference point:

- 1187 1. PEs from the current cycle falling into the along-track bin for the along-track point are
1188 collected
- 1189 2. The initial height and along-track slope are estimated for each beam in the pair
- 1190 3. The heights and surface windows are iteratively refined for each beam in the pair
- 1191 4. Corrections for subsurface scattering, first-photon bias, median offsets, and error
1192 estimates are calculated for each beam based on the edited PEs
- 1193 5. The across-track slope is calculated

1194 Steps 1-5 are described in the “Processing Procedure” subsection.

1195 **5.2 Input Parameters**

1196 Steps 1-6 in 5.1.1 can be calculated based on ATL03 inputs. Steps 5 and 6 require information
1197 about the background rate, which is provided with the atmospheric data

1198 **Table 5-1** lists parameters needed from ATL03 and ATL09 for generation of ATL06.

1199 Individual PE heights, times, IDs, and geolocations are provided by ATL03. A variety of tidal
1200 and atmospheric-delay parameters are derived from subsamples of ATL03 fields or by
1201 interpolation into data tables used during ATL03 processing. Some ATL03 parameters are
1202 provided for every PE (e.g. height and horizontal position). These are averaged over the selected
1203 PEs for each segment. Others are provided for ‘reference’ photons spaced approximately every
1204 40 m along track. For these fields, ATL06 values are interpolated as a function of along-track x
1205 from the values for the ‘nominal’ photons to the segment centers.

1206 In addition, parameters from the atmospheric channel are used to define the blowing-snow height
1207 parameter, the blowing-snow confidence parameter, and the cloud-flag confidence parameter.

1208 The 200-Hz background-rate parameter is used to estimate background rates for each segment, as
1209 is the 50-Hz background-rate parameter based on the full atmospheric window. An estimate of
1210 the optical depth for the 3 km above the ground and a blowing-snow height estimate and
1211 confidence flag are also calculated based on ATL09 parameters.

1212 The transmit-pulse shape is used to correct the truncated means and medians used in estimating
1213 the surface shape to reduce potential biases in the recovered surface height.

Table 5-1. Inputs for ATL06

Parameter	Source	Description
podppd flag	<i>/gtxx/geolocation/podppd_flag</i>	Flag indicating low/high quality geolocation
Segment_ID	ATL03: <i>/gtxx/geolocation</i>	ATL03 segment ID
Ph_index_beg	ATL03: <i>/gtxx/geolocation</i>	First photon in the segment
Segment_ph_cnt	ATL03: <i>/gtxx/geolocation</i>	Number of PE in each segment
Segment_dist_x	ATL03: <i>/gtxx/geolocation</i>	Along-track distance for each ATL03 segment
Segment_length	ATL03: <i>/gtxx/geolocation</i>	Along-track length of each ATL03 segment.
Velocity_sc	ATL03: <i>/gtxx/geolocation</i>	Spacecraft ground speed
Sigma_across	ATL03: <i>/gtxx/geolocation</i>	across-track component of geolocation error
Sigma_along	ATL03: <i>/gtxx/geolocation</i>	Along-track component of geolocation error
Sigma_h	ATL03: <i>/gtxx/geolocation</i>	Vertical component of geolocation error
Delta_time	ATL03: <i>/gtxx/geolocation</i>	Time for each PE
H_ph	ATL03: <i>/gtxx/heights</i>	WGS-84 PE height
Lat_ph	ATL03:	PE latitude

	/gtxx/heights	
Lon_ph	ATL03: /gtxx/heights	PE longitude
Signal_conf_ph	ATL03: /gtxx/heights	Signal-classification confidence
Ph_id_channel	ATL03: /gtxx/heights	Channel number for each PE
Ph_id_pulse	ATL03: /gtxx/heights	Pulse number for the current PE
Pce_mframe_cnt	ATL03: /gtxx/heights	Major frame number for the current PE
Dist_ph_along	ATL03: /gtxx/heights	Along-track distance relative to the current segment start
Dist_ph_across	ATL03: /gtxx/heights	Along-track distance relative to the RGT
bckgrd_rate	ATL03: /gtxx/bckgrd_atlas	Background rate calculated from the 50-pulse altimetric histogram
delta_time (corresponding to bckgrd_rate)	ATL03: /gtxx/bckgrd_atlas	Time for the first shot in the 50-pulse altimetric histogram
DEM elevation	Standard DEMs	Best-available DEMs (see 4.3.5) interpolated to each segment location
Tide model values	ATL03: /gtxx/geophys_corr	Various tide-model parameters
Tep_hist	ATL03: Atlas_impulse_response/ beam_x/histogram	Transmitter-echo-pulse histogram for the strong/weak spot (should match current spot)

Tep_hist_x	ATL03: Atlas_impulse_response/ beam_x/histogram	Times for transmitter-echo-pulse histogram bins
Tep_bckgrd	ATL03: Atlas_impulse_response/ beam_x/histogram	Transmitter-echo-pulse per-bin background count
Tep_tod	ATL03: Atlas_impulse_response/ beam_x/histogram	Day/time for the TEP measurement used
Channel dead-time estimates	ATL03	dead-time estimates for each channel, from ATL03 parameters /atlas_impulse_response/dead_time
Blowing-snow flag	ATL09	Blowing-snow flag
Blowing-snow confidence	ATL09	Blowing-snow confidence
Cloud flag	ATL09	Cloud flag and confidence

1214

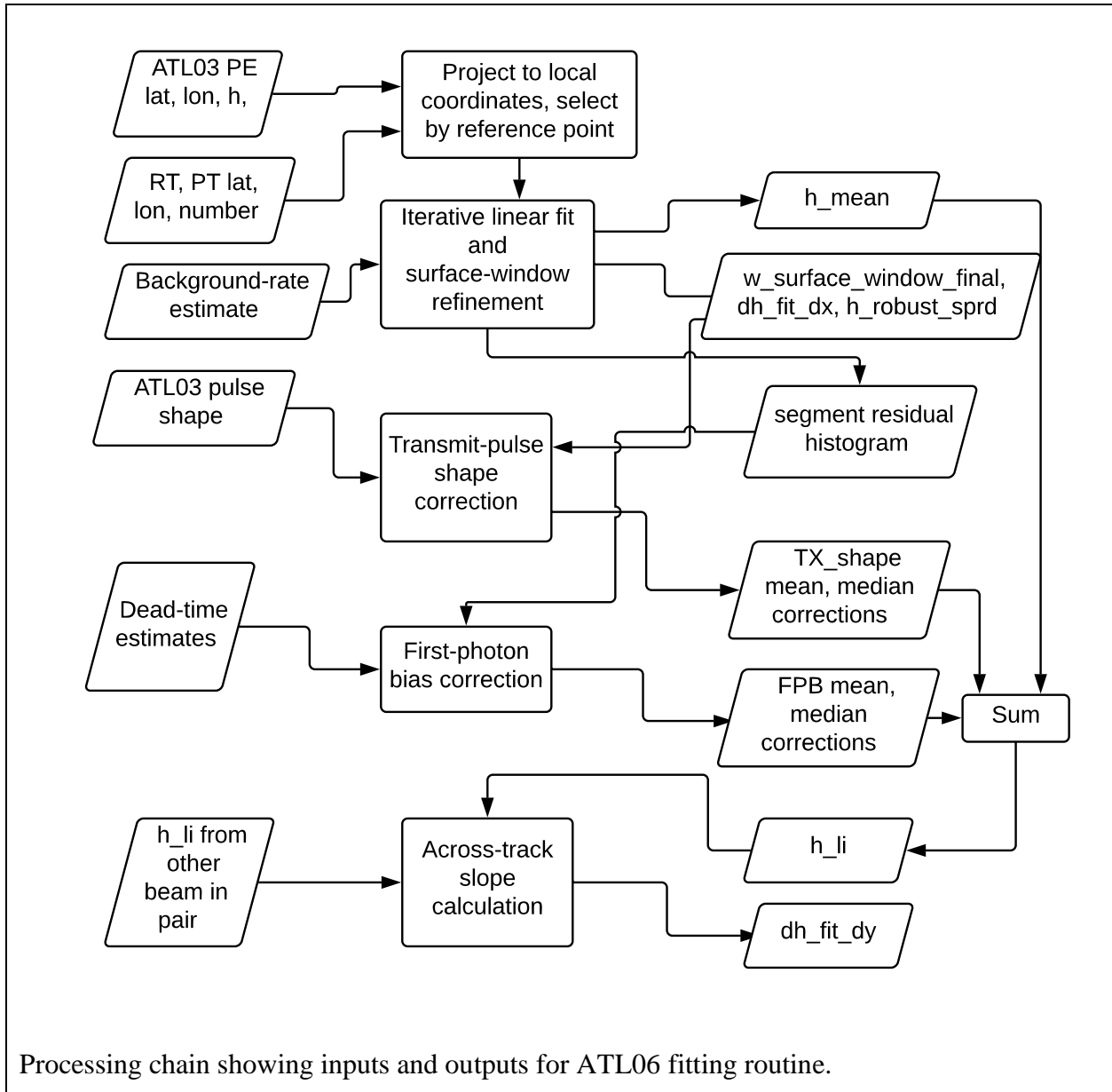
1215 Note that some parameters that are provided for each segment in ATL03 are needed for each PE
 1216 in ATL06. For example, the along-track distance for a PE is the sum of *segment_dist_x*
 1217 (provided per segment) and *dist_ph_along* (provided for each PE). To allow us to access these
 1218 fields, we generate an internal *ph_seg_num* variable, based on the ATL03
 1219 *geolocation/ph_index_beg* variables, assigning all photons between the *i*-th value of
 1220 *geolocation/ph_index_beg* and 1 less than the *i+1*-th value a *ph_seg_num* value of *i*. The
 1221 background rate is provided in ATL03 on a 50-shot sampling interval; we convert this to the per-
 1222 PE rate by interpolating as a function of *delta_time*.

1223

1224 5.3 Processing Procedure for Parameters

1225 In this section, we give pseudocode for the calculation of ATL06 parameters. The flow chart for
 1226 this process is summarized in Figure 5-1. The code is made up of several functions that call one
 1227 another, following the process described in Section 5.1.

Figure 5-1. Flow chart for top-level ATL06 processing



1228

1229 **5.4 Top-Level Fitting Routine**

1230 This routine calls the other routines in the processing chain to derive the final heights and
 1231 corrections. It corresponds to all the steps described in 3.2.

1232

1233 **Inputs**, for each beam, for ATL03 segments $m-1$ and m :

1234 x_{PE} : along-track coordinates of the land-ice PEs, meters

1235 y_{PE} : across-track coordinates of the land-ice PEs, meters

1236 *h_PE*: heights of the PE, meters
1237 *t_PE*: times for PE.
1238 *Ice_confidence_flag* : Confidence with which the PE has been identified as coming from
1239 the surface, unitless
1240 *bckgrd* : estimated background PE rate for the current segment, counts/second
1241 *ch_deadtime*: Deadtime estimate for each channel
1242 *x0_seg* : along-track coordinate of the current reference point
1243 *bckgrd_rate*: 50-shot-resolution background rate, derived from ATL03, interpolated to
1244 the center of the segment.
1245 *Spacecraft_ground_speed*: The speed of the nadir point below the spacecraft as it moves
1246 along the geoid.
1247 *Podppd_flag*: ATL03 flag indicating high or low quality geolocation
1248 **Outputs** (repeated for left and right beams)
1249 *delta_time*: time offset with respect to the beginning of the granule
1250 *h_li* : land-ice height, meters
1251 *h_li_sigma* : error in the ice-sheet height, meters
1252 *h_robust_sprd* : ice-sheet residual robust spread, meters
1253 *h_rms_misfit* : RMS residual for the residual spread, meters
1254 *n_fit_photons*: The number of photons used to define the segment.
1255 *w_surface_window* : width of the refined window used to select PEs, meters
1256 *h_expected_rms* : expected standard deviation of PEs based on surface geometry and
1257 signal levels, meters
1258 *dh_fit_dx* : along-track slope for the segment, unitless
1259 *signal_selection* parameters : parameters indicating how the initial PE were selected
1260 *fpb_corr_mean* : first-photon bias correction for the mean surface height, meters
1261 *fpb_corr_median*: first-photon bias correction for the median surface height, meters
1262 *tx_median_corr*: return-truncation correction to the median-based segment height
1263 *tx_mean_corr*: return-truncation correction to the mean-based segment height
1264 *fpb_n_corr* : corrected PE count from the first-photon bias, meters
1265 *y_seg_RGT*: segment across-track coordinate
1266 *lat_seg_center*: segment-center latitude
1267 *lon_seg_center*: segment-center longitude

1268 *tide* and *dac* parameters: geophysical parameters that are averaged and passed on from
 1269 ATL03

1270 *SNR*: Estimated signal-to-noise ratio for the segment

1271 *atl06_quality_summary*: Summary parameter indicating whether a problem in the
 1272 segment fitting was identified

1273 **Output** for both beams together:

1274 *dh_fit_dy* : across-track slope, unitless

1275 **Internal variable**, that is tracked through the fitting procedure:

1276 *h_range_input*: The range of heights provided as an input to the fitting algorithm.

1277 **Parameters:**

1278 *granule_start_time*: the starting time of the granule

1279 *dx_seg* = 40 meters

1280 *sigma_beam*: sigma value for pulse surface footprint (expected to be equal to 4.25 m)

1281 *SNR_F_table*: 3-d table giving the probability of finding a segment with the given SNR
 1282 for noise-only inputs

1283 *PRF*: Pulse repetition frequency for ATLAS (equal to 10,000 s⁻¹)

1284 **Procedure:**

1285 1. Select PE for the initial fit.

1286 1a. If the *podppd_flag* indicates degraded geolocation for any pulses, skip to the next
 1287 segment.

1288 1b. For each beam, select PE with ATL03 *segment_id* of *m* or *m-1*. Set *h_range_input*
 1289 equal to the difference between the maximum and minimum of the PE heights. Eliminate any
 1290 photons that are identified by ATL03 as part of the TEP.

1291 1c. Set initial values for the geolocation and time parameters: set *lat_seg_center*,
 1292 *lon_seg_center* and *delta_time* to the means of the corresponding reference photon values.

1293 1d. Calculate *n_seg_pulses* based on the spacecraft ground speed, and the lengths of
 1294 segments *m-1* and *m*: $n_seg_pulses = (\text{sum of segment lengths} * PRF) / \text{spacecraft_ground_speed}$.

1295 1e Based on the *ice_confidence_flag* values (see **PE selection based on ATL03 flags**),
 1296 and assign values to *signal_selection_source*, *signal_selection_status_confident*, and
 1297 *signal_selection_status_all*. If *signal_selection_source* is equal to 0 or 1, set *h_range_input* equal
 1298 to *H_win*.

1299 1f. If both *signal_selection_status_confident* and *signal_selection_status_all* are nonzero,
 1300 select PE using the **backup PE selection** routine. If *signal_selection_status_backup* is greater
 1301 than 1, skip fitting for the current beam and reference point, report invalid for *h_mean*, and for
 1302 *n_fit_photons*. If *signal_selection_status_backup* is equal to 0 set *h_range_input* equal to
 1303 *H_win*.

1304 Note: If h_range_input is not set in 1d or 1e, it remains equal to the value set in 1a: the
 1305 difference between the maximum and minimum heights of all photons found in segments m and
 1306 $m-1$.

1307

1308 Output values assigned: $signal_selection_source$, $signal_selection_status_confident$,
 1309 $signal_selection_status_all$, $signal_selection_status_backup$.

1310 Internal values assigned: PE_selection_flag.

1311 2. For each beam, estimate the surface height and slope using the **iterative least-squares fitting**
 1312 routine. Set $n_fit_photons$ to the number of PE in the final selection. If the final selection
 1313 includes fewer than 10 PE, or if the along-track spread is less than 20 m, or if the final window
 1314 width is larger than 20 m, report an invalid fit and set h_mean to its invalid value (NaN) and
 1315 return.

1316 Output values assigned, for each beam: $n_fit_photons$, dh_fit_dx , h_mean , h_rms_misfit ,
 1317 h_robust_sprd , med_r_fit , $w_surface_window_final$, SNR .

1318 Internal values assigned, for each beam: h_mean , r_fit , $selected_PE$, h_range_input

1319

1320 3. For each beam, calculate the first-photon bias correction

1321 For each beam, estimate the first-photon bias correction to the mean height, the first-
 1322 photon-bias corrected median height, and the corrected return-time histogram based on the
 1323 residuals to the segment heights calculated in step 3.

1324 3a. Run the first-photon-bias-correction routine on PE flagged with $selected_PE$ (see
 1325 below)

1326 Internal values assigned: fpb-corrected residual histogram, estimated gain.

1327 Output values assigned for each beam: fpb_mean_corr , $fpb_mean_corr_sigma$,
 1328 fpb_median_corr , $fpb_median_corr_sigma$, FPB_N_PE

1329

1330 4. Calculate the pulse-truncation correction

1331 Based on the h_robust_sprd and $w_surface_window_final$ values calculated in the last
 1332 step of the iterative least-squares fit and the SNR calculated in step 2, calculate the pulse-
 1333 truncation correction (See pulse-truncation-correction section).

1334 Output values assigned for each beam: tx_med_corr , tx_mean_corr

1335

1336 5. Calculate remaining output parameters

1337 5a. Calculate h_li :

$$1338 \quad h_li = h_mean + fpb_med_corr + tx_med_corr$$

1339 Output values assigned: h_li

1340

1341 5b. Calculate y_seg_RGT , equal to the median of all y_PE_RGT values.

1342 Output values assigned: y_seg_RGT

1343 5c. Calculate seg_time , lat_seg_center and lon_seg_center by regressing (respectively)
 1344 $time_PE$, lat_PE and lon_PE as a function of x_PE to $x0_seg$ for selected PE. For those
 1345 segments for which fitting has failed, but for which the other beam in the pair has a valid
 1346 segment, report the latitude and longitude of the valid segment, displaced by 90 m to the left or
 1347 right in the across-track direction (depending on which segment is valid).

1348 Output values assigned: seg_time , lat_seg_center , lon_seg_center , $delta_time$

1349 5d. Estimate the final cross-track slope, equal to the difference between the h_li values
 1350 divided by the difference between the y_seg_RGT values for the two beams.

1351 Output values assigned: dh_fit_dy

1352 5e. Calculate error estimates for each beam.

1353 *i.* For each segment, calculate $h_expected_RMS$ based on the footprint size, the along-
 1354 track track slope, and the transmit pulse duration (equation 1):

1355
$$h_expected_RMS = \text{sqrt}((dh_fit_dx \sigma_beam)^2 + (c/2 \sigma_xmit)^2)$$

1356 *ii.* Add the effects of background noise to $\sigma_expected$ to calculate σ_PE_est .

1357
$$\sigma_PE_est = ((N_signal h_expected_RMS^2 + N_noise(0.287 H_win)^2) / N_tot)^{1/2}$$

1358 *iii.* Calculate linear-fit-model errors. Multiply $h_mean_sigma_unit$ and
 1359 $dh_fit_dx_sigma_unit$ by $\max(\sigma_PE_est, h_rms_misfit)$ to obtain h_mean_sigma and
 1360 $dh_fit_dx_sigma$.

1361 Output values assigned: σ_h_mean , $\sigma_dh_fit_dx$, σ_PE_est , h_rms_misfit .

1362 5f. Set h_li_sigma equal to the maximum of σ_h_mean and $fpb_med_corr_sigma$.

1363 Output values assigned for each beam: h_li_sigma .

1364 5g. Calculate the uncorrected reflectance, based on the first-photon-bias-corrected total
 1365 PE count. Equation given in 3.4.3.3.

1366 Output values assigned, for each beam: r_eff

1367 5h. Calculate $SNR_significance$, by interpolating into the SNR_F_table as a linear
 1368 function of the table parameters BGR , SNR , and $w_surface_window_initial$.

1369 Output value assigned: $SNR_significance$

1370 5i: calculate $atl06_quality_summary$: $atl06_quality_summary$ is zero unless
 1371 $h_robust_sprd > 1$ m or $h_li_sigma > 1$ m or $SNR_significance > 0.02$ or
 1372 $N_fit_photons/w_surface_window_final < 4$ (for strong beams) or < 1 (for weak beams) or
 1373 $signal_selection_source > 1$.

1374 5j: Calculate pass-through parameters: For tide parameters, error parameters, and the dac ,
 1375 calculate ATL06 values from the average values for the ATL03 segments.

1376 5k: Calculate systematic error estimates: Based on geolocation error estimates and surface
1377 slope, calculate $h_{li_sigma_systematic}$ based on equation 36.

1378 **5.5 Signal selection based on ATL03 flags**

1379 **Inputs**, from one beam only, for each PE

1380 x_{PE} : along-track coordinates of the land-ice PE for the current segment

1381 h_{PE} : height of PE for the current segment

1382 $Ice_confidence_flag$: ATL03 classification of the land-ice PE. 0=undetected, 1=PE in the
1383 pad region, but not identified as signal PE, 2=low confidence, 3=medium confidence, 4=high
1384 confidence.

1385 **Input**, one per segment:

1386 $x0$: the along-track location of the segment center.

1387 BGR : the interpolated background PE rate for the segment.

1388 **Parameters:**

1389 $Sigma_beam$: The one-sigma expected horizontal spread of the photons on the ground.
1390 Equal to 4.25 m (pre-launch estimate)

1391 $Sigma_xmit$: The one-sigma temporal duration of the transmit pulse.

1392 **Outputs:**

1393 $PE_selection$: binary flag, one per input PE, showing whether to use that PE in the initial
1394 fit.

1395 $Signal_selection_source$: parameter indicating the how the signal was selected. See
1396 Table 3-1 for values.

1397 $signal_selection_status_confident$: parameter indicating the success/failure of signal
1398 selection using low-or-better confidence PEs.

1399 $signal_selection_status_all$: parameter indicating the success/failure of signal selection
1400 using all flagged PEs.

1401 H_win : Height of the window around the best-fitting line used to select PE.

1402

1403 **Procedure:**

1404 1. If the inputs are empty (no PE are in the along-track window), set $signal_selection_source$ to
1405 3, set $signal_selection_status_confident$ to 3, set $signal_selection_status_all$ to 3 set
1406 $signal_selection_status_backup$ to 4, and return.

1407 2. Check if the confidently detected PE are adequate to define an initial segment.

1408 2a. Set $PE_selection$ to true for all PE with $Ice_confidence_flag \geq 2$, to zero for all
1409 others

1410 2b: If the difference in x_{PE} between the first and last PE in $PE_selection$ is less than 20
1411 m set $signal_selection_status_confident$ to 1.

1412 2c: If there are fewer than 10 true elements in $PE_selection$, but the spread between the
1413 first and last PE in $PE_selection$ is greater than 20 m, set $signal_selection_status_confident$ to 2.

1414 2d. If there are fewer than 10 true elements in $PE_selection$, and the spread between the
1415 first and last PE is less than 20 m, set $signal_selection_status_confident$ to 3.

1416

1417 3. Check if the combination of confidently detected PE and the padded PE are adequate to define
1418 an initial segment. If $signal_selection_status_confident$ is zero, skip this step.

1419 3a. Set $PE_selection$ to true for all PE with non-zero $ice_confidence_flag$.

1420 3b: If the difference in x_{PE} between the first and last PE in $PE_selection$ is less than 20
1421 m set $signal_selection_status_all$ to 1.

1422 3c: If there are fewer than 10 true elements in $PE_selection$, but the spread between the
1423 first and last PE in $PE_selection$ is greater than 20 m, set $signal_selection_status_all$ to 2.

1424 3d. If there are fewer than 10 true elements in $PE_selection$, and the spread between the
1425 first and last PE is less than 20 m, set $signal_selection_status_all$ to 3.

1426 3e: If $signal_selection_status_all$ is equal to zero, set $signal_selection_source$ to 1 and
1427 proceed to step 4, otherwise set $signal_selection_source$ to 2, and return.

1428 4. Calculate the vertical spread of the selected PE, make the selection consistent with a vertical
1429 window around a sloping segment.

1430 4a. Calculate the least-squares fit line between $(x_{PE}-x_0)$ and h_{PE} for the selected PE.
1431 Internal variables set: $along_track_slope$, seg_center_height .

1432 4b. Calculate r_{PE} , the residual between the best-fitting line and h_{PE} .

1433 4c. Calculate σ_r , the robust spread (accounting for noise) of r_{PE} , based on the
1434 background density, $BG_density$, with z_{min} and z_{max} set to the minimum and maximum
1435 values of r_{PE} . See the **robust_dispersion** section for description.

1436 4d. Calculate the expected PE spread, $\sigma_{expected}$, based on the current slope
1437 estimate:

$$1438 \quad \sigma_{expected} = [(c/2 \sigma_{xmit})^2 + \sigma_{beam}^2 \text{along_track_slope}^2]^{1/2}$$

1439 4e. Calculate H_{win} :

$$1440 \quad H_{win} = \max(H_{win_min}, 6 \sigma_{expected}, 6 \sigma_r)$$

1441 4f. Select all PE that have $abs(r_{PE}) < H_{win}/2$. Report the number of selected PE as
1442 $N_{initial}$.

1443 5.6 Backup PE-selection routine.

1444 **Inputs:**

1445 x_{PE} : along-track coordinates of all PE for the current beam

1446 h_{PE} : heights of all PE for the current beam

1447 x_0 : along-track bin center for the current bin.

1448 $Ice_confidence_flag$: ATL03 classification of the land-ice PE. 0=undetected, 1=PE in the
1449 pad region, but not identified as signal PE, 2=low confidence, 3=medium confidence, 4=high
1450 confidence

1451 $signal_selection_source$: Flag indicating the how the signal was selected. See Table 3-1
1452 for values.

1453 **Outputs:**

1454 $PE_selection$: selected PE for the current bin.

1455 $signal_selection_source$: Flag indicating the how the signal was selected. See Table 3-1
1456 for values, updated based on the results of this algorithm

1457 $signal_selection_status_backup$ flag indicating the success/failure of signal selection
1458 using backup selection algorithm

1459 H_win : Vertical extent of the selected window

1460 **Internal variables:**

1461 $Test_window_center$: Vector of test window centers

1462 $Window_center_height$: Estimated window center height

1463 **Procedure:**

1464 1. Attempt to center the window on any ATL03 flagged PE that are present.

1465 1a. If any padded or detected PE are found, set w_0 to the maximum of 10 m and the
1466 difference between the maximum and minimum selected PE heights, and set $PE_selection$ to true
1467 for all PE that have heights within 5 m of the median of the selected PE heights. Set H_win
1468 equal to 10 m.

1469 1b. If the horizontal spread in the PE marked in $PE_selection$ is greater than 20 m, and if
1470 10 or more PE are selected, then set $signal_selection_status_backup$ to zero, set
1471 $signal_selection_source$ to 2, and return.

1472 2. Find the 80-m along-track by 10-m vertical bin that contains the largest number of PEs

1473 2a. Select all PE from ATL03 segments $m-2$ to $m+1$, inclusive.

1474 2b. Loop over $test_window_center$ values between $floor(\min(h_{PE}))+0.25$ and
1475 $ceil(\max(h_{PE}))$ in 0.5 m steps. For each $test_window_center$ value, count the PE in a 10-m
1476 (vertical) bin centered on the $test_window_center$ value.

1477 2c. Find the maximum of the window counts, C_{max} , and calculate its uncertainty,
1478 $C_{sigma}=\sqrt{C_{max}}$. If C_{max} is less than 16, then set $PE_selection$ to null (no selected PE) and
1479 skip to step 3.

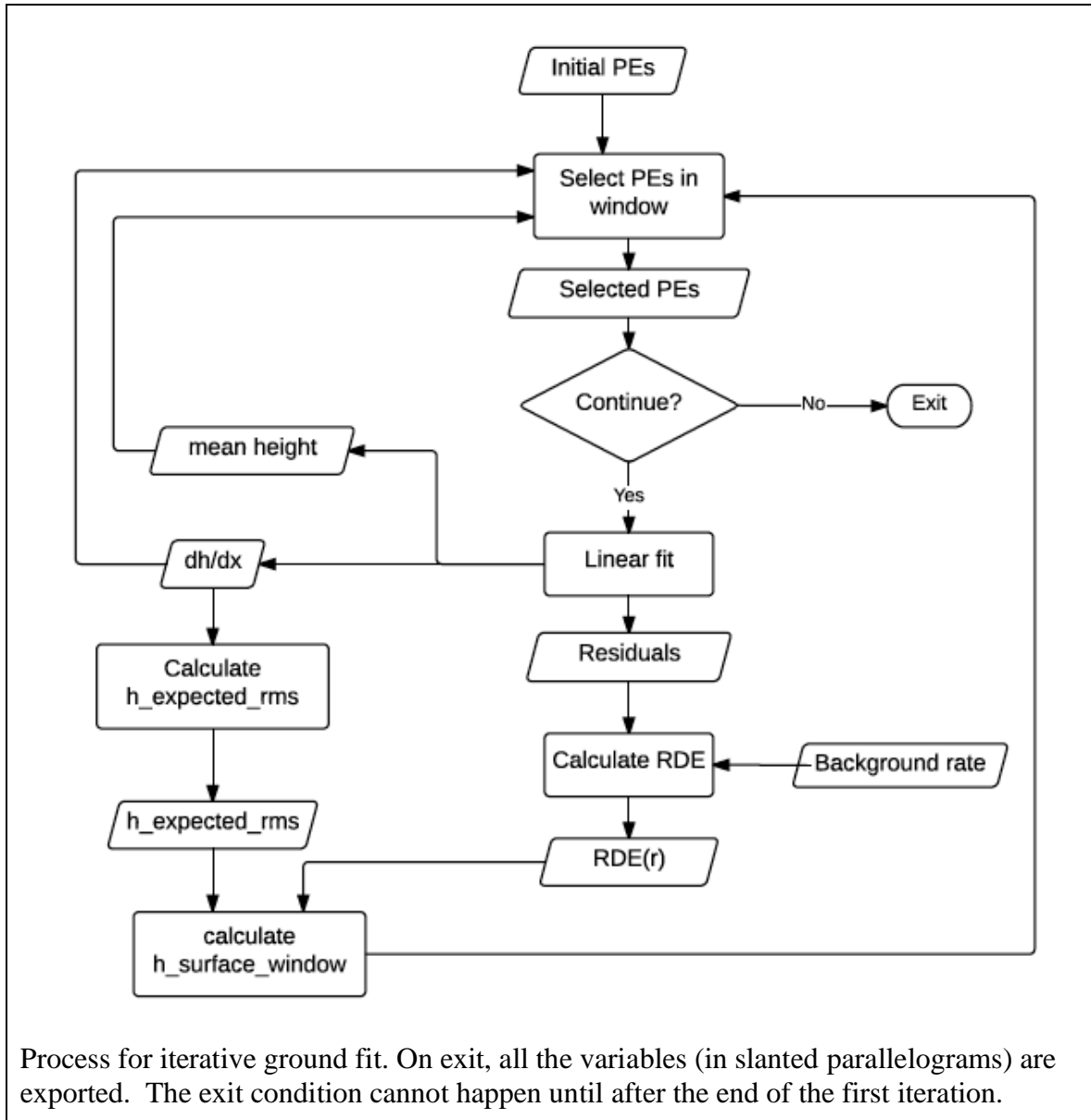
- 1480 2d. Set *window_center_height* equal to the center of the range of *test_window_center*
1481 values that have a count greater than *Cmax-Csigma*. Set *H_win* to the difference between the
1482 minimum and maximum of *test_window_center* values that have a count greater than *Cmax-*
1483 *Csigma*, plus 10 m.
- 1484 2e. Set *PE_selection* to 1 for all PE in ATL03 segments *m-1* and *m*, with a height within
1485 *H_win/2* of *window_center_height*.
- 1486 3. Evaluate the selection.
- 1487 3a. Set *signal_selection_status_backup* to 1.
- 1488 3b: If the difference in *x_PE* between the first and last PE in *PE_selection* is less than 20
1489 m set *signal_selection_status_backup* to 2.
- 1490 3c: If there are fewer than 10 true elements in *PE_selection*, but the spread between the
1491 first and last PE in *PE_selection* is greater than 20 m, set *signal_selection_status_backup* to 3.
- 1492 3d. If there are fewer than 10 true elements in *PE_selection*, and the spread between the
1493 first and last PE is less than 20 m, set *signal_selection_status_backup* to 4.
- 1494 3e. If *signal_selection_status_backup* is 1, set *signal_selection_source* to 2, if greater
1495 than 1, set *signal_selection_source* to 3.

1496

1497 **5.7 Iterative Least-Squares Fitting Routine**

1498 This routine performs the iterative least-squares fit to refine the surface window and determine
1499 the along-track slope. The process for this step is shown in Figure 5-2.

Figure 5-2. Flow chart for iterative ground fit



1500

1501 **Inputs:**

- 1502 x_{PE} : along-track coordinates of PE for the current beam
- 1503 y_{PE} : across-track coordinates of PE for the current beam
- 1504 $input_PE_selection$: Flag defining the PE selected by the initial selection routine
- 1505 h_{PE} : heights of selected PE for the current beam
- 1506 $x0$: along-track bin center for the current bin.
- 1507 $bckgrd$: Interpolated background-PE rate estimate for the segment
- 1508 H_{win} : Initial surface-window height.

1509 *signal_selection_source*: Flag indicating the source of the initial signal selection

1510 *N_it*: maximum number of iterations

1511 **Parameters:**

1512 *Sigma_xmit*: transmitted pulse duration (seconds)

1513 *Sigma_beam*: sigma value for pulse surface footprint (expected to be equal to 4.25 m)

1514 *L0*: Along-track length of the window

1515 *N_seg_pulses*: Number of pulses in a 40-meter segment (equal to 58 assuming 7 km/s

1516 ground-track speed)

1517 *H_win_min*: Minimum allowed surface window height, equal to 3m.

1518 **Outputs:**

1519 *H_win*: the height of the window around the best-fitting segment within which PE are

1520 selected.

1521 *dh_fit_dx*: The along-track slope of the best-fitting segment

1522 *h_mean*: The mean-based height of the best-fitting segment

1523 *PE_fit_flag*: A flag indicating whether a particular PE has been selected based on the

1524 segment height and slope and *H_win*.

1525 *r0*: Residuals to the best-fitting segment

1526 *h_mean_sigma_unit*: Estimated error in *h_mean* per unit of PE-height error

1527 *dh_fit_dx_sigma_unit*: Estimated error in *dh_fit_dx* per unit of PE-height error.

1528 *N_signal* : Estimated number of signal PE

1529 *N_BG* : Estimated number of background PE

1530 *h_robust_sprd* : robust spread of residuals

1531 *h_rms_misfit*: RMS misfit of residuals

1532 *SNR*: signal-to-noise ratio for window.

1533 **Procedure:**

1534 1. Initialize the fit.

1535 1a. If *signal_selection_source* is zero or 1, eliminate all PE not marked as 1 in

1536 *input_PE_selection*, set *PE_fit_flag* to 1 for all remaining PE.

1537 1b. If *signal_selection_source* is nonzero, Set *PE_fit_flag* to 1 for all PE marked in

1538 *input_PE_selection*, zero for all others.

1539 1c. Calculate the vertical noise-photon density:

1540 $BG_density = N_seg_pulses \text{ median}(bckgrd) / (c/2)$

1541 2. Iterate the fit.

1542 2a. Check whether enough PE are selected to define a window. If fewer than 10 PE are
1543 selected in *PE_fit_flag*, set *H_win*, *dh_fit_dx*, *H_mean*, and *r0* to invalid, and return.

1544 2b. Calculate the least-squares linear fit between *h_PE* and *x_PE-x0* for the PE selected
1545 in *PE_fit_flag*. The intercept of the fit is *h_mean*, the slope is *dh_fit_dx*. Calculate the residual to
1546 this fit for the selected PE, *r0* and for all PE, *r*. If the along-track spread between the first and
1547 last selected PE is less than 10 m, fit for the height only, and set the along-track slope estimate to
1548 zero.

1549 2c. Calculate *sigma_r*, the robust spread (accounting for noise) of *r0*, based on the
1550 background density, *BG_density*, and current window height, *H_win*. The variables input to the
1551 **robust dispersion including a background estimate** routine are $z=r0$, $z_{min}=-H_{win}/2$,
1552 $z_{max}=H_{win}/2$, $N_{BG}=H_{win} BG_{density}$. If the resulting *sigma_r* is greater than 5 m, set it to
1553 5 m.

1554 2d. Calculate the expected PE spread, *sigma_expected*, based on the current slope
1555 estimate:

1556 $sigma_expected = [(c/2 \sigma_{xmit})^2 + \sigma_{beam}^2 \text{along_track_slope}^2]^{1/2}$

1557 2e. Save the value of *H_win* in *H_win_previous*, then calculate the window height from
1558 *sigma_expected* and *sigma_r*.

1559 $H_{win} = \max(H_{win_min}, 6 \sigma_{expected}, 6 \sigma_r, 0.75 H_{win_previous})$

1560 2f. Save the values of *PE_fit_flag* in *PE_fit_flag_last*.

1561 2g. Select PE within *H_win/2* of the segment fit.

1562 $PE_fit_flag = 1$ for PE with $r < H_{win}/2$, 0 for PE with $r > H_{win}/2$

1563 2h. Evaluate the newly selected PE. If there are fewer than 10 selected PE, or if the
1564 along-track spread between the first and last PE is less than 20 m, set *PE_fit_flag* to
1565 *PE_fit_flag_last*, *H_win* to *H_win_previous*, and continue to step 3.

1566 2i. If fewer than *N_iterations* have been completed, and if the values for *PE_fit_flag* have
1567 changed since the previous iteration, return to step 2a. Otherwise continue to step 3.

1568 3. Propagate the error in the fit parameters assuming unit data errors (see 3.6, with $\sigma_{photon}=1$).
1569 This gives the unit errors *h_mean_sigma_unit*, *dh_fit_dx_sigma_unit*.

1570 4. Calculate the number of signal and background PE, and the SNR.

1571 $N_{BG} = bckgrd H_{win} / 2 / c N_{seg_pulses}$

1572 $N_{signal} = \max(0, \text{number of selected PE} - N_{BG})$

1573 $SNR = N_{signal} / N_{BG}$

1574 5. Calculate output error statistics:

1575 $h_{rms_misfit} = \text{RMS misfit of selected PE}$

1576 $h_{robust_sprd} = \sigma_r$ from the last iteration

1577 **5.8 Robust dispersion calculation from a collection of points, not including a background**
 1578 **estimate**

1579 **Input:**

1580 z: sampled values

1581 **Output:**

1582 RDE : the robust dispersion estimate for z.

1583

1584 **Procedure:**

- 1585 1. Sort z. z_s is equal to z, sorted in ascending order. Let N_z equal to the number of elements in z.
 1586 2. Calculate an abscissa for z_s ,
 1587 2a. Generate *ind*, equal to the sequence of integers between 1 and N_z .
 1588 2b. Calculate ind_N , equal to $(ind-0.5)/N_z$.
 1589 3. Interpolate the percentiles of z. Interpolate the values of z_s as a function of ind_N at values
 1590 0.16 and 0.84. Half the difference between these values is *RDE*.
 1591

1592 **5.9 Robust dispersion calculation from a collection of points, including a background**
 1593 **estimate**

1594 **Inputs:**

1595 z: sampled values

1596 z_{min} , z_{max} : window from which the values in z are sampled

1597 N_{BG} : Estimate of the number of background events between z_{min} and z_{max} .

1598 **Output:**

1599 *RDE* : the robust dispersion estimate for z.

1600 **Parameter:**

1601 *Scale_factor*: equal to $\sqrt{2}(erfinv(0.5)-erfinv(-0.5))$, where *erfinv*() is the inverse error
 1602 function, or 1.3490.

1603 **Procedure:**

- 1604 1. Estimate the background rate and signal count.
 1605 1a. *bckgrd* is equal to N_{BG} divided by the difference between z_{max} and z_{min} .
 1606 1b. N_{sig} is equal to the number of elements in z, minus N_{BG} .
 1607 1c. If $N_{sig} \leq 1$, the RDE is equal to $(z_{max}-z_{min})/(the\ number\ of\ elements\ in\ z)$, and the
 1608 rest of the calculation is skipped.

- 1609 2. Sort z . z_s is equal to z , sorted in ascending order. Let N_z equal to the number of elements in z .
- 1610 3. Calculate an abscissa for z_s . Generate ind , equal to the sequence of integers between 1 and N_z ,
1611 minus 0.5.
- 1612 4. Find the indices for the smallest potential percentiles of z .
- 1613 4a. $i0$ is equal to the index of the greatest value of ind for which $ind < (0.25N_{sig} + (z_s -$
1614 $z_{min})bckgrd)$.
- 1615 4b. $i1$ is equal to the index of the smallest value of ind for which $ind > (0.75N_{sig} + (z_s -$
1616 $z_{min})bckgrd)$.
- 1617 5. If $i1 < i0$, reselect $i0$ and $i1$ to measure spread of the central $N_{sig}/2$ values of the distribution:
- 1618 5a: $i0$ is equal to the index of the greatest value of ind for which $ind < N_z/2 - N_{sig}/4$.
- 1619 5b: $i1$ is equal to the index of the smallest value of ind for which $ind > N_z/2 + N_{sig}/4$.
- 1620 6. Calculate RDE . RDE is equal to the difference between the z_s values at $i0$ and $i1$, divided by
1621 $scale_factor$.

1622 5.10 First- Photon Bias Correction

1623 These routines calculate the first-photon bias for a collection of residual photon heights. Most of
1624 the calculation is done as a function of time, and the results are converted back to height at the
1625 end of the routine.

1626

1627 **Inputs:**

1628 r_p : PE heights, corrected for the along-track segment fit, converted to time (multiplied by $-2/c$)

1629 N_seg_pulses : the number of pulses in the segment

1630 N_px : the number of pixels in the detector.

1631

1632 **Outputs:**

1633 G_est : the estimated detector gain

1634 N_hist : The uncorrected PE count histogram (in units of PE)

1635 N_PEcorr : the estimated PE count histogram (in units of PE)

1636 t_full : the time vector for the PE count histogram.

1637 FPB_med_corr : the FPB correction to the median height

1638 $Sigma_FPB_med_corr$: the error estimate for FPB_med_corr

1639 FPB_mean_corr : The FPB correction to the mean height

1640 $FPB_mean_corr_sigma$: the error estimate for FPB_mean_corr .

1641 $Fpb_N_photons$: the FPB-corrected estimate of the number of PE in the return.

1642

1643 **Parameters:**

1644 t_{dead} : the mean detector dead time for the beam.

1645 N_{seg_pulses} : the number of pulses in the segment

1646 N_{px} : the number of pixels in the detector.

1647 dt : duration of a histogram bin.

1648

1649 **Procedure:**

1650

1651 *1. Generate a residual histogram*

1652 Convert PE height residuals to time residuals (multiply by $-2/c$). Generate a histogram of time
1653 residuals, N_{hist} , in bins of size dt .

1654 *2. Calculate the gain from the histogram*

1655 P_{dead} for bin i is the sum over bins $i-N_{dead}$ to $i-1$ of N_{hist} , divided by $N_{seg_pulses} N_{px}$.

1656 G_{est} is equal to $1 - P_{dead}$, where N_{dead} is the deadtime expressed in histogram bins.

1657 *3. Check if the correction is valid. If the minimum value for G_{est} is less than $2/(N_{seg_pulses}$*

1658 $N_{px})$, set all return values equal to invalid (NaN) and return.

1659 *4. Calculated the corrected histogram:*

1660 N_{PEcorr} is equal to N_{hist} divided by G_{est} .

1661 *5. Calculate height statistics*

1662 Calculate the gain-corrected mean and median and their errors for the segment, based on the full
1663 gain estimate and the full histogram:

1664 FPB_{med_corr} : $-1/2c$ times the gain-corrected median time based on N_{PE} and G_{est} . See
1665 5.11.

1666 $\Sigma_{FPB_{med_corr}}$: the error estimate for FPB_{med_corr}

1667 FPB_{mean_corr} : $-1/2c$ times the gain-corrected mean time based on N_{PE} and G_{est} . See 5.12.

1668 $FPB_{mean_corr_sigma}$: the error estimate for FPB_{mean_corr} .

1669 $Fpb_{N_photons}$: the sum of N_{PEcorr} .

1670

1671

1672 **5.11 Gain-corrected median**

1673 **Inputs:**

1674 N : The uncorrected histogram

1675 G : The gain estimate,
 1676 x : the abscissa for the bin centers, corresponding to N and G .

1677

1678 Outputs:

1679 x_{med} : the median of N based on G

1680 $sigma_x_med$: the error in x_{med}

1681

1682 **Procedure:**

1683 1. Calculate the corrected histogram:

1684 N_{corr} is equal to N divided by G .

1685

1686 2. Calculate the CDF of N_{corr}

1687 The CDF, C , is calculated at the bin centers, and at each bin center, j , is equal to the sum of all
 1688 values of N_{corr} for bin centers $i < j$. C is normalized so that its last value is equal to 1.

1689

1690 3. Calculate the 40th, 50th, and 60th percentiles of N_{corr}

1691 C is treated as a function that increases linearly across each bin, such that the upper edge of the
 1692 i th bin is greater than the lower edge of the i th bin by N_i . The abscissa for C runs from zero at
 1693 $x_l - dx/2$, to $x_m + dx/2$, where x_l is the first bin center, x_m is the last bin center, and dx is the spacing
 1694 between bin centers. The 40th, 50th, and 60th percentiles of N_{corr} are calculated by interpolating
 1695 into the vector of bin edges as a function of C . If more than one bin has a CDF within numerical
 1696 precision of the calculated percentile, report the mean x value of all such bins.

1697

1698 4. Calculate the error in the CDF at the 50th percentile

1699 The error in any value of N_{corr} ($sigma_N_{corr}$) is the inverse gain value for that bin times the
 1700 square root of N for that bin. $sigma_CDF$ for any x is found by calculating the RSS of all
 1701 $sigma_N_{corr}$ values for bins less than x , and dividing by the sum of N_{corr} .

1702 The value for $sigma_CDF$ at the 50th percentile is found by interpolating $sigma_CDF$ as a
 1703 function of C at a C value of 0.5.

1704

1705 5. calculate $sigma_x_med$

1706 $Sigma_x_med$ is found:

$$sigma_x_med = \frac{dz_{60} - dz_{40}}{0.2} \sigma_{cdf}(dz_{med})$$

1707

1708 Here d_{z60} and d_{z40} are the 40th and 60th percentiles of N_{corr} from step 3.

1709

1710 **5.12 Gain-corrected mean**

1711 Inputs

1712 N : The uncorrected histogram

1713 G : The gain estimate

1714 x : the abscissa for the bin centers, corresponding to N and G .

1715

1716 **Outputs:**

1717 x_{mean} : the mean of N based on G

1718 $sigma_x_mean$: the error in x_{mean}

1719

1720 1. Calculate the corrected histogram:

1721 N_{corr} is equal to N divided by G .

1722

1723 2. Calculate the corrected mean:

1724 Calculate the mean:

$$x_{mean} = \sum \frac{N_{corr,i}}{N_{tot}} x_i$$

1725

1726 3. Calculate the error in the corrected histogram:

$$\sigma_{N,corr,i} = \frac{N_{0,i}^{1/2}}{G_i}$$

1727

1728 4. Calculate the error in the corrected mean:

$$sigma_x_mean = \left[\sum \left(\sigma_{N,corr,i} \frac{x_i - x_{mean}}{N_{corr,tot}} \right)^2 \right]^{1/2} \quad 49$$

1729

1730 **5.13 Transmit-pulse-shape correction**

1731 This routine uses the most recent estimate of the transmit-pulse shape calculated from the
 1732 transmitter-echo pulse to calculate median and mean offsets for a windowed, truncated received
 1733 pulse. This correction depends the shape of the transmit pulse, and on three parameters that are
 1734 unique to each segment: the estimated width of the return pulse, the refined surface-window
 1735 height, and the signal-to-noise ratio.

1736

1737 **Inputs:**

1738 -Transmit-pulse-shape estimate (t_{tx} , P_{tx}). The time vector, t_{tx} is shifted so that P_{tx} has a
 1739 zero centroid (see 5.15).

1740 -Received-pulse width estimate (W_{rx})

1741 -Surface-window time duration (dt_W)

1742 -Signal-to-noise ratio estimate within the truncated window (SNR)

1743 **Outputs:**

1744 Height offsets for the mean and median transmit-pulse-shape correction.

1745

1746 **Procedure:**

1747 This correction works by generating a synthetic return pulse that matches the width of the actual
 1748 return pulse, and truncating it in the same way that the return pulse has been truncated. The
 1749 median and the mean of the synthetic pulse are then calculated.

1750

1751 *1. Calculate the time by which the received pulse was broadened*

1752 The spreading needed to broaden the transmitted pulse to match the received pulse is equal to
 1753 $W_{spread} = \sqrt{\max(0.01e^{-9}, W_{RX}^2 - W_{TX}^2)}$.

1754

1755 *2. Generate a synthetic received pulse*

1756 *2a: Calculate the shape of the expected spread pulse:*

1757 The synthetic received pulse is generated by convolving the transmitted pulse with a Gaussian
 1758 function of with a sigma parameter equal to W_{spread} . The Gaussian should have enough
 1759 samples to include at least $4 * W_{spread}$ worth of samples on either side of its center. The
 1760 synthetic pulse and its time vector are $N_{hist_synthetic}$ and $t_{synthetic}$.

1761

1762 *2b: Calculate the median of the broadened synthetic pulse:*

1763 Calculate the median of the synthetic received pulse, $t_{synthetic_med}$, and set
 1764 $t_{ctr} = t_{synthetic_med}$.

1765

1766 *2c: Normalize the waveform and add an estimated noise signal:*

1767 *N_hist_synthetic* is normalized so that its sum is equal to 1, and a background count of $1/SNR$

1768 (dt/dt_W) is added to *N_hist_synthetic*.

1769

1770 *3. Calculate the centroid of the synthetic received pulse*

1771 To find the centroid of the truncated synthetic waveform, an iterative procedure is used:

1772 *3a: Calculate the centroid of the synthetic waveform*

1773 *t_ctr* is set to the centroid of the truncated synthetic received waveform, windowed by $t_ctr -$

1774 $dt_W/2$ and $t_ctr + dt_W/2$

1775 *3b: Check for convergence and iterate*

1776 Unless the current and previous values of *t_ctr* are consistent to within 0.1 mm (0.00067 ns) or if

1777 50 iterations are complete, return to *4a*.

1778

1779 *4. Calculate the median of the synthetic received pulse*

1780 The median of the synthetic received waveform is calculated the synthetic received waveform

1781 from 4b, windowed by $t_ctr - dt_W/2$ and $t_ctr + dt_W/2$

1782

1783 5. The corrections for the median and mean heights are equal to $c/2$ times the median and mean

1784 time offsets.

1785 **5.14 Residual_histogram calculation**

1786 **Inputs:**

1787 *Segment_lat* : latitude for each segment center

1788 *Segment_lon* : longitude for each segment center

1789 *Segment_x_ATC*: along-track (x) coordinate for each segment center

1790 *Segment_h_mean*: mean-based land-ice height for each segment center

1791 *Segment_slope*: along-track slope for each segment center

1792 *Segment_SNR*: SNR values for segment fits

1793 *Segment_BGR*: Background rate estimate for each segment

1794 *N_seg_pulses* Number of pulses in each segment (including those contributing no PE to the fit).

1795 *x_pe*: along-track(x) coordinates for all ATL03 PE in the segment

1796 *h_pe*: ATL03 surface height for all PE in the segment.

1797 **Parameters:**

1798 N_{hist} : Number of groups of segments in the histogram (number of horizontal divisions)

1799 N_{bins} : Number of vertical bins in the residual histogram

1800 bin_{top_h} : Tops of the histogram bins, listed from bottom to top

1801 **Outputs:**

1802 *Count*: $N_{bins} \times N_{hist}$ -element array giving the number of residual photons in each bin
 1803 (N_{bins} is the vertical dimension, N_{hist} is the horizontal dimension)

1804 *bckgrd_per_m*: $1 \times N_{hist}$ -vector giving the expected background count per vertical
 1805 meter in each column of the histogram based on the observed background rate (*bckgrd*) and the
 1806 number of segments included in the histogram

1807 *Segment_id_list*: $10 \times N_{hist}$ -element array list of segment IDs included in the histogram

1808 *Lat_mean*: N_{hist} -element list giving the mean latitude of all segments included in each
 1809 horizontal histogram bin

1810 *Lon_mean*: N_{hist} -element list giving the mean longitude of all segments included in
 1811 each horizontal histogram bin

1812 *x_ATC_mean*: N_{hist} -element list giving the mean along-track (x) coordinate of all
 1813 segments included in each horizontal histogram bin

1814 **Procedure**

1815 1. Calculate the bin-edge heights. There are $N_{bins}+1$ edges. The second through last edges are
 1816 equal to the input bin_{top_h} values. The first (lowest) edge is 1 m lower than the second (i.e.
 1817 equal to the first value of $bin_{top_h} - 1$).

1818 2. Group segment centers into 10-segment groups: For each RGT, segments 1-10 would be in the
 1819 first group, 11-20 in the second, etc.

1820 3. For each group, gather all valid segments that have high-quality surface-height estimates
 1821 (*ATL06_quality_summary*=0). If any high-quality segments are present, calculate the histogram
 1822 count. Otherwise, report the histogram count as all zeros, and report *lat_mean*,
 1823 *lon_mean*, *x_atc_mean*, and *segment_id_list* as invalid.

1824 3a. For each valid segment, calculate the histogram and background count.

1825 3a.1: Gather the PE that have $x_{segment} - 10 \text{ m} < x_{pe} \leq 10 \text{ m}$.

1826 3a.2: Calculate the residual between the segment and the gathered PE: $r = h_{mean_segment} -$
 1827 $(x_{pe} - segment_x_ATC) \times segment_slope$.

1828 3a.3: For each vertical bin in the histogram, count the PE with residuals that fall
 1829 into the bin

1830 3a.4: For each valid segment, add the expected background count per vertical
 1831 meter, as estimated from the segment background count to the total background-per-meter
 1832 (*bckgrd_per_m*) for the segment. The contribution for each segment is: $segment_BGR \times$
 1833 $N_{seg_pulses} / 2 / (c/2)$. [N.B. The factors of 2 in the previous statement cancel, leaving :
 1834 $segment_BGR \times N_{seg_pulses} / c$.]

- 1835 3b. Add the segment histograms together to calculate the 10-segment histogram
- 1836 3c. Calculate the mean values for latitude, longitude, and x_{ATC} for the segment. List
- 1837 the selected segments in *segment_id_list*

1838

1839 **5.15 Transmit-echo-pulse initialization**

1840 This calculation centers the transmit-echo-pulse reported by ATL03 on its centroid, after using

1841 an iterative edit to distinguish between signal and noise. It should be performed each time a new

1842 night-time TEP estimate of the waveform becomes available. The TEP consists of the power

1843 (*tep_hist*) and time (*tep_hist_x*) that are input from ATL03. Two TEP histograms are available,

1844 obtained for laser spot 1 and 3. The ATL03 *tep_valid_spot* parameter specifies with which TEP

1845 histogram is used for each of the ground tracks, and the ATL03 *tep_range_prim* parameter

1846 specifies the valid range of times for each TEP histogram.

1847 **Inputs:**

1848 *-tep_hist_x* : Time for the Transmit-pulse-shape estimate

1849 *-tep_hist*: power (or signal count) for the transmit-pulse-shape estimate

1850 The time-sampling interval these is *dt_input*. The transmit pulse is sampled so that at least the

1851 first 5 ns and the last 10 ns are representative of the background noise for the transmit pulse.

1852 **Outputs:**

1853 *-t_tx*: time vector for the transmit pulse estimate, shifted such that P_{tx} has a zero centroid

1854 *-P_tx*: Power for the transmit-pulse estimate,

1855 **Algorithm:**

1856 1. *Identify noise-only and signal samples*: mark index *noise_samples* as true for the first 5 ns

1857 and last 10 ns of samples in *tep_hist*. Set *sig_samples* to the inverse of *noise_samples*

1858 2. *Calculate the noise value for the transmit pulse*: N_{tx} = the mean of *tep_hist* for the samples

1859 in *noise_samples*. Subtract N_{tx} from *tep_hist* to give P_{tx} .

1860 3. *Calculate the centroid of the transmit pulse*: $T0_{tx} = \text{sum}(P_{tx} * t_{tx}) / \text{sum}(P_{tx})$. The sum

1861 is carried out over the samples in *sig_samples*.

1862 4. *Calculate the RDE of the transmit pulse*: The width of the transmitted pulse (W_{TX}) is equal

1863 to half the difference between the 84th percentile and the 16th percentile of the portion of P_{tx} in

1864 *sig_samples*.

1865 5. *Re-establish the noise-only samples*: mark *noise_samples* as true for all samples with times

1866 more than 6 W_{TX} away from $T0_{tx}$, set *sig_samples* to the inverse if *noise_samples*. If

1867 *sig_samples* has changed from its previous values, and if fewer than 10 iterations have taken

1868 place, return to 1b.

1869 6. *Center the transmit pulse on its centroid*: Subtract $T0_{tx}$ from *t_tx_input* to give *t_tx*.

1870

1871

1872 **6 TEST DATA AND SOFTWARE REQUIREMENTS**

1873 This section describes a very simple test data set that has been derived to verify the performance
1874 of the ATL06 surface code.

1875 **6.1 ATL06 Test Data Setup**

1876 The ATL06 test data are a set of synthetic data generated based on a planar, sloping surface with
1877 a slope of 0.02. Separate data sets are generated for surface reflectance values between 1/16 and
1878 1, and for surface roughness values between zero and 2 m. A detector model with a dead time of
1879 3.2 ns is used to simulate the effects of the first-photon bias. For each segment, a full set of
1880 ATL06 parameters are generated using the Matlab prototype code, and with the ASAS
1881 production code, and the two are compared. Small numerical differences between the codes can
1882 produce different results in the early stages of the signal-finding code, so the most valid
1883 comparisons between the results of the two codes are for segments with moderate signal strength
1884 (reflectance greater than 0.25). We consider the two codes to produce equally valid results when
1885 the difference between the results for any parameter is not significantly different from zero, and
1886 when the spreads of the two sets of parameters are not significantly different from one another
1887 for segments based on the same number of photons with the same surface window size.

1888 **7 BROWSE PRODUCTS AND Q/A STATISTICS**

1889 **7.1 Browse Products**

1890 Browse products include two kinds of plots: Data-quality maps, and profile plots.

1891 Data-quality maps are based on the *signal_selection_source* parameter. Each map shows a
1892 background image based on the MODIS mosaics of Greenland or Antarctica (Scambos and
1893 others, 2007), with color-coded points showing the mean segment location for each kilometer of
1894 the beam track, with the color showing the largest bit in *signal_selection_source* that is set for
1895 more than 50% of all segments in that kilometer of data, assuming that for segments with no
1896 data, all bits are set. The plots are made separately for the strong and weak beams, because the
1897 two beams are, at the granule scale, very close to one another and would otherwise overlap.

1898 Profile plots are generated separately for each beam pair in the granule. Each plot shows the
1899 surface height as a function of along-track distance, and the height for each beam in the pair. A
1900 second set of axes, aligned with the first, shows the number of PE per segment (*N_fit_photons*)
1901 and the height error estimate, *h_li_sigma*.

1902 **7.2 Q/A Statistics**

1903 Quality assessment statistics are provided for each beam, for each 10-km increment along track.
1904 For each increment we provide:

1905 A synopsis of the *signal_selection_source* parameter:

1906 -The fraction of possible segments with *signal_selection_source* equal to zero.

1907 -The fraction of segments with *signal_selection_source* equal to 1.

1908 -The fraction of segments with *signal_selection_source* equal to 2.

1909 -The fraction of segments with *signal_selection_source* equal to 3.

1910 [Add parameters for the entire file]

1911

1912

1913 **8 APPENDIX A: GLOSSARY**

1914 This appendix defines terms that are used in ATLAS ATBDs, as derived from a document
1915 circulated to the SDT, written by Tom Neunann. Some naming conventions are borrowed from
1916 **Spots, Channels and Redundancy Assignments** (ICESat-2-ATSYS-TN-0910) by P. Luers.
1917 Some conventions are different than those used by the ATLAS team for the purposes of making
1918 the data processing and interpretation simpler.

1919

1920 **Spots.** The ATLAS instrument creates six spots on the ground, three that are weak and three that
1921 are strong, where strong is defined as approximately four times brighter than weak. These
1922 designations apply to both the laser-illuminated spots and the instrument fields of view. The
1923 spots are numbered as shown in Figure 1. At times, the weak spots are leading (when the
1924 direction of travel is in the ATLAS +x direction) and at times the strong spots are leading.
1925 However, the spot number does not change based on the orientation of ATLAS. The spots are
1926 always numbered with 1L on the far left and 3R on the far right of the pattern. Not: beams,
1927 footprints.

1928

1929 **Laser pulse (pulse for short).** Individual pulses of light emitted from the ATLAS laser are
1930 called laser pulses. As the pulse passes through the ATLAS transmit optics, this single pulse is
1931 split into 6 individual transmit pulses by the diffractive optical element. The 6 pulses travel to
1932 the earth's surface (assuming ATLAS is pointed to the earth's surface). Some attributes of a laser
1933 pulse are the wavelength, pulse shape and duration. Not: transmit pulse, laser shot, laser fire.

1934

1935 **Laser Beam.** The sequential laser pulses emitted from the ATLAS instrument that illuminate
1936 spots on the earth's surface are called laser beams. ATLAS generates 6 laser beams. The laser
1937 beam numbering convention follows the ATLAS instrument convention with strong beams
1938 numbered 1, 3, and 5 and weak beams numbered 2, 4, and 6 as shown in the figures. Not:
1939 beamlet.

1940

1941 **Transmit Pulse.** Individual pulses of light emitted from the ICESat-2 observatory are called
1942 transmit pulses. The ATLAS instrument generates 6 transmit pulses of light from a single laser
1943 pulse. The transmit pulses generate 6 spots where the laser light illuminates the surface of the
1944 earth. Some attributes of a given transmit pulse are the wavelength, the shape, and the energy.
1945 Some attributes of the 6 transmit pulses may be different. Not: laser fire, shot, laser shot, laser
1946 pulse.

1947

1948 **Reflected Pulse.** Individual transmit pulses reflected off the surface of the earth and viewed by
1949 the ATLAS telescope are called reflected pulses. For a given transmit pulse, there may or may
1950 not be a reflected pulse. Not: received pulse, returned pulse.

1951

1952 **Photon Event.** Some of the energy in a reflected pulse passes through the ATLAS receiver
1953 optics and electronics. ATLAS detects and time tags some fraction of the photons that make up
1954 the reflected pulse, as well as background photons due to sunlight or instrument noise. Any
1955 photon that is time tagged by the ATLAS instrument is called a photon event, regardless of
1956 source. Not: received photon, detected photon.

1957

1958 **Reference Ground Track (RGT).** The reference ground track (RGT) is the track on the earth at
1959 which a specified unit vector within the observatory is pointed. Under nominal operating
1960 conditions, there will be no data collected along the RGT, as the RGT is spanned by GT2L and
1961 GT2R (which are not shown in the figures, but are similar to the GTs that are shown). During
1962 spacecraft slews or off-pointing, it is possible that ground tracks may intersect the RGT. The
1963 precise unit vector has not yet been defined. The ICESat-2 mission has 1387 RGTs, numbered
1964 from 0001xx to 1387xx. The last two digits refer to the cycle number. Not: ground tracks, paths,
1965 sub-satellite track.

1966

1967 **Cycle Number.** Over 91 days, each of the 1387 RGTs will be targeted in the polar regions once.
1968 In subsequent 91-day periods, these RGTs will be targeted again. The cycle number tracks the
1969 number of 91-day periods that have elapsed since the ICESat-2 observatory entered the science
1970 orbit. The first 91-day cycle is numbered 01, the second 91-day cycle is 02, and so on. At the
1971 end of the first 3 years of operations, we expect the cycle number to be 12. The cycle number
1972 will be carried in the mid-latitudes, though the same RGTs will (in general) not be targeted more
1973 than once.

1974

1975 **Sub-satellite Track (SST).** The sub-satellite track (SST) is the time-ordered series of latitude
1976 and longitude points at the geodetic nadir of the ICESat-2 observatory. In order to protect the
1977 ATLAS detectors from damage due to specular returns, and the natural variation of the position
1978 of the observatory with respect to the RGT throughout the orbit, the SST is generally not the
1979 same as the RGT. Not: reference ground track, ground track.

1980

1981 **Ground Tracks (GT).** As ICESat-2 orbits the earth, sequential transmit pulses illuminate six
1982 ground tracks on the surface of the earth. The track width is approximately 10m wide. Each
1983 ground track is numbered, according to the laser spot number that generates a given ground
1984 track. Ground tracks are therefore always numbered with 1L on the far left of the spot pattern
1985 and 3R on the far right of the spot pattern. Not: tracks, paths, reference ground tracks, footpaths.

1986

1987 **Reference Pair Track (RPT).** The reference pair track is the imaginary line half-way between
1988 the planned locations of the strong and weak ground tracks that make up a pair. There are three
1989 RPTs: RPT1 is spanned by GT1L and GT1R, RPT2 is spanned by GT2L and GT2R (and may be
1990 coincident with the RGT at times), RPT3 is spanned by GT3L and GT3R. Note that this is the
1991 planned location of the midway point between GTs. We will not know this location very
1992 precisely prior to launch. Not: tracks, paths, reference ground tracks, footpaths, pair tracks.

1993

1994 **Pair Track (PT).** The pair track is the imaginary line half way between the actual locations of
1995 the strong and weak ground tracks that make up a pair. There are three PTs: PT1 is spanned by
1996 GT1L and GT1R, PT2 is spanned by GT2L and GT2R (and may be coincident with the RGT at
1997 times), PT3 is spanned by GT3L and GT3R. Note that this is the actual location of the midway
1998 point between GTs, and will be defined by the actual location of the GTs. Not: tracks, paths,
1999 reference ground tracks, footpaths, reference pair tracks.

2000

2001 **Pairs.** When considered together, individual strong and weak ground tracks form a pair. For
2002 example, GT2L and GT2R form the central pair of the array. The pairs are numbered 1 through
2003 3: Pair 1 is comprised of GT1L and GT1R, pair 2 is comprised of GT2L and GT2R, and pair 3 is
2004 comprised of GT3L and 3R.

2005

2006 **Along-track.** The direction of travel of the ICESat-2 observatory in the orbit frame is defined as
2007 the along-track coordinate, and is denoted as the +x direction. The positive x direction is
2008 therefore along the Earth-Centered Earth-Fixed velocity vector of the observatory. Each pair has
2009 a unique coordinate system, with the +x direction aligned with the Reference Pair Tracks.

2010

2011 **Across-track.** The across-track coordinate is y and is positive to the left, with the origins at the
2012 Reference Pair Tracks.

2013

2014 **Segment.** An along-track span (or aggregation) of PE data from a single ground track or other
2015 defined track is called a segment. A segment can be measured as a time duration (e.g. from the
2016 time of the first PE to the time of the last PE), as a distance (e.g. the distance between the
2017 location of the first and last PEs), or as an accumulation of a desired number of photons.
2018 Segments can be as short or as long as desired.

2019

2020 **Signal Photon.** Any photon event that an algorithm determines to be part of the reflected pulse.

2021

2022 **Background Photon.** Any photon event that is not classified as a signal photon is classified as a
2023 background photon. Background photons could be due to noise in the ATLAS instrument (e.g.
2024 stray light, or detector dark counts), sunlight, or mis-classified signal photons. Not: noise
2025 photon.

2026

2027 **h_{**}.** Signal photons will be used by higher-level products to determine height above the
2028 WGS-84 reference ellipsoid, using a semi-major axis (equatorial radius) of 6378137m and a
2029 flattening of 1/298.257223563. This can be abbreviated as ‘ellipsoidal height’ or ‘height above
2030 ellipsoid’. These heights are denoted by h; the subscript ** will refer to the specific algorithm

2031 used to determine that elevation (e.g. is = ice sheet algorithm, si = sea ice algorithm, etc...). Not:
2032 elevation.

2033

2034 **Photon Cloud.** The collection of all telemetered photon time tags in a given segment is the (or
2035 a) photon cloud. Not: point cloud.

2036

2037 **Background Count Rate.** The number of background photons in a given time span is the
2038 background count rate. Therefore a value of the background count rate requires a segment of PEs
2039 and an algorithm to distinguish signal and background photons. Not: Noise rate, background
2040 rate.

2041

2042 **Noise Count Rate.** The rate at which the ATLAS instrument receives photons in the absence of
2043 any light entering the ATLAS telescope or receiver optics. The noise count rate includes PEs
2044 due to detector dark counts or stray light from within the instrument. Not: noise rate,
2045 background rate, background count rate.

2046

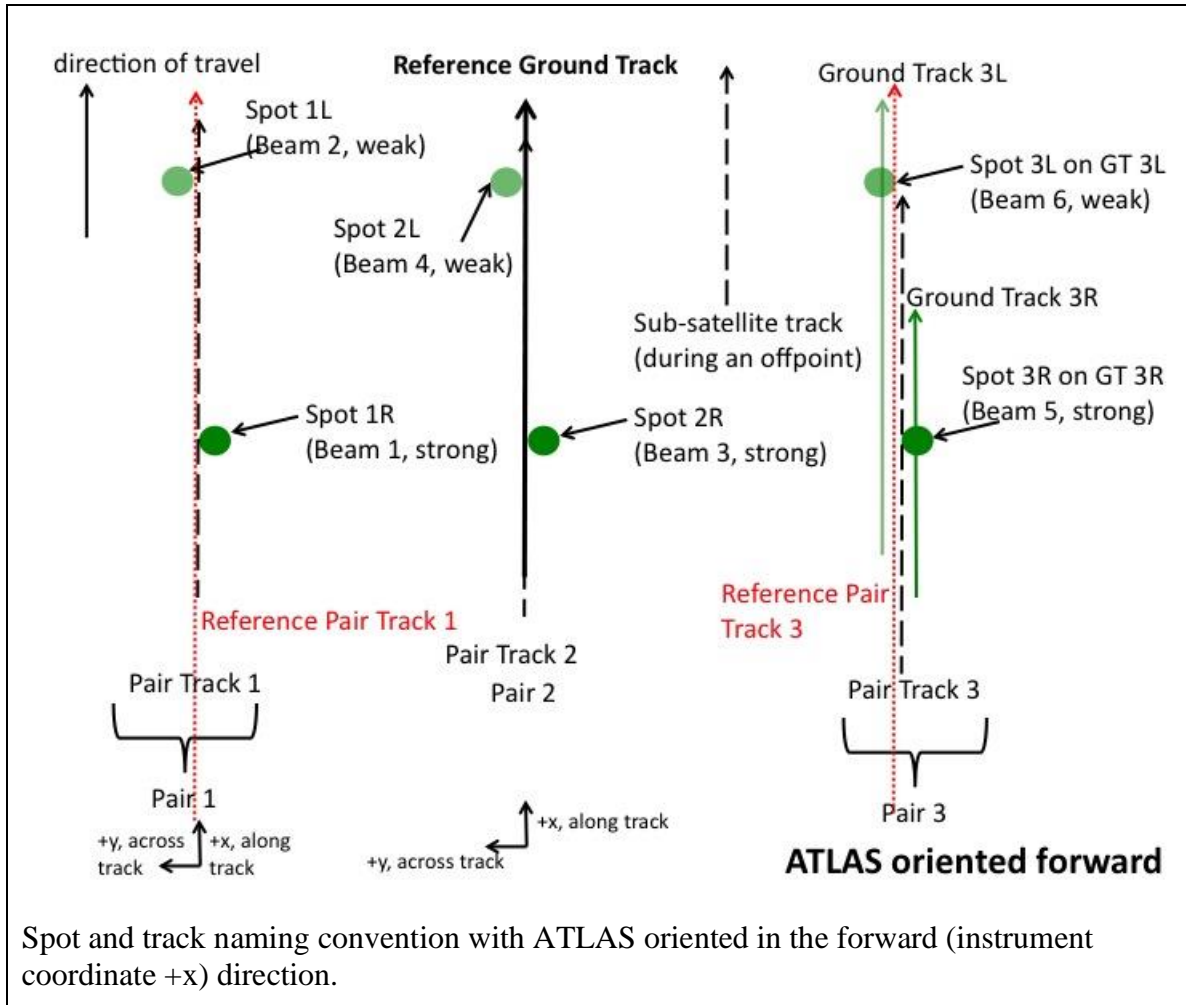
2047 **Telemetry band.** The subset of PEs selected by the science algorithm on board ATLAS to be
2048 telemetered to the ground is called the telemetry band. The width of the telemetry band is a
2049 function of the signal to noise ratio of the data (calculated by the science algorithm onboard
2050 ATLAS), the location on the earth (e.g. ocean, land, sea ice, etc...), and the roughness of the
2051 terrain, among other parameters. The widths of telemetry bands are adjustable on-orbit. The
2052 telemetry band width is described in Section 7 or the ATLAS Flight Science Receiver
2053 Algorithms document. The total volume of telemetred photon events must meet the data volume
2054 constraint (currently 577 GBits/day).

2055

2056 **Window, Window Width, Window Duration.** A subset of the telemetry band of PEs is called a
2057 window. If the vertical extent of a window is defined in terms of distance, the window is said to
2058 have a width. If the vertical extent of a window is defined in terms of time, the window is said to
2059 have a duration. The window width is always less than or equal to the telemetry band.

2060

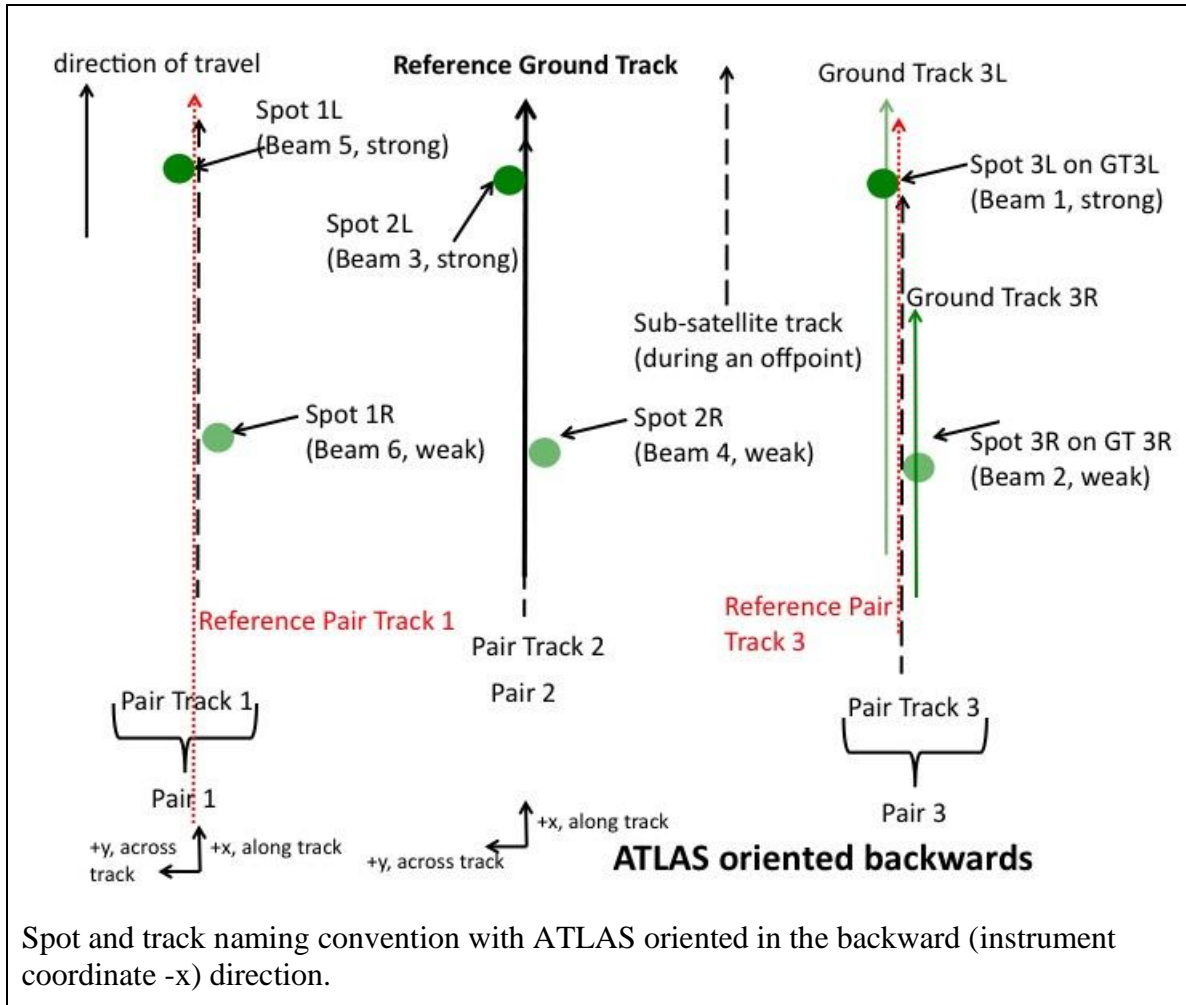
Figure 8-1. Spots and tracks, forward flight



2061

2062

Figure 8-2. Spots and tracks, forward flight



2063

2064

Glossary/Acronyms

ASAS	ATLAS Science Algorithm Software
ATBD	Algorithm Theoretical Basis Document
ATLAS	ATLAS Advance Topographic Laser Altimeter System
CDF	Cumulative Distribution Function
DEM	Digital Elevation Model
GSFC	Goddard Space Flight Center
GTs	Ground Tracks
ICESat-2	Ice, Cloud, and Land Elevation Satellite-2
MABEL	Multiple altimeter Beam Experimental Lidar
MIS	Management Information System
NASA	National Aeronautics and Space Administration
PE	Photon Event
POD	Precision Orbit Determination
PPD	Precision Pointing Determination
PRD	Precise Range Determination
PSO	ICESat-2 Project Science Office
PTs	Pair Tracks
RDE	Robust Dispersion Estimate
RGT	Reference Ground Track
RMS	Root Mean Square
RPTs	Reference Pair Tracks
RT	Real Time
SCoRe	Signature Controlled Request

SIPS ICESat-2 Science Investigator-led Processing System

TBD To Be Determined

TL/DR Too Long/Didn't Read.

2065

References

2066 Bamber, J.L., J.L. Gomez-Dans and J.A. Griggs 2009. A new 1 km digital elevation model of the
2067 Antarctic derived from combined satellite radar and laser data - Part 1: Data and methods.
2068 *Cryosphere*, **3**(1): 101-111.

2069 Menke, W. 1989. *Geophysical data analysis: discrete inverse theory*. San Diego, CA, Academic
2070 Press.

2071 Scambos, T.A., T.M. Haran, M.A. Fahnestock, T.H. Painter and J. Bohlander 2007. MODIS-
2072 based Mosaic of Antarctica (MOA) data sets: Continent-wide surface morphology and snow
2073 grain size. *Remote Sensing of Environment*, **111**(2-3): 242-257.

2074 Warren, S.G., R.E. Brandt and T.C. Grenfell 2006. Visible and near-ultraviolet absorption
2075 spectrum of ice from transmission of solar radiation into snow. *Applied Optics*, **45**(21): 5320-
2076 5334.

2077 Yang, Y., A. Marshak, S.P. Palm, T. Varnai and W.J. Wiscombe 2011. Cloud Impact on Surface
2078 Altimetry From a Spaceborne 532-nm Micropulse Photon-Counting Lidar: System Modeling for
2079 Cloudy and Clear Atmospheres. *Ieee Transactions on Geoscience and Remote Sensing*, **49**(12):
2080 4910-4919.

2081 Yang, Y., A. Marshak, S.P. Palm, Z. Wang and C. Schaaf 2013. Assessment of Cloud Screening
2082 With Apparent Surface Reflectance in Support of the ICESat-2 Mission. *Ieee Transactions on*
2083 *Geoscience and Remote Sensing*, **51**(2): 1037-1045.

2084 Yi, D.H. and C.R. Bentley 1999. Geoscience Laser Altimeter System waveform simulation and
2085 its applications. *Annals of Glaciology, Vol 29, 1999*, **29**: 279-285.

2086